USGS
science for a changing world

Debris Flows and Floods in Southeastern Arizona from Extreme Precipitation in July 2006—Magnitude, Frequency, and Sediment Delivery

Open-file Report 2008-1274

U.S. Department of the Interior
U.S. Geological Survey

Cover Photograph. (November 21, 2006) Debris-flow initiation and transport zones on the western side of Sabino Canyon, southern Santa Catalina Mountains, as seen from the Sabino Canyon road close to its end. (R.H. Webb, Stake 3803x).

USGS
science for a changing world

Prepared in Cooperation with the Pima County Regional Flood Control District

Debris Flows and Floods in Southeastern Arizona from Extreme Precipitation in July 2006—Magnitude, Frequency, and Sediment Delivery

By Robert H. Webb, Christopher S. Magirl, Peter G. Griffiths, and Diane E. Boyer

Open-file Report 2008-1274

U.S. Department of the Interior
U.S. Geological Survey

U.S. Department of the Interior
DIRK KEMPTHORNE, Secretary

U.S. Geological Survey
Mark D. Myers, Director

U.S. Geological Survey, Reston, Virginia 2008

For product and ordering information:
World Wide Web: http://www.usgs.gov/pubprod
Telephone: 1-888-ASK-USGS

For more information on the USGS—the Federal source for science about the Earth,
its natural and living resources, natural hazards, and the environment:
World Wide Web: http://www.usgs.gov
Telephone: 1-888-ASK-USGS

Suggested citation:
Webb, R.H., Magirl, C.S., Griffiths, P.G., and Boyer, D.E., 2008, Debris flows and floods in the southeastern Arizona from extreme precipitation in July 2006—Magnitude, frequency, and sediment delivery: U.S. Geological Survey Open-file Report 2008-1274.

Contents

Figures

Tables

Conversion Factors

Inch/Pound to SI

Multiply	By	To obtain
	Length	
inch (in.)	2.54	centimeter (cm)
inch (in.)	25.4	millimeter (mm)
foot (ft)	0.3048	meter (m)
mile (mi)	1.609	kilometer (km)
yard (yd)	0.9144	meter (m)
	Area	
acre	4,047	square meter (m^2)
acre	0.4047	hectare (ha)
square foot (ft^2)	929.0	square centimeter (cm^2)
square foot (ft^2)	0.09290	square meter (m^2)
square mile (mi^2)	259.0	hectare (ha)
square mile (mi^2)	2.590	square kilometer (km^2)
	Volume	
cubic yard (yd^3)	0.76455	cubic meter (m^3)
inch per hour (in/h)	0 .0254	meter per hour (m/h)
mile per hour (mi/h)	1.609	kilometer per hour (km/h)
	Mass	
pound, avoirdupois (lb)	0.4536	kilogram (kg)
ton, short (2,000 lb)	0.9072	megagram (Mg)
	Density	
pound per cubic foot (lb/ft^3)	16.02	kilogram per cubic meter (kg/m^3)
	Flow rate	
cubic foot per second (ft^3/s)	0.02832	cubic meter per second (m^3/s)

SI to Inch/Pound

Multiply	By	To obtain
	Length	
millimeter (mm)	0.03937	inch (in.)

Vertical coordinate information is referenced to the North American Vertical Datum of 1988 (NAVD 88).
Horizontal coordinate information is referenced to the North American Datum of 1983 (NAD 83 HARN).

Debris Flows and Floods in Southeastern Arizona from Extreme Precipitation in July 2006—Magnitude, Frequency, and Sediment Delivery

By Robert H. Webb, Christopher S. Magirl, Peter G. Griffiths, and Diane E. Boyer

Abstract

From July 31 to August 1, 2006, an unusual set of atmospheric conditions aligned to produce record floods and an unprecedented number of slope failures and debris flows in southeastern Arizona. During the week leading up to the event, an upper-level low-pressure system centered over New Mexico generated widespread and locally heavy rainfall in southeastern Arizona, culminating in a series of strong, mesoscale convective systems that affected the region in the early morning hours of July 31 and August 1. Rainfall from July 27 through 30 provided sufficient antecedent moisture that the storms of July 31 through August 1 resulted in record streamflow flooding in northeastern Pima County and eastern Pinal County. The rainfall caused at least 623 slope failures in four mountain ranges, including more than 30 near Bowie Mountain in the northern Chiracahua Mountains, and 113 at the southern end of the Huachuca Mountains within and adjacent to Coronado National Memorial. In the Santa Catalina Mountains north of Tucson, 435 slope failures spawned debris flows on July 31 that, together with flood runoff, damaged structures and roads, affecting infrastructure within Tucson's urban boundary. Heavy, localized rainfall in the Galiuro Mountains on August 1, 2006, resulted in at least 45 slope failures and an unknown number of debris flows in Aravaipa Canyon.

In the southern Santa Catalina Mountains, the maximum 3-day precipitation measured at a climate station for July 29-31 was 12.04 in., which has a 1,200-year recurrence interval. Other rainfall totals from late July to August 1 in southeastern Arizona also exceeded 1,000-year recurrence intervals. The storms produced floods of record along six watercourses, and these floods had recurrence intervals of 100-500 years. Repeat photography suggests that the spate of slope failures was historically unprecedented, and geologic mapping and cosmogenic dating of ancient debris-flow deposits indicate that debris flows reaching alluvial fans in the Tucson basin are extremely rare events. Although recent watershed changes—particularly the impacts of recent wildland fires—may be important locally, the record number of slope failures and debris flows were related predominantly to extreme precipitation, not other factors such as fire history.

The large number of slope failures and debris flows in an area with few such occurrences historically underscores the rarity of this type of meteorological event in southeastern Arizona. Most slope failures appeared to be shallow-seated slope failures of colluvium on steep slopes that caused deep scour of chutes and substantial aggradation of channels downstream. In the southern Santa Catalina Mountains, we estimate that 1.5 million tons of sediment were released from slope failures into the channels of ten drainage basins. Thirty-six percent of this sediment (527,000 tons) is gravel-sized or smaller and is likely to be transported by streamflow out of the mountain drainages and into the drainage network of metropolitan Tucson. This sediment poses a potential flood hazard by reducing

conveyance in fixed-section flood control structures along Rillito Creek and its major tributaries, although our estimates suggest that deposition may be small if it is distributed widely along the channel, which is expected.

Using the stochastic debris-flow model LAHARZ, we simulated debris-flow transport from slope failures to the apices of alluvial fans flanking the southern Santa Catalina Mountains. Despite considerable uncertainty in applying coefficients developed from worldwide observations to conditions in the southern Santa Catalina Mountains, we predicted the approximate area of depositional zones for several 2006 debris flows, particularly for Soldier Canyon. Better results could be achieved in some canyons if sediment budgets could be developed to account for alternating transport and deposition zones in channels with abrupt expansions and contractions, such as Rattlesnake Canyon.

Introduction

Landslides induced by heavy rainfall, which can spawn debris flows, are a significant geologic hazard throughout the world (Larsen, 2008). The desert regions of the southwestern United States are no exception, although the frequency of damaging events may be orders of magnitude lower than in more humid regions. The alluvial fans skirting the mountains of the Tucson basin (figs. 1 and 2) are popular locations for expensive homes and resorts, but few property owners realize that the ground below was built up by debris-flow deposition, particularly near the mountain fronts (Youberg and others, 2008). Although geologists have long recognized the debris-flow process as having a large role in alluvial-fan building (for example, Wells and Harvey, 1987), most had assumed debris-flow aggradation was restricted to the wetter climates of the Pleistocene and early Holocene. Debris flows are known to occur following fire in southeastern Arizona (Wohl and Pearthree, 1991) but were not believed to be a geologic hazard in the absence of fire or other disturbances under present-day climate. Supporting this assumption, historical records in the Tucson basin in the past 150 years report few instances of debris flows affecting areas downslope from the mountains (Pearthree and Youberg, 2006).

Heavy rainfall in southeastern Arizona from July 27 through August 1, 2006, led to record flooding at U.S. Geological Survey (USGS) streamflow gaging stations on a number of watercourses. The list of long-term gaging stations with new floods of record is given in table 1, and the annual flood series of three of these gaging stations are given in figure 3. The most significant flooding occurred in the Tucson basin, where runoff from the southern Santa Catalina Mountains and the western Rincon Mountains gathered in Rillito Creek, causing bankfull to near-bankfull flow in the soil-cemented channel designed to convey 100-year flood discharges. In Sabino Creek, rainfall on July 29, 30, and 31 generated significant floods culminating in a new flood-of-record (fig. 4*A*). Aravaipa Canyon had a series of large floods, culminating in a record event on August 1 (fig. 3*A*).

The heavy rainfall also triggered a historically unprecedented number of slope failures (at least 623), many of which coalesced and mobilized into debris flows in at least four mountain ranges in southeastern Arizona. The rainfall caused more than 30 debris flows near Bowie Mountain in the northern Chiracahua Mountains, 113 slope failures at the southern end of the Huachuca Mountains within and adjacent to Coronado National Memorial, and more than 45 debris flows in Aravaipa Canyon in the Galiuro Mountains. In the Santa Catalina Mountains north of Tucson, Arizona, 435 slope failures spawned damaging debris flows in an area where less than 10 small debris flows had been documented in the past 25 years (figs. 2 and 5). At least 13 debris flows damaged roads and bridges in the heavily used Sabino Canyon Recreation Area (*http://wwwpaztcn.wr.usgs.gov/rsch_highlight/articles/200611.html*, accessed June 12, 2008). In five canyons of the Santa Catalina Mountains, debris flows reached or passed the heads of alluvial fans on the edge of the Tucson metropolitan area.

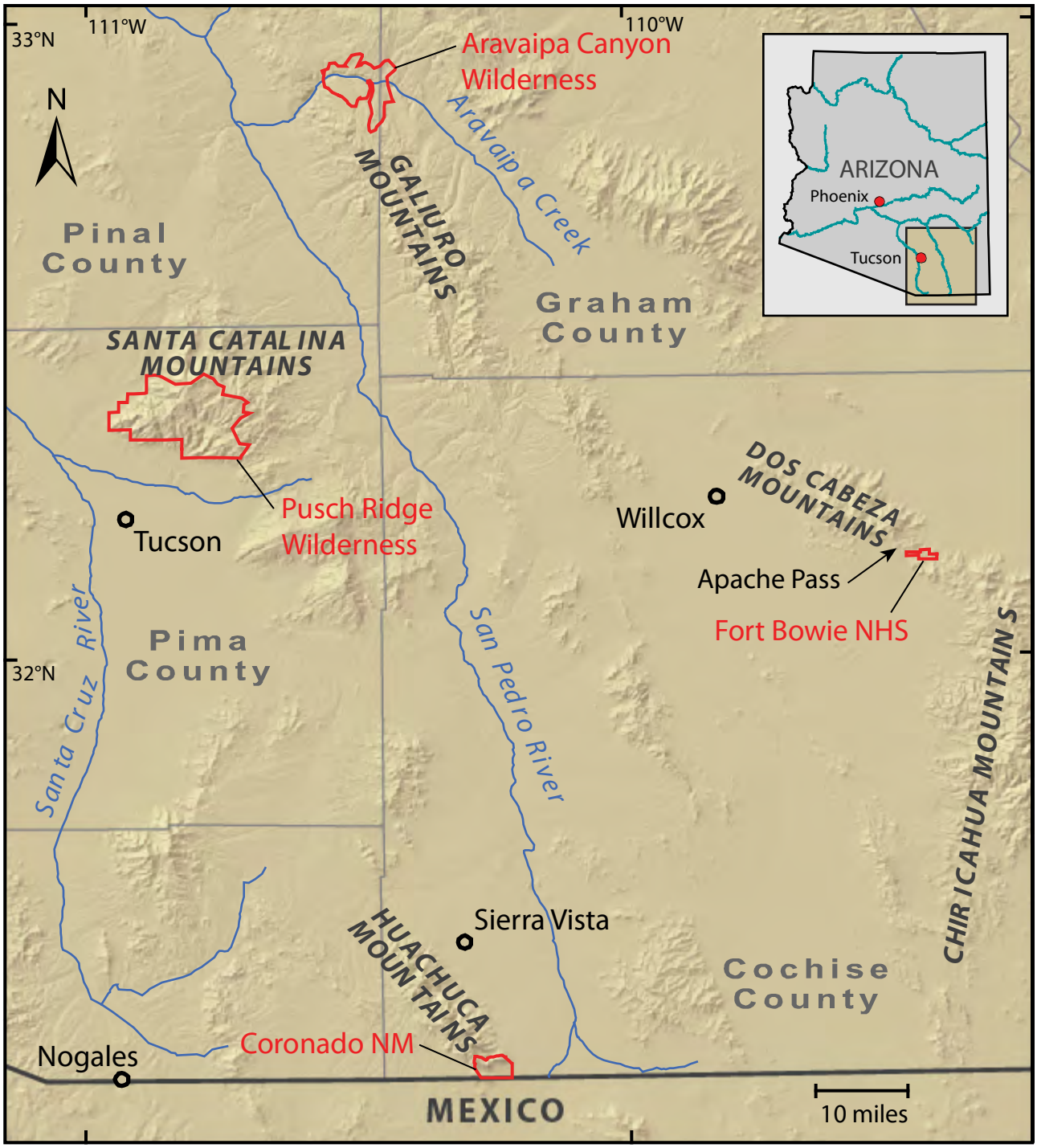

Figure 1. Map of southeastern Arizona showing the locations of areas affected by flooding and debris flows during the July 31 and August 1, 2006, storms. NM, National Monument; NHS, National Historic Site.

Table 1. Floods of record that occurred on July 31 or August 1, 2006, in southeastern Arizona.

Watercourse	Gaging Station Name	Drainage Area (mi^2)	Years of Record	Previous Flood of Record (ft^3/s)	Date of Previous Record Flood	New Flood of Record (ft^3/s)
Aravaipa Creek	Near Mammoth (09473000)	537	56	70,800[1]	1983	28,000
Rincon Creek	Near Tucson (09485000)	44.8	54	9,670	1971	15,000
Pantano Wash	At Broadway Blvd at Tucson (09485450)	599	23[2]	11,000	1983	15,900
Sabino Creek	Near Tucson (0984000)	237	75	14,100[3]	1999	15,700
Tanque Verde Creek	Tanque Verde Creek at Tucson (09484500)	219	39	24,500	1993	26,600
Rillito Creek	Near Tucson (combined record, see text)	918	86	29,700	1983	38,700

[1]This discharge, from Roeske and others (1989), is widely believed to be an overestimate of the peak discharge for the 1983 flood. Roberts (1986) estimated this peak discharge to be 27,500 ft^3/s, which is the value we accept.

[2] The gaging station Pantano Wash near Vail, AZ (09484600) has 49 years of record; however, the peak discharge at this site was 5,100 ft^3/s on July 27, 2006, which is not a particularly high discharge for the record. Most of the runoff on July 31 came from downstream of this gaging station.

[3] This value was reduced from 15,400 ft^3/s after the 2006 flood owing to reexamination of the stage-discharge relation.

The purpose of this report is to discuss the magnitude and frequency of the storm and floods of July-August 2006 in southeastern Arizona, to provide quantitative estimates of sediment moved from cliffs and hill slopes into channels in the southern Santa Catalina Mountains, and to use a stochastic model (LAHARZ) to estimate the potential for future debris flows to exit the Santa Catalina mountain front and affect alluvial fans on the fringe of the Tucson Metropolitan Area. The occurrence of extreme rainfall in four different mountain ranges, and the large number of slope failures that resulted, underscores our conclusion that the record floods and debris flows were caused by an extreme meteorological event irrespective of other watershed changes, particularly those introduced by wildland fire.

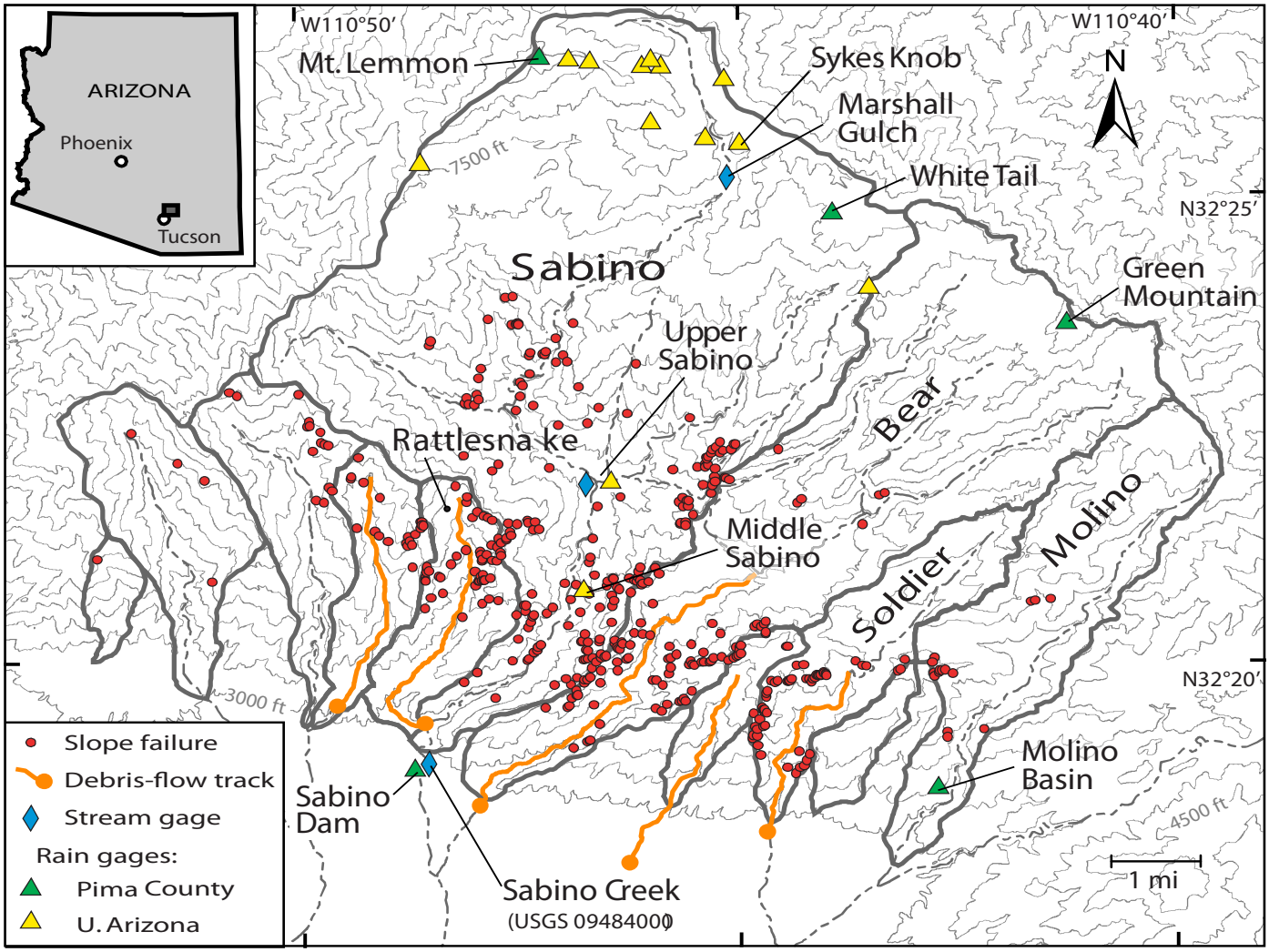

Figure 2. Map of 435 slope failures that occurred on July 31, 2006, the tracks of five large debris flows that approached or exited the mountain front, and the locations of climate stations and streamflow gaging stations in the southern Santa Catalina Mountains north of Tucson, Arizona. Many of the locations for University of Arizona climate stations overlap at this map scale. The elevation contour interval is 300 feet. Click on the figure to see and control animation (courtesy of Google Earth).

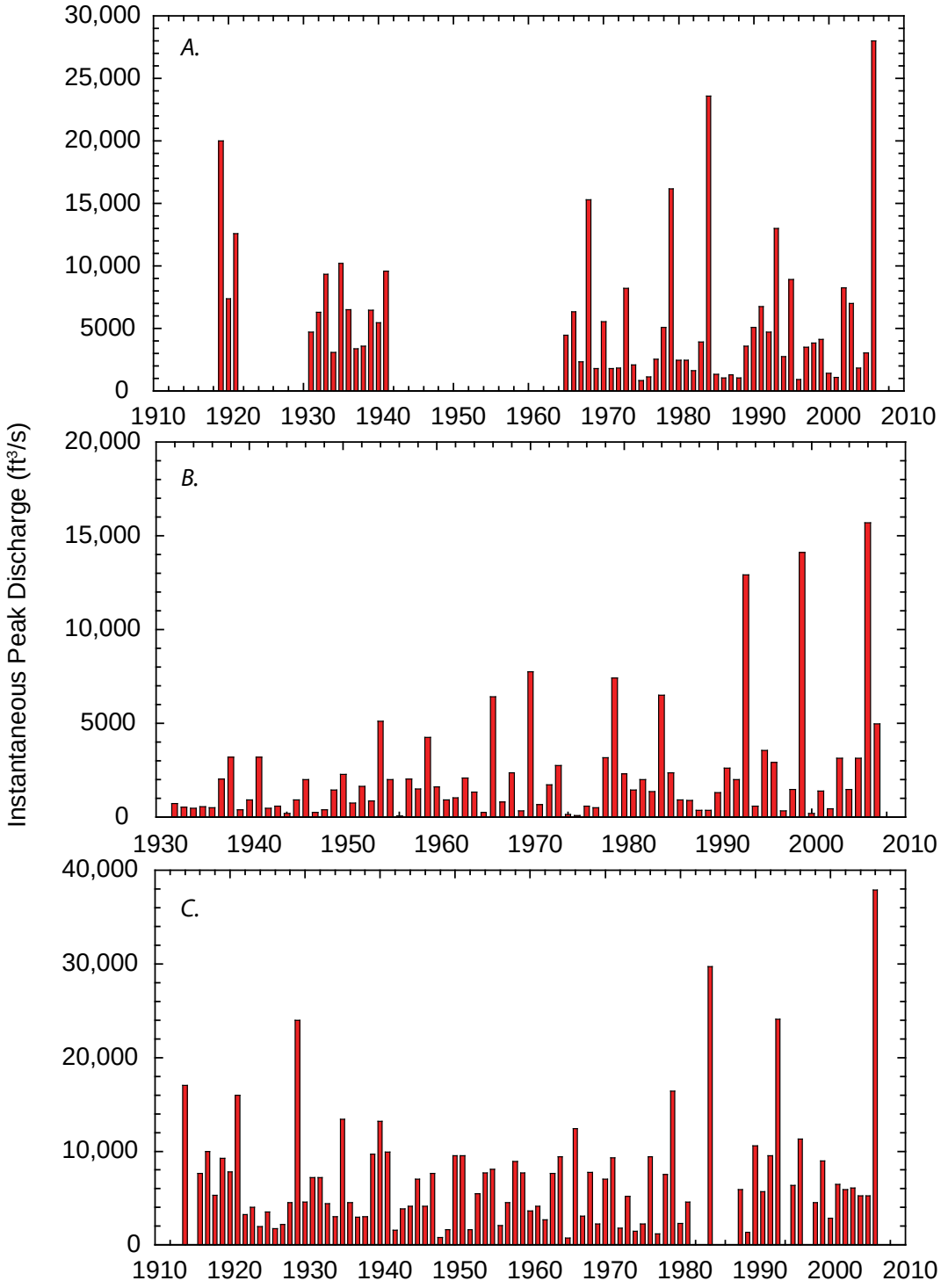

Figure 3. Annual flood series of three streams in southeastern Arizona that had record flooding on July 31 and August 1, 2006. A, Aravaipa Creek near Mammoth, AZ (09473000), showing the revised estimate for the 1983 flood (see text). The 2006 flood peak occurred on August 1. B, Sabino Creek near Tucson, AZ (09484000). C, Combined record for Rillito Creek near Tucson, AZ (09486000; 1915-1984) and Rillito Creek at Dodge Boulevard at Tucson, AZ (09485700; 1988-2006).

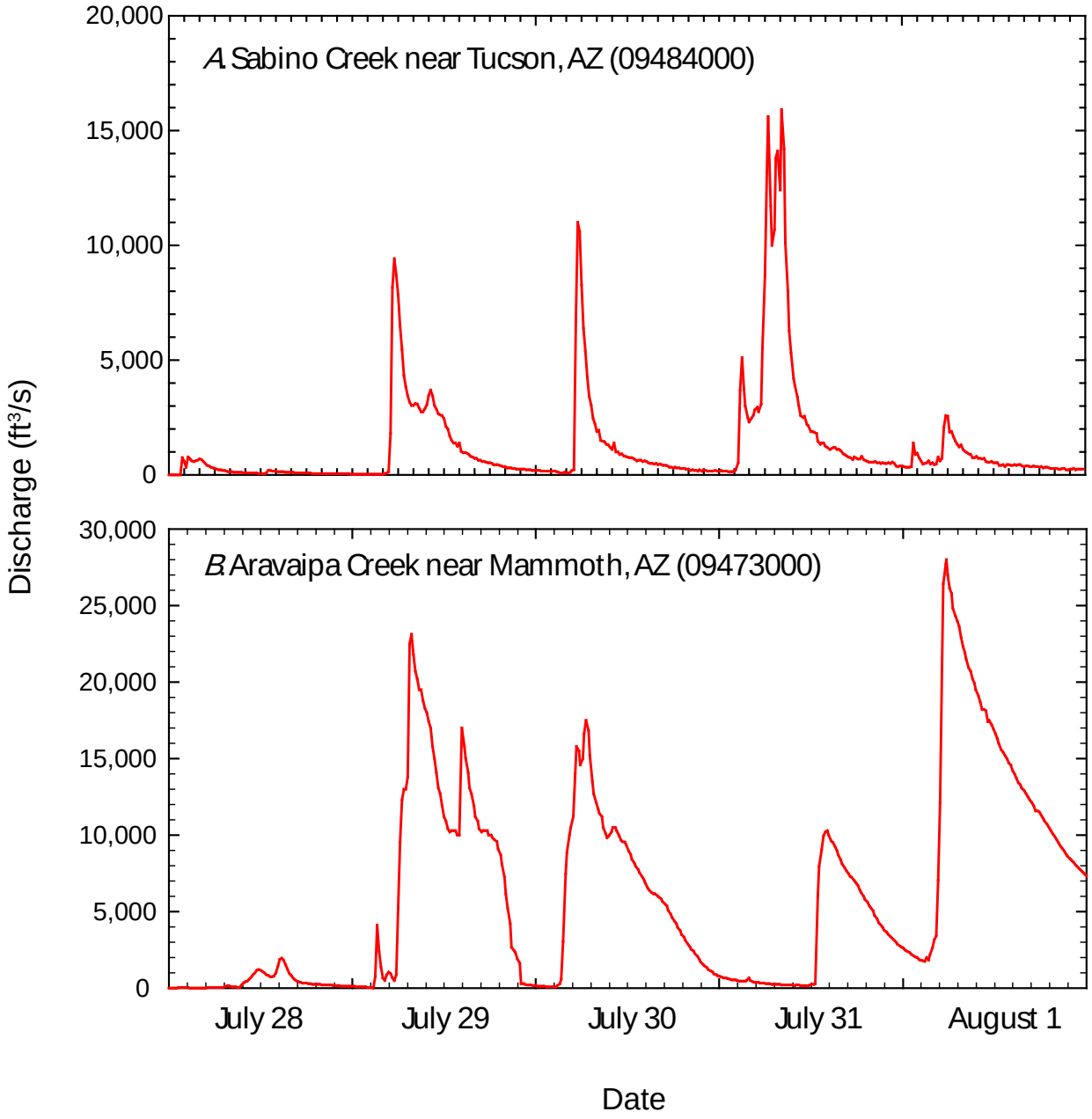

Figure 4. Hydrograph of flow from July 27 through August 1, 2006. *A*, Sabino Creek near Tucson, AZ (09484000). *B*, Aravaipa Creek near Mammoth, AZ (09473000).

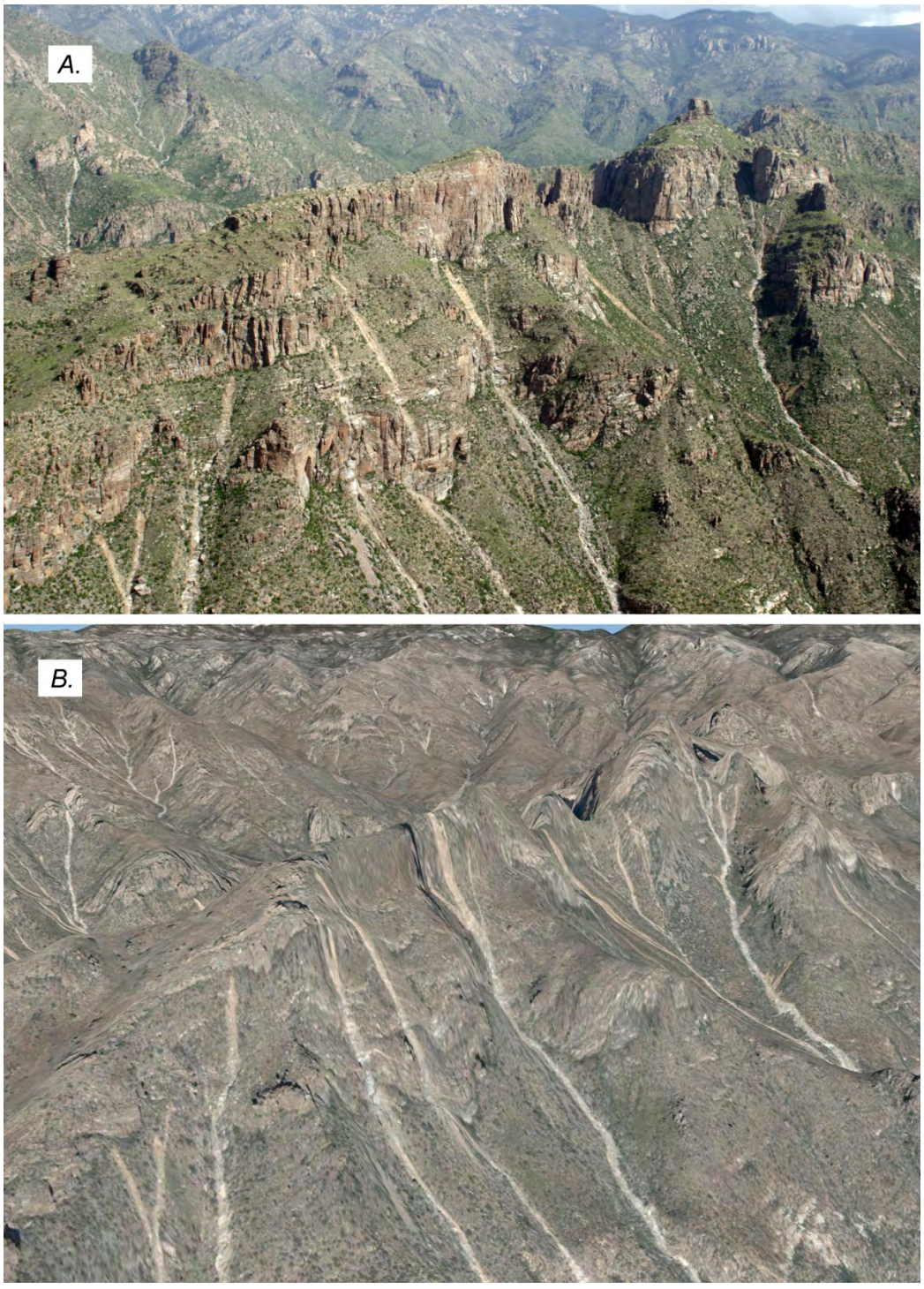

Figure 5. Slope failures in Bear Canyon, southern Santa Catalina Mountains, that occurred on July 31, 2006. *A*, August 18, 2006, aerial photograph (R.H. Webb). *B*, October 2006 satellite imagery (courtesy of Google Earth).

Definitions

In this report, we use a number of specific hydrologic and geomorphic terms, some of which are modified from their worldwide general application, to describe floods and debris flows in southeastern Arizona. We urge readers unfamiliar with these terms to use our Glossary section, where we provide explicit definitions. Only the most widely used terms are discussed here.

We differentiate the types of flooding that were observed in southeastern Arizona in 2006 into the categories of streamflow flood, hyperconcentrated flow, and debris flow (Pierson and Costa, 1987). All of these flow types are two-phase media containing water and sediment in varying mixtures. Streamflow is Newtonian flow that typically contains less than 40 percent sediment and is the most common type of floodflow observed in this region. A debris flow typically contains less than 60 percent sediment and is a non-Newtonian flow (Iverson, 1997); debris flows commonly are modeled as granular mass flows (Iverson and Vallance, 2001). Hyperconcentrated flow is a poorly understood phenomena, but the term is used to describe fluid flow with sediment concentrations between streamflow and debris flow. For many canyons in southeastern Arizona that flooded in 2006 (for example, Soldier Canyon), all three types of flow occurred at some point in the event hydrograph (see Melis and others, 1997, for examples of hydrographs of debris flows from Grand Canyon National Park, Arizona).

The potential complexities of the event hydrograph are unknown for the 2006 debris flows but are well known in other areas; readers should refer to several web sites and videos (for example, *http://elnino.usgs.gov/landslides-sfbay/photos.html*, *http://ca.water.usgs.gov/news/NewsVideos.html*, *http://landslides.usgs.gov/recent/events/laconchita/*, *http://vulcan.wr.usgs.gov/Projects/PP1671/framework.html*, all accessed June 20, 2008) for graphic depictions of debris-flow mobilization and remobilization possibilities. Costa and Williams (1984) is an early report with video imagery of debris flows and is highly recommended. Most debris flows have multiple pulses separated in the hydrograph by either streamflow or hyperconcentrated flow; only relatively small debris flows from small watersheds tend to travel as a single, discrete pulse. The 2006 debris flows in southeastern Arizona differ from debris flows elsewhere because in most cases substantial recessional streamflow or hyperconcentrated flow followed the peak of the debris flow, obliterating evidence or obscuring deposits.

In southeastern Arizona, we use the generic term slope failure to describe the initiation points for debris flows. In many parts of the world, the term landslide is used, and landslides typically are deep-seated failures (thickness typically is much greater than 3 ft) of relatively large spatial extent that typically initiate movement of a saturated or partially saturated sediment body on a curvimetric failure plane. Slope failures in southeastern Arizona tend to be small-scale, fully saturated colluvial masses with failure surfaces at a depth of 3 ft or slightly less, and the failure surface in many cases is bedrock. The sediment produced by a slope failure could either move a short distance and stop or mobilize into a debris flow that travels hundreds of feet to several miles. Sediment from closely spaced slope failures coalesced in many cases to mobilize the largest debris flows that we observed in this region.

Debris flows maintain their downstream motion through both particle-to-particle impacts and the presence of a slurry of water and fine-grained sediment, known as the flow matrix, that buoys larger particles in the flow and maintains down-slope motion (Iverson, 1997). Consistent with the mechanics of debris flows observed elsewhere (Pierson and Costa, 1987; Costa, 1988; Iverson, 1997), debris flows in the Santa Catalina Mountains left signature lateral and medial levees and snouts of relatively large particles up to and greater than 6-ft in diameter. Downstream from the depositional zone, debris flows transitioned to hyperconcentrated flow and then to streamflow flood in a downstream direction, a behavior that is widely observed elsewhere (Pierson and Scott, 1985; Iverson, 1997) and termed runout. In contrast to debris flows elsewhere, however, the supporting matrix of the debris flows in southeastern

Arizona generally flows away from the debris-flow deposits or was washed away by following streamflow floods, leaving behind deposits of piled boulders.

We used a set of criteria to evaluate whether a debris flow occurred in a watershed. These criteria include (1) the presence of a definable snout of coarse debris, particularly boulders, at the termination point of the debris flow; (2) the presence of a slope failure or failures associated with the debris flow; (3) the presence of depositional evidence, including boulder levees, boulder trains, secondary snouts, and debris fans along the route of the debris flow; and (4) the presence of fine-grained matrix deposits within lateral flow levees or in snouts. Debris flows occur within a larger event hydrograph (Melis and others, 1997), and if subsequent flood flow has a higher stage than the preceding debris flow (termed a type III event by Melis and others, 1997), debris-flow deposits can be reworked and evidence of the event can be obscured. This is particularly true for debris-flow deposits and whether or not matrix deposits remain identifiable on the landscape.

Finally, we generalize debris-flow initiation through deposition into three zones. The initiation zone is where slope failures occur and debris flows mobilize. The initiation zone is on steep slopes and always represents net sediment addition to the debris flow beginning with a discrete slope failure and continuing through scour of hillslope hollows and steep chutes. We use the term scar to refer to the landscape modification that occurs in the initiation zone as a result of a debris flow, and we measured the dimension of scars to determine the volume of slope failures. The transport zone is highly variable and represents a channelized setting with little or no net change in flow volume; generally, field evidence suggests that sediment additions are offset by deposition in the transport zone. Small debris flows may lack a transport zone if deposition occurs at the toe of the slope leading to the slope failure. Finally, the deposition zone is where either the debris flow terminates in a snout or, as in channel expansion zones, where significant amounts of debris-flow sediments are deposited in levees, boulder trains, or mid-channel secondary snouts. These types of deposits are diagnostic for debris-flow occurrence in this region.

In watersheds with narrow channels confined within bedrock, debris flows begin in an initiation zone, flow through the transport zone with little net additions or losses, and terminate in a deposition zone. Watersheds with complex channel geometries featuring alternating expansion-contraction reaches may have complex and alternating transport and deposition zones. We will illustrate some of these complexities in a later discussion of 2006 debris flows in the Santa Catalina Mountains.

Data Sources and Methods

Precipitation and Streamflow

For many studies of extreme events in Arizona, rainfall and streamflow gaging data are relatively sparse, owing to the typically remote locations of watersheds. For watersheds affected by the July 31, 2006, storm in the southern Santa Catalina Mountains, considerable hydrologic data is available owing to a convergence of scientific studies by the University of Arizona (Desilets and others, 2007), nearby weather radar operated by the National Weather Service (NWS), early warning systems installed by Pima County Regional Flood Control District (PCRFCD), and on-going streamflow gaging by the USGS and PCRFCD (Magirl and others, 2007). For other flood-affected areas of southeastern Arizona, relatively few data document the events of July 2006 and its antecedent conditions.

Rainfall and streamflow gages were distributed throughout the Sabino Creek watershed to study, among other things, the hydrologic response to the 2003 Aspen Fire (Desilets and others, 2007; Magirl and others, 2007). Considerable rainfall data are available for this storm (Griffiths and others, in press), including 24 temporary rainfall gages operated by the University of Arizona and positioned mostly at

the upper elevations of Mount Lemmon (fig. 2). The Pima County ALERT system of rainfall gages and stage recorders has nine stations within the flood-affected area *(http://alert.rfcd.pima.gov*, accessed June 18, 2008*)*. A NWS Doppler weather radar (WSR-88D), positioned 31 mi southeast of the southern Santa Catalina Mountains, has an unimpeded view of the atmosphere above these mountains. At this distance, the weather radar recorded high-frequency rainfall amounts at a resolution of approximately 0.36 mi^2 (Griffiths and others, in press).

Rainfall gages are widely spaced elsewhere in southeastern Arizona and generally are not in mountainous areas, so other regions affected by the July 2006 storms have little quantitative precipitation data. Rainfall data were collected in storage gages by The Nature Conservancy in Aravaipa Canyon, at the headquarters of Fort Bowie National Historic Site by the National Park Service, and by the Agricultural Research Service in the vicinity of Coronado National Memorial (A. Youberg, Arizona Geological Survey, written commun., 2008). USGS automatically records precipitation at its gaging station on Aravaipa Creek, and the Bureau of Land Management (BLM) maintains recording rainfall gages in Horse Camp Canyon, 1.6 mi north of Aravaipa Creek in Aravaipa Canyon, and in Goodwin Canyon, in Apache Pass about 2.5 mi northwest of the failures near Fort Bowie.

Streamflow gaging stations operated by the USGS record stage at numerous sites in the Tucson basin, including Sabino Creek and the master drainage of Rillito Creek and its major tributaries. Many of these sites are long-term; for example, the gaging record for Sabino Creek has a record length of 75 years (table 1). In addition, several temporary streamflow gaging stations were established by the University of Arizona to monitor the effects of the Aspen Fire (Magirl and others, 2007), but these short-record gaging stations were mostly at elevations higher than the most heavily affected zone and their short records preclude any frequency analyses of the event. For Aravaipa Creek, a long-term USGS gaging station records flow at the western end of Aravaipa Canyon, but no streamflow gaging stations are located in the vicinity of Fort Bowie and Coronado National Memorial, although runoff from Coronado National Memorial flows into the San Pedro River upstream from the Palominas gaging station (see later section on Coronado National Memorial).

Frequency analysis of rainfall in this region is estimated using standardized techniques developed by the National Oceanic and Atmospheric Administration (NOAA) and published in NOAA Atlas 14 (Bonin and others, 2006); a calculator is available on-line (*http://hdsc.nws.noaa.gov/hdsc/pfds/sa/az_pfds.html*, accessed June 3, 2008). Flood frequency is estimated using standard techniques (U.S. Water Resources Council, 1981) implemented in USGS computer program PeakFQ (*http://water.usgs.gov/software/PeakFQ/*, accessed June 18, 2008). This program implements a log-Pearson type III probability distribution and recommends use of a generalized skew coefficient averaged with the station skew to reduce uncertainty in the tail of probability distributions, which is where extreme events are identified. We used PeakFQ with a regional generalized skew coefficient of 0.0 in our analyses.

Repeat Photography of Slope Failures

Repeat photography is a time-honored technique for evaluating landscape change worldwide. This technique has been used throughout southern Arizona to document change, particularly in perennial vegetation (Turner and others, 2003) but also flood-related channel change (for example, Betancourt, 1990) and change in riparian vegetation (Webb and others, 2007b). The Desert Laboratory Collection of Repeat Photography (Webb and others, 2007a) is the largest collection of oblique repeat photography in the world, and imagery is collected with rigorous, well-documented techniques using large-format film cameras. All camera stations for repeat photographs are identified in our database with unique stake numbers (see captions for repeat photographs).

We used repeat photography primarily to document debris-flow and flood effects on channels, such as Sabino and Soldier Creeks, and also to provide some information on the recurrence interval of slope failures. We examined all of the historic oblique imagery of the southern Santa Catalina Mountains stored in archives (1890-present) or made available from private individuals (1984-present) to determine if slope failures could be documented. This involves the assumption that the physical evidence of slope failures persists long enough to be captured in repeat imagery as a highly visible scar. To attempt to evaluate this assumption, we revisited slope failures in Bear Canyon that occurred during the October 1983 floods. These failures remain highly visible but are easily distinguished from the 2006 failures in the same drainage. Although recovery of slope failures may be highly variable, our observations suggest that if an historical spate of slope failures occurred before 2006, it probably would be recorded on historical imagery.

Sediment Yield from Slope Failure and Debris Flow

The sudden occurrence of hundreds of slope failures and associated debris flows within a limited area necessarily introduced an unknown but likely significant amount of entrainable sediment to the canyon washes of the southern Santa Catalina Mountains. As the washes from these canyons drain directly into the urban washes of metropolitan Tucson, this new sediment supply may become a maintenance concern for PCRFCD, dependent on the rate at which this sediment is transported downstream. We estimated the mass of available sediment released by these failures using a variety of data collected by remote sensing and field reconnaissance. First, slope failures were identified and cataloged with aerial and satellite imagery, then their plan areas were outlined on orthorectified imagery and the data transferred to a GIS. Using LIDAR-derived elevation data, plan areas of slope failures were converted to slope areas, which were then multiplied by average failure depth to obtain the volumes of individual slope failures. These volumes were converted to total mass of all sediment as well as the masses of individual particle-size fractions.

Identification of Slope Failures

Slope failures were first identified and cataloged using 1:13,000 black-and-white aerial photography collected on July 28, 2007; 2-ft color satellite imagery collected on October 20, 2006; and 1-ft color aerial orthophotographs collected in August and September 2002. PCRFCD provided the black-and-white photography as tiff files scanned at high resolution (10.5 μm) and the 2002 color orthophotographs as georeferenced tiff files. The color satellite imagery was accessible during the project within Google Earth software (*http://earth.google.com*, accessed June 26, 2008). Slope failures are readily apparent in the color imagery on hill slopes, identifiable by the sharp contrast of freshly abraded white granite against adjacent green vegetation and reddish-brown colluvium, and color imagery was the principal means of failure identification (fig. 5). The 2007 black-and-white photography was used east of 110°43’W longitude, where color imagery was not available.

Vertical white lines of high contrast on hill slopes were initially classified as slope failures if they were more than 3 ft wide and oriented downslope. Candidates for slope failures were then compared against the 2002 color orthophotographs to identify and eliminate failures that predated the 2006 event. Similarly, well-worn bedrock stream channels were identified and then eliminated from consideration as slope failures. Each slope failure > 3.3 ft wide was counted as a separate failure, even if it merged downslope with other failures, which frequently occurred (fig. 5).

Sediment Volume and Mass

Each slope failure mapped in the southern Santa Catalina Mountains was outlined on the color aerial photography within Google Earth to provide a georeferenced polygonal area. For the slope

failures east of 110°43'W longitude, we orthorectified 2007 black-and-white images using control points derived from the 2002 orthophotos and mapped the remaining failure areas on those images. All data were then imported into a GIS for further processing. Using aerial LIDAR collected in March 2007 (4.59 ft horizontal and 0.59 ft vertical resolution), we built a surface model (TIN) of the entire area that encompassed all failures in the Santa Catalina Mountains. We then projected the slope-failure outlines collected from the aerial and satellite imagery onto this TIN. Each failure polygon was evaluated and adjusted by hand to account for error inherent to the Google Earth data and to better fit the LIDAR surface model. Once adjusted to the LIDAR model, the plan area of each failure was converted to actual slope or surface area using a 3.28-ft resolution digital-elevation model (DEM) also derived from the LIDAR data. To calculate the volume of sediment from each failure, slope area was multiplied by the average depth of slope failure. Average depth was determined through a combination of field reconnaissance and GIS techniques. Finally, sediment volume was converted to mass using an estimated debris-flow bulk density of 125 lbs/ft^3 (Webb and others, 2000). Mass estimates were then aggregated by primary drainage basin (fig. 2).

Particle-Size Distribution

In evaluating the particle-size distribution of slope-failure sediments, we deviate from the English system of units because particle sizes traditionally are given in mm in sediment-transport calculations. Given the large size (b-axis >32 mm) of many particles in these sediments, accurate determination of sediment particle-size distribution by standard mass-based sieving methods was impossible. Instead, we used point counts (Wolman, 1954; Rice and Church, 1996) in combination with standard sieving techniques (Kellerhals and Bray, 1971; Folk, 1974) to obtain a complete view of the distribution of particles in the failure sediments. This combination has been used successfully to evaluate debris-flow deposits in Grand Canyon and elsewhere and is described in detail in Webb and others (2000). Point counts were obtained on the surface of sufficiently large, undisturbed sediment deposits and sample particles with a b-axis >2 mm (gravel and larger). Finer particles were evaluated from 4-11 lb samples of debris-flow matrix, which were collected wherever complete debris-flow deposits were preserved. Typically, these samples were composed of gravel-sized and finer particles (b-axis <64 mm).

Although a wide range of particle sizes—from large boulders to clay-size particles—were released by each slope failure, only the finer particles are likely to be entrained by typical streamflow floods. To obtain an upper limit of the particle sizes typically carried into the washes of the Tucson basin, we sampled surficial streamflow sediment from the thalweg of washes exiting the mountains at 16 locations (see fig. 36). Three 10-lb samples were collected at each sampling location from a depth of 0 – 0.5 ft (surface samples), sieved and analyzed for weight-percent particle-size distribution, and the results averaged for one mean distribution at that location. These samples were analyzed in the same manner as the debris-flow matrix samples, providing an upper limit to the size of sediment carried by streamflow out of the mountain basins.

Stochastic Modeling of Debris Flows (LAHARZ)

Due to complex particle interaction and non-Newtonian fluid mechanics (Iverson, 1997), deterministic modeling of debris flows can be challenging and inaccurate. One of the better ways of predicting mobility and inundation potential of debris flows is to use stochastic modeling. Examining worldwide data from lahars, which are a common type of debris flow spawned from volcanic eruptions, Iverson and others (1998) found a correlation between the volume of debris flow, the planimetric area of deposition, and the largest cross-sectional area through which the debris flow has passed. The relations between area and volume follow a 2/3 power law of the form:

$$A = c_1 V^{2/3} \text{ and} \quad (1)$$

$$B = c_2 V^{2/3}, \quad (2)$$

where A is the largest cross-sectional area of the debris flow, B is the total planimetric area of deposition of the debris flow, and c_1 and c_2 are proportionality coefficients (fig. 6). For lahars, Iverson and others (1998) found that c_1 = 0.05 and c_2 = 200 produced results that most closely matched the observed worldwide data. They also developed a GIS-based tool named LAHARZ that uses the equations (1) and (2) in combination with digital topographic data to predict the depositional area of a lahar (Schilling, 1998). The user must input the volume of sediment to be deposited, the topography across which the lahar will move in the form of a digital elevation model, and the point in the travel path where deposition begins; the model returns the boundary of the predicted area of deposition.

Recently, Griswold and Iverson (2008) extended the methodology of LAHARZ to include non-volcanic debris flows and rock avalanches. Specifically for debris flows, they found the best proportionality coefficients to be c_1 = 0.1 and c_2 = 20. Because they form in volcanic settings, lahars tend to have smaller particles than other debris flows, and volcanic ash in the matrix make lahars less viscous. Desert debris flows not associated with volcanic eruptions, in contrast, tend to have large particles and a matrix richer in clays, making them appear to have a higher relative viscosity. Therefore, the deposits from these debris flows tend to have larger cross-sectional areas and cover a smaller planimetric area than their volcanic counterparts.

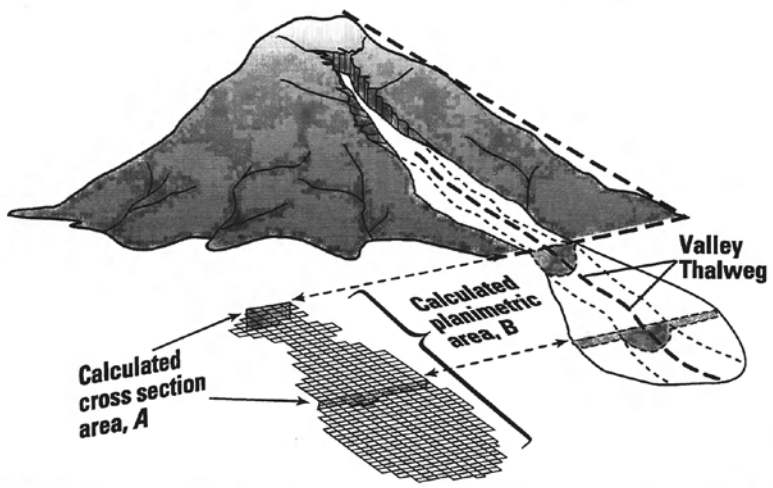

Figure 6. Cartoon illustrating the cross-sectional area (*A*) and planimetric area of deposition (*B*) used by the LAHARZ modeling tool to delineate areas of debris-flow deposition (adapted from Schilling, 1998).

Synoptic-Scale Meteorology of the Storm

Southeastern Arizona receives about half of its annual precipitation from July to September during the North American Monsoon (Adams and Comrie, 1997), when incursions of moist, subtropical air promote localized convective thunderstorms. The source of moisture varies from the Gulf of Mexico to the Pacific Ocean with an unknown contribution from the Gulf of California (Douglas, 1995) that varies seasonally and inter-annually. In Arizona, surges of moist air from the Gulf of California can enhance monsoonal activity (Douglas, 1995), and these impulses contribute to the formation of severe thunderstorms (McCollum and others, 1995). Precipitation in this region generally begins in early July

and extends through September. Normally, weak atmospheric steering mechanisms move relatively small (1-5 mi^2) thunderstorms into the Tucson basin.

During the last week of July 2006, an upper-level low-pressure system stalled over northwestern New Mexico, steering moisture-laden air into central and southern Arizona from the north (*http://www.hpc.ncep.noaa.gov/dailywxmap/index_20060727.html*, accessed June 1, 2008). Combined with a surge of humid, tropical air from the south, this large-scale circulation feature generated widespread, early-morning thunderstorms over southeastern Arizona during a 5-day period. Many of these storms were mesoscale convective systems of relatively broad spatial extent (Magirl and others, 2007). Mesoscale convective systems commonly occur during the summer months in Arizona (Hales, 1975; McCollum and others, 1995; Maddox and others, 1995) when high surface dew points, large moisture content throughout the atmospheric column, and weak to moderate vertical wind shear coincide (Maddox and others, 1979). Subtropical upper-level lows are believed to promote the coverage and intensity of mesoscale convective systems (Pytlak and others, 2005); sinking air within the upper-level low tends to suppress convection while instability tends to promote strong convective activity on the periphery of the low, particularly its west side. Atmospheric instability induced by desert mountain ranges in Arizona produces additional lifting and enhances precipitation potential.

Debris Flows and Floods in the Santa Catalina Mountains

Storm Dynamics on July 31

On July 31, heavy rainfall began shortly after midnight and lasted 6 to 8 hours. A strong mesoscale complex of thunderstorms developed in the Phoenix area in an atmospheric deformation zone that formed on the back side of the upper-level disturbance. High atmospheric-moisture content coupled with cooling aloft generated two mesoscale thunderstorms that moved southeast from the formation point near Phoenix into the Tucson basin. Simultaneously, a relatively strong, low-level southwesterly inflow jet (18-21 mi/h) developed with an orographic upslope component over the south face of the Santa Catalina Mountains. The presence of a strong near-surface jet of moist air impinging on a mountain front is known to increase the severity of storms traveling over complex terrain (Landel and others, 1999).

The first of the mesoscale thunderstorms had a cold cloud-top structure (-74°C) and passed through the region around 3:00 AM (MST). A second mesoscale thunderstorm with a warm cloud-top structure (-55°C) developed near dawn and persisted after 8:00 AM (MST). The low-level, southwesterly jet provided lifting and fed additional moisture directly into the southwest-trending canyons along the mountain range. This atmospheric combination sustained heavy rainfall for several hours in three increments in the southern Santa Catalina Mountains: (1) moderate intensity rainfall from 2-6 AM, (2) high intensity rainfall from 6-7 AM, and (3) a final burst of rainfall from 8-9 AM (Griffiths and others, in press). Storms occurred later in the morning at other sites in southeastern Arizona as the storms moved towards the southeast and dissipated, as discussed later in this report.

Rainfall Magnitude and Frequency

Point rainfall measurements were highly variable as the two convective thunderstorms swept across southern Santa Catalina Mountains on July 31. At six long-term ALERT rain gages maintained by Pima County, 6-hour rainfalls ranged from 0.65 in. at Green Mountain to 3.85 in. at Molino Canyon. Based on preliminary analyses using the NOAA statistics on rainfall magnitude and frequency, these 6-hour rainfalls had recurrence intervals of less than 1 year and 600 years, respectively (fig. 7). Griffiths and others (in press) collated data from 24 short-term rainfall gages operated by the University of

Arizona, and similarly report 6-hour rainfall ranging from 1.16 in. (RI <1 yr) near the mountain top (7,743 ft elevation) to the maximum recorded gage value of 5.03 in. (RI >500 yr) in the middle of lower Sabino Canyon (3,690 ft elevation). Record flooding from the Rincon Mountains, southeast of the Santa Catalina Mountains, suggests that rainfall was also high in this area, but there were no rainfall gages in this wilderness area.

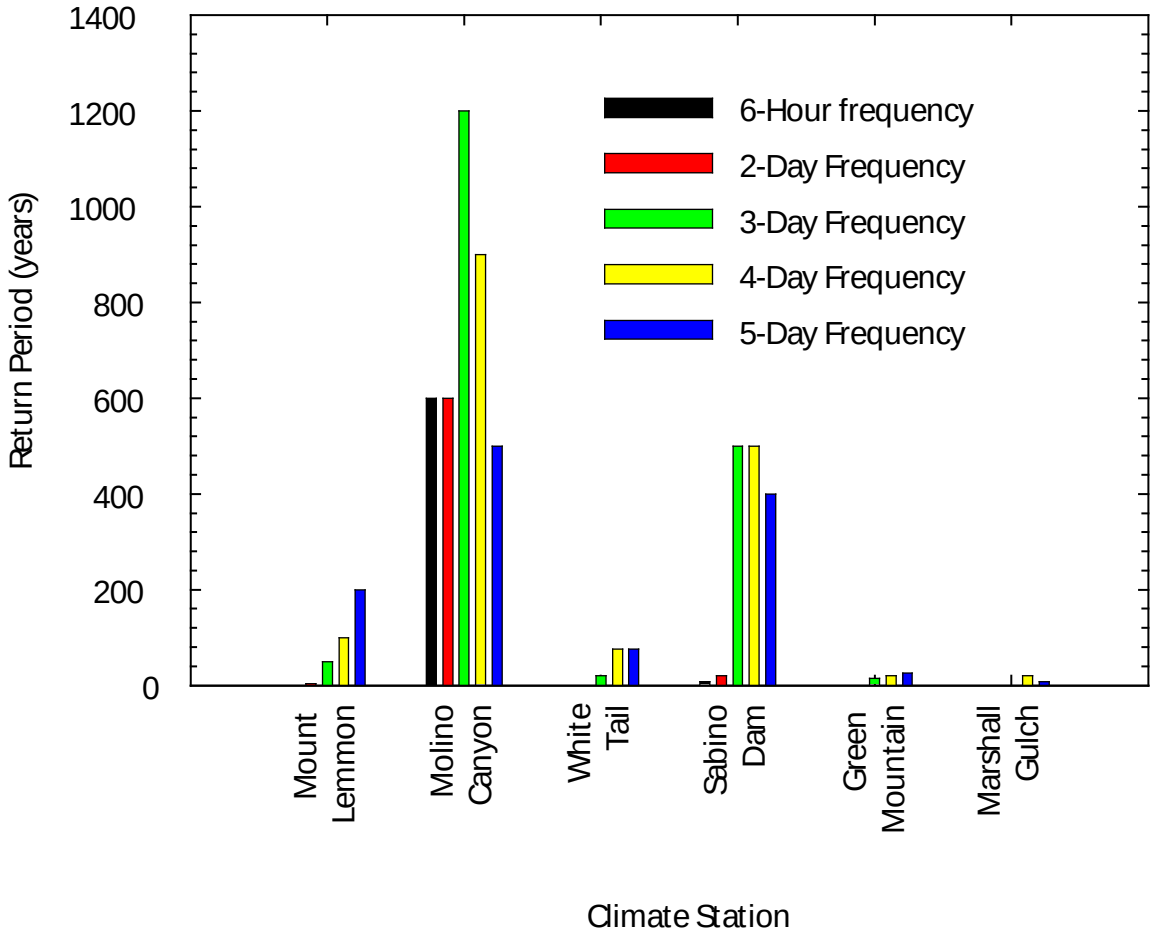

Figure 7. Rainfall frequency at selected Pima County ALERT rainfall gages in the southern Santa Catalina Mountains, southeastern Arizona (Michael Schaffner, National Weather Service, written commun., 2006).

Griffiths and others (in press) analyzed weather radar data, estimating mean rainfall over each of 754 grid cells (about 0.36 mi^2 each) over the southern Santa Catalina Mountains (figs. 8 and 9) to illustrate the spatial variability of rainfall. Total daily rainfall on July 31 was highest in a focused band along the northwest to southeast path of both storms, mostly in the middle elevations, ranging generally from 2 to 4 in. (fig. 8*A*). Most areas, however, including the higher elevations and mountain front, received only 1 to 2 in. of rain. At this spatial scale of averaging, the recurrence interval for general 1-day rainfall over the southern Santa Catalina Mountains is quite low, ranging from <1 year to 5 years (fig. 8*B*). Rainfall intensity in the early morning hours of July 31 had maximums of 0.85 in/h averaged over the radar study area, which is not an unusually high intensity for summer thunderstorms in

southeastern Arizona. Rainfall at six Pima County ALERT rainfall gages ranged from 0.31 to 1.42 in/h, which is similarly typical in terms of expected frequency of occurrence.

Rainfall becomes increasingly extreme, however, when totaled over multiple days. It rained daily over the southern Santa Catalina Mountains beginning on July 27 with the highest rainfall totals occurring on July 29 (Griffiths and others, in press). The 3-day rainfall total at the Molino Canyon gage was 8.30 in., a rainfall depth that has an estimated 1,200-year recurrence interval (fig. 7) (M. Schaffner, National Weather Service, written commun., 2006). Griffiths and others (in press) found that 4-day rainfall (July 28-31) averaged 6.6 in. (fig. 9*A*) with an average recurrence interval exceeding 50 years over all 754 radar cells (fig. 9*B*). The average recurrence interval exceeded 100 years, however, when averaged over radar cells that included one or more slope failures. Some individual cells had recurrence intervals of about 1,000 years, reflecting the high degree of rainfall variability within the storms and the extreme nature of the multiday storm at particular locations.

Streamflow Flooding

Sabino Creek

In Sabino Creek, late July runoff from each day's thunderstorm(s) drained rapidly from the 237 mi^2 watershed (fig. 4*A*). The hydrograph for the Sabino Creek near Tucson, Ariz., gaging station (09484000), showed that, other than increased antecedent moisture on hillslopes and in channel sediments, the July 29 flood had little effect on the July 30 flood, and the July 30 flood had little effect on the July 31 flood because flow in the channel lowered to near baseflow (160 ft^3/s) between events (fig. 4*A*). The peak discharges on July 29 and 30 were 9,400 and 11,000 ft^3/s, respectively.

The July 31 flood had four separate peaks, the highest having a peak discharge of 15,700 ft^3/s (fig. 4*A*). This flow represents the largest flood in the 75-year gaging record (1932-2006; table 1). The same day, other non-USGS gaging stations located higher in the watershed had much smaller peak discharges (Magirl and others, 2007), showing that rainfall during the July 31 storm was focused in the middle elevations of the watershed (Griffiths and others, in press). Excluding the peak discharge of July 31, 2006, from the analysis, the estimation of the recurrence interval for this flood is about 200 years.

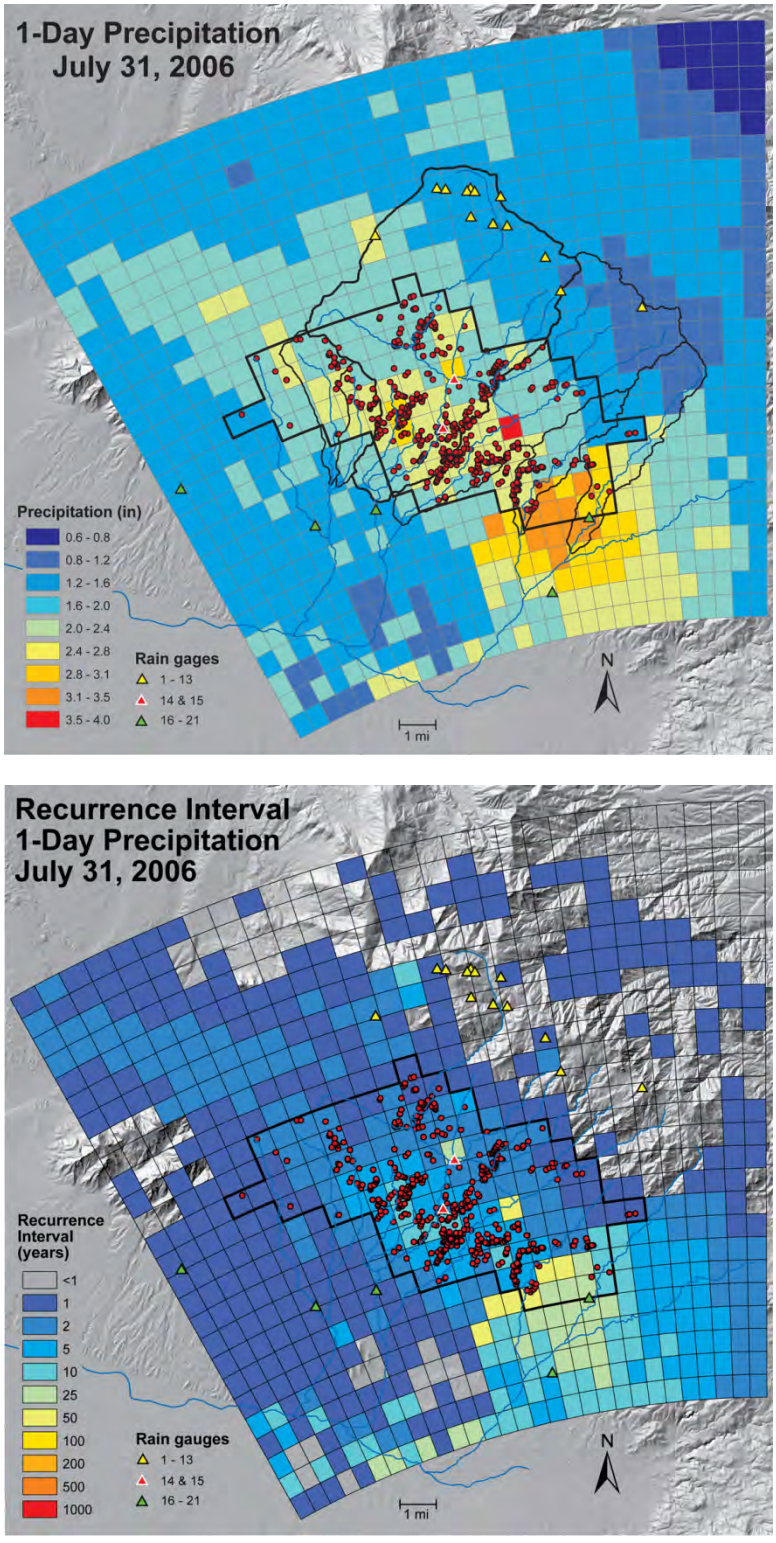

Figure 8. Maps of total 1-day rainfall derived from weather-radar data for July 31, 2006. Red circles indicate slope failures and the slope-failure zone is outlined in black. (From Griffiths and others, in press) A, one-day precipitation (P) in millimeters. *B*, Recurrence intervals (RI) for one-day precipitation in years.

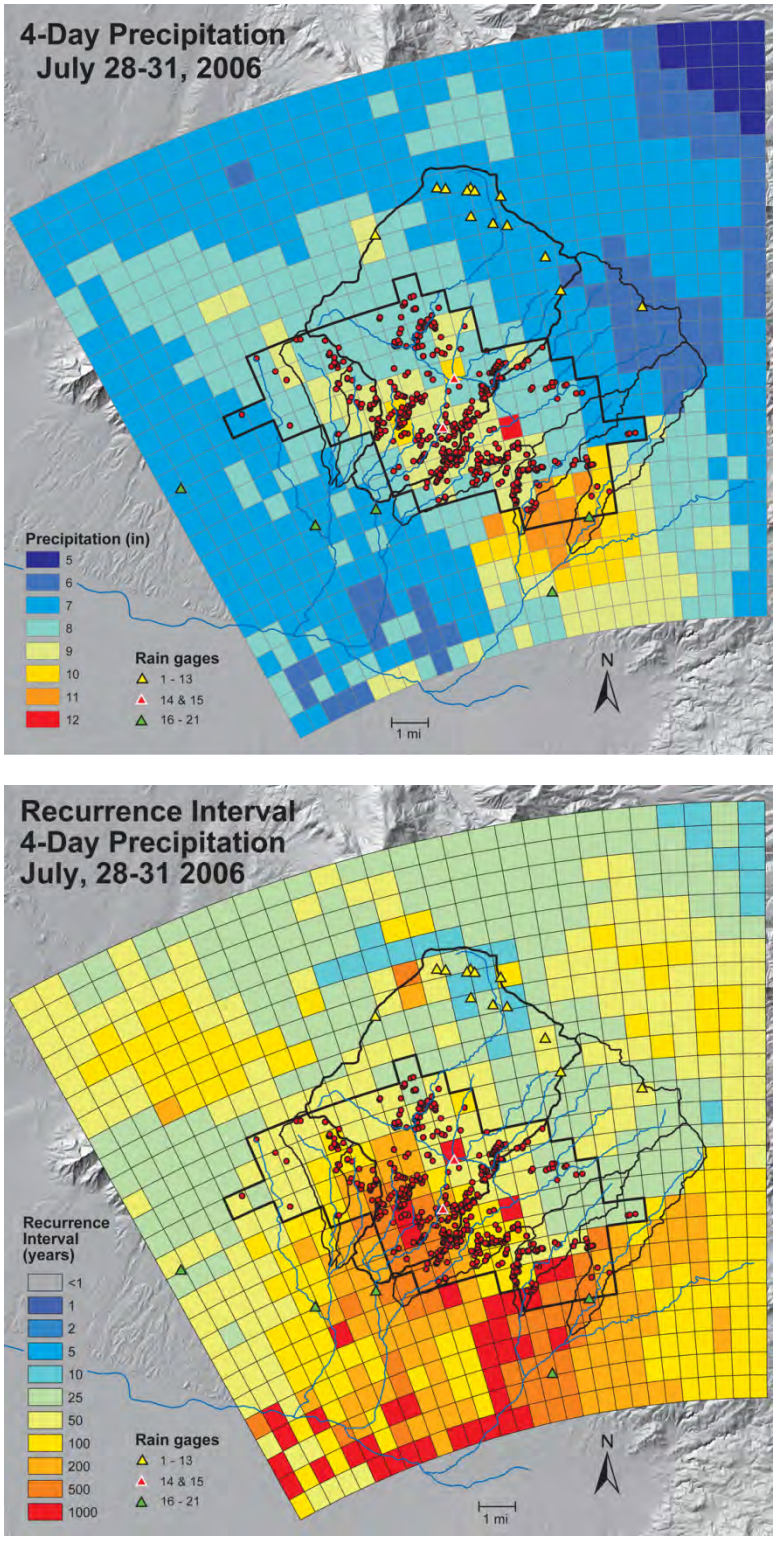

Figure 9. Maps of cumulative 4-day rainfall derived from weather radar data for the period of July 28-31, 2006. Red circles indicate slope failures and the slope-failure zone is outlined in black (From Griffiths and others, in press). *A*, 4-day precipitation (P) in millimeters. *B*, Recurrence intervals (RI) of 4-day precipitation in years.

Although the flood of July 31 is significant historically, the sequence of large floods on three consecutive days is exceptional. Analyzing the three floods with a stationary log-Pearson III distribution and annual flood data from 1932-2005, the floods of July 29-31 would have recurrence intervals of 40, 60, and about 200 years on consecutive days. This analysis, while violating the assumption of independence among these flood peaks, serves to underscore the condition of the watershed on July 31, which was approximately 92 percent saturated (Griffiths and others, in press). The total runoff volume for the 3-day period of July 29-31, 2006, was 8,900 acre-ft, which is second in the record for Sabino Creek behind the runoff of January 8, 1993, which had a peak discharge of 12,900 ft^3/s and a total runoff volume over 3 days of 10,000 acre-ft from a combination of rainfall and snowmelt. More telling in terms of the extreme nature of the flooding is that flood peaks previously exceeded 1,000 ft^3/s on consecutive days only once in the 75-year gaging record at Sabino Creek (September 13-14, 1964), and those floods had peak discharges of 1,310 and 1,210 ft^3/s, respectively.

Rillito Creek

Flooding along Rillito Creek was severe on July 31. Peaks of record were set at several gaging stations, notably at five stations with record lengths longer than 23 years (table 1). Most of the runoff was generated from the western Rincon Mountains (Rincon Creek watershed, draining into Pantano Wash) and the southern Santa Catalina Mountains (Tanque Verde Creek, merging with Pantano Wash to form Rillito Creek). The peak discharge for the July 31, 2006, flood in Rillito Creek, measured at the Rillito Creek at Dodge Boulevard near Tucson, AZ (09485700), was 38,700 ft^3/s. Downstream from the confluence of Rillito Creek and the Santa Cruz River, the gaging station Santa Cruz River at Cortaro Road near Tucson, AZ (09486500), had a peak discharge of 40,900 ft^3/s (2nd highest flood on record). Upstream from the confluence, the gaging station Santa Cruz River at Tucson (09482500) had a rather ordinary peak discharge of 7,200 ft^3/s.

Estimation of flood frequency for Rillito Creek is somewhat problematic because of changes in the location of the gaging station. From 1915-1981, the gaging station Rillito Creek near Tucson, AZ (09486000) was operated from the bridge at 1st Avenue, 3.36 mi downstream from Dodge Boulevard. The discharge for the 1983 flood was indirectly estimated for this gaging station (Roeske and others, 1989). From 1988-2006, streamflow was measured at two gaging stations, Rillito Creek at La Cholla Blvd near Tucson, AZ (09486055), and Rillito Creek at Dodge Boulevard. We chose to combine the original record (09486000) with the new record from Dodge Boulevard, which is closer to 1st Avenue, to create a combined record with a total length of 86 years, with gaps in 1982 and 1984-87 (fig. 3*C*). There are no significant tributaries between these two gaging stations and infiltration losses during floods can be assumed to have negligible effects on peak discharges.

Peak discharges of floods in October 1983 and January 1993 were 29,700 and 24,100 ft^3/s, respectively, which makes the 2006 flood, with its peak discharge of 38,700 ft^3/s, the largest in the combined record. Using the combined data from 1915-2005 and the 1983 peak discharge in the analyses, the recurrence interval for the 2006 flood on Rillito Creek is greater than 500 years.

Slope Failures and Debris Flows

The southern flanks of the Santa Catalina Mountains consist of many near-vertical bedrock outcrops of the Wilderness Granite (Force, 1997), and steep talus slopes below these outcrops are covered by relatively thin colluvium. The slope failures from July 2006 occurred between elevations of 4,000 and 6,000 ft (fig. 2), mostly on steep colluvial slopes (figs. 10 and 11). Sabino Canyon, a heavily used recreation area administered by the U.S. Forest Service (fig. 2), was the epicenter of mass wasting where at least 13 debris flows removed structures, destroyed the roadway in multiple locations, and closed public access for months (figs. 10-14). Within Sabino Canyon, most debris flows traveled short

distances down chutes and stopped upon reaching either the road that traverses the canyon or Sabino Creek (fig. 13). Numerous large boulders were entrained, adding mass to debris flows and compounding damage to roads, bridges, and structures in Sabino Canyon.

The debris flow informally known as Ocho Grande (fig. 13) was one of the largest of these debris flows. Repeat photography shows that a previous event, smaller in size (P. Pearthree, Arizona Geological Survey, written commun., 2006), occurred in this small drainage in 2003 (fig. 15), but the July 2006 debris flow was more visible in the repeat imagery. Longer-record repeat photography from Sabino Canyon suggests that a spate of debris flows of this magnitude had not occurred during the 20th century (fig. 16). Photography from Sabino Creek away from the junctures with debris-flow tributaries shows flood damage but little change that can be attributed to the debris flows (figs. 17 and 18). At least one set of photographs (fig. 17) suggests the possibility of significant coarse-grained aggradation in the channel before 2006, but it is unknown if this aggradation resulted from debris-flow activity or flooding before the start of the gaging record in 1933.

Figure 10. (August 18, 2006) This aerial photograph shows numerous slope failures, debris-flow deposits, and the channel of Sabino Creek in Sabino Canyon Recreation Area. The prominent slope failure at lower center is the same one shown on the cover of this report (R.H. Webb).

Figure 11. (August 8, 2006) Slope failures and debris-flow deposits along Sabino Creek in Sabino Canyon Recreation Area. A large chute that passed a debris flow, with its multiple contributing initiation points, appears in the center of the view. A total of 56 slope failures occurred in the Sabino Canyon Recreation Area, which encompasses most of lower Sabino Canyon (C.S. Magirl).

Figure 12. (August 11, 2006) Debris-flow deposits on the Sabino Canyon road in Sabino Canyon Recreation Area downstream from bridge 9. Debris-flow matrix, mostly fine gravel to clay-sized particles, appears in the right foreground (P.G. Griffiths).

Figure 13. (August 8, 2006) The July 2006 debris flow, informally named “Ocho Grande,” covered and damaged the Sabino Canyon Road in Sabino Canyon Recreation Area. The debris flow filled the two culverts with coarse sediment and flowed into Sabino Creek, which flows from left to right in this view. Note the person standing on what is left of the roadway in the midground for scale. This debris flow had a superelevation stage of more than 20 ft on the right side of this view. Cosmogenic ^{10}Be dates obtained from the two large boulders on the left side of the channel (channel right) indicated that these boulders most likely were deposited during the latest Pleistocene; see appendix 1 for details and Youberg and others (2008) for full results (C.S. Magirl).

Figure 14. (August 18, 2006) This photograph of the eastern wall of Sabino Canyon shows the large debris flows of Ocho Grande (right center) and the debris flow that deposited coarse sediment over tram stop 9 (center) (R.H. Webb).

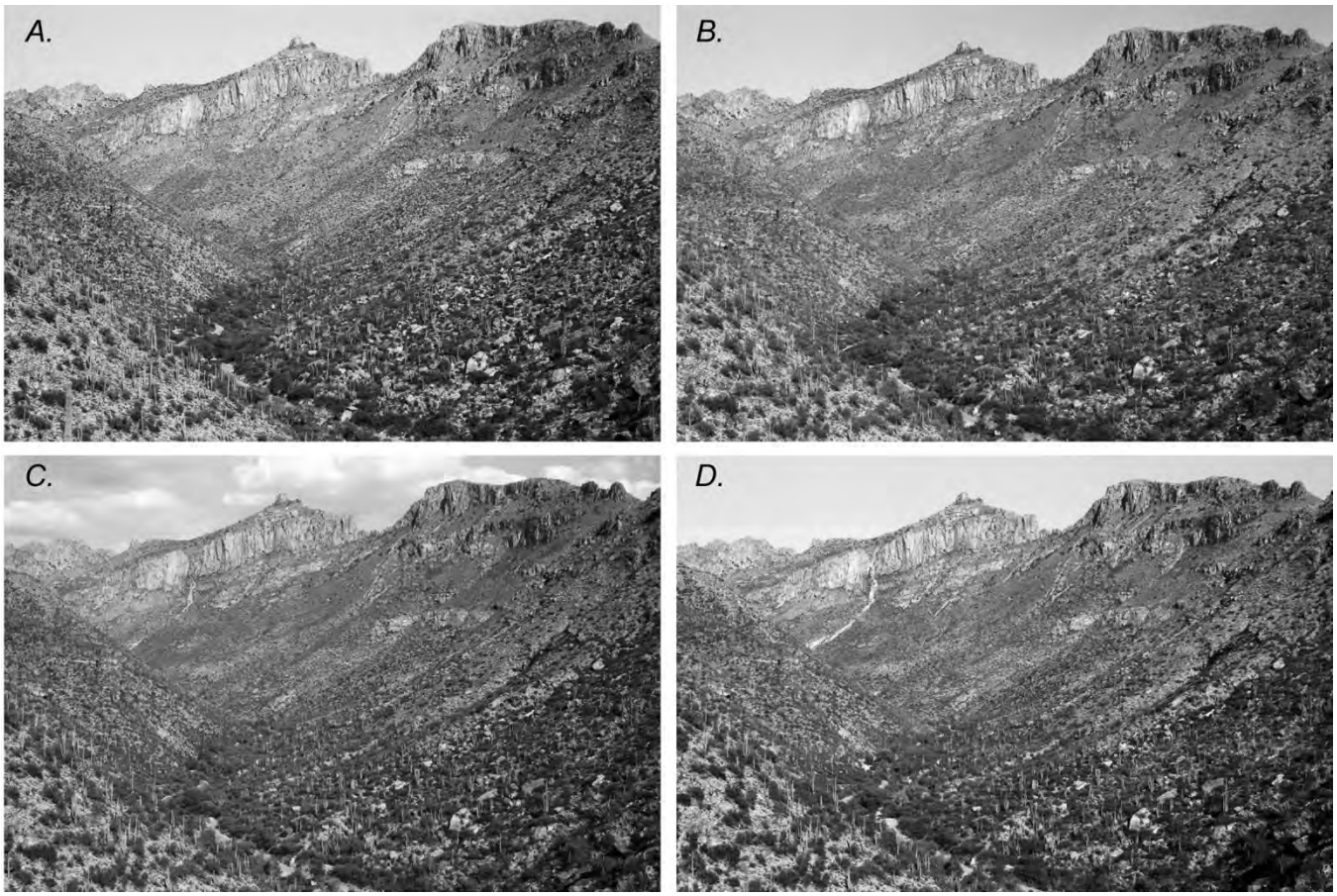

Figure 15. Repeat photographs of Sabino Canyon Recreation Area. *A*, (October 10, 1982) This photograph looks northeast into upper Sabino Canyon from a slope above the first bridge across Sabino Creek. Thimble Peak is visible on the horizon at center; the dominant vegetation along the slopes includes saguaro (*Carnegia gigantea*), foothill paloverde (*Cercidium microphyllum*), and mesquite (*Prosopis* sp.) (D.W. Lazaroff, PX 10-8A). *B*, (October 9, 2002) In 1995, the Sabino Fire ignited near the bottom center of view, spreading upslope to the right, then up canyon, stopping short of Thimble Peak (D.W. Lazaroff, PX15-11). *C*, (October 16, 2003) The Aspen Fire burned along the ridge top near Thimble Peak in the early summer of 2003. A small slope failure that can be seen along the cliff near the base of Thimble Peak occurred in an unnamed tributary during that year's summer monsoon (D.W. Lazaroff, PX 22-14). *D*, (October 10, 2006) On July 31, 2006, the slope failure informally named "Ocho Grande" was considerably larger than the slope failure that occurred in 2003 (D.W. Lazaroff, PX 24-16, Stake 4877).

Figure 16. Repeat photographs of Sabino Canyon Recreation Area. *A*, (ca. 1909) This image, from a souvenir view book of Tucson-area photographs, shows an upstream view of Sabino Canyon with Mount Lemmon in the distance. The trail was the main canyon access; the road had not been built at this time. The dominant vegetation includes saguaro (*Carnegia gigantea*), ocotillo (*Fouquieria splendens*), catclaw acacia (*Acacia greggii*), and babybonnet (*Coursetia glandulosa*) (R. Rasmessen, courtesy of James Klein). *B*, (April 3, 1990) This approximate match, taken nearly 80 years after the original was made, has a smaller field of view than the original. The trail, now known as the Historic Sabino Trail, fell into disuse in 1912 after construction of the Phoneline Trail, which is upslope to the right. The density of the vegetation has increased, particularly the cottonwoods (*Populus fremontii*) that line Sabino Creek on the left side of the view (D.W. Lazaroff, 523-20, courtesy of the photographer). *C*, (November 21, 2006) In July 2006, a debris flow bisected the foreground of the view, scouring vegetation and largely burying the large boulder visible in the lower right. Debris-flow transport zones are also visible at left midground and in the distance at right center (D.E. Boyer, Stake 4958).

Figure 17. Repeat photographs of the channel of Sabino Creek downstream from the second bridge in Sabino Canyon Recreation Area. *A*, (February 1901) Samuel J. Holsinger shot some of the earliest known photographs of Sabino Canyon, including this image just downstream from where the second bridge is now located. The trees are mostly leafless (S.J. Holsinger, courtesy of James Klein). *B*, (September 26, 2003) Views *A* and *B* originally appeared in Webb and others (2007b, p. 282). In the 102 years since the original image was taken, the channel has changed considerably, and none of the original boulders can be recognized. The dominant trees are sycamore (*Platanus wrightii*) and Bonpland willow (*Salix bonplandiana*), along with some cottonwood (*Populus fremontii*) and coyote willow (*Salix exigua*). Non-native giant reed (*Arundo donax*) is also present. Driftwood suggests recent flood occurrence, and the sediments are laden with ash from the Aspen Fire (R.M. Turner). *C*, (September 1, 2006) Surprisingly little has changed in the view between 2003 and 2006 in spite of the debris flows upstream in Sabino Canyon and the record streamflow flood. Most of the boulders visible in 2003 are still in the same positions, although some have shifted slightly. The sycamores in the midground survived the recent flood, and the giant reeds in the foreground have grown (R.H. Webb, Stake 4693).

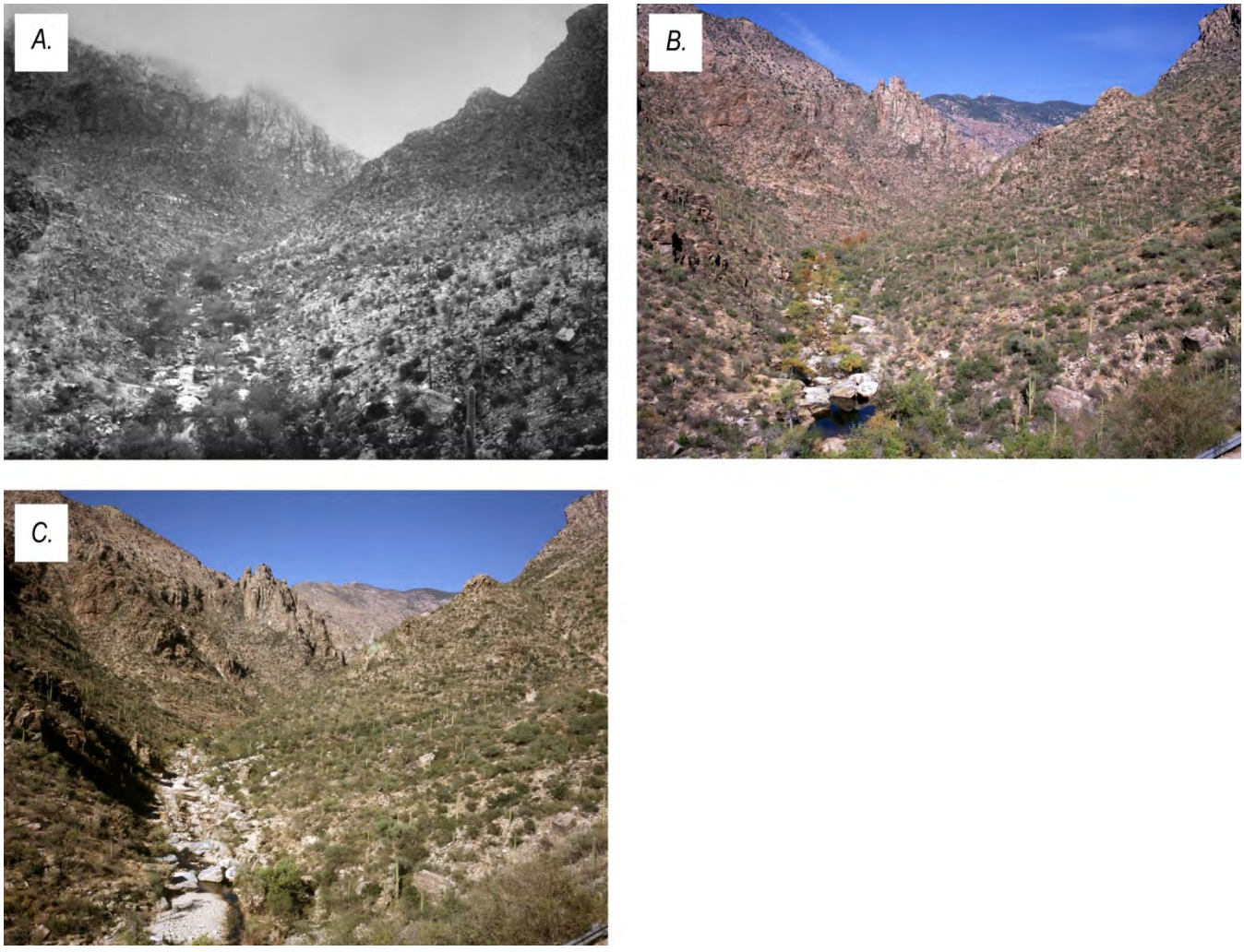

Figure 18. Upstream views of Sabino Creek near the end of the Sabino Road in Sabino Canyon Recreation Area. *A*, (March 1902) This view, one of the earliest photographs of upper Sabino Canyon, looks almost due north from a point that is now between tram stops eight and nine. The channel is thickly lined with vegetation, and many small pools are present. The background mountains are not completely visible, due in part to the poor quality of the photograph (D. Griffiths, 83-FB-902, courtesy of the National Archives). *B*, (November 19, 1998) Many of the large boulders in the channel appear to be in the same locations 96 years after the original image was taken, although the sediments have shifted. Most of the channel vegetation appears to have changed, and mountains clearly appear in the background (D. Oldershaw, Stake 3803). *C*, (November 21, 2006) This image was made eight years after the previous match and four months after the debris flows of July 31, 2006. The channel vegetation has been freshly scoured. Many of the large boulders are still visible in the same locations, but there has been considerable sediment deposition, filling in some of the pools visible in the 1998 view. Some slope failures are visible in the upper right corner of the view (R.H. Webb, Stake 3803).

Figure 19. (September 1, 2006) This photograph shows the snout of a debris flow that stopped in the channel of Rattlesnake Creek during the floods of July 31, 2006. This snout is several miles upstream from the confluence of Rattlesnake and Sabino Creeks, and the large boulders are typical of the largest particles transported during debris flows in the southern Santa Catalina Mountains. Most of these boulders likely were transported from debris-flow initiation zones, although some may have been entrained from the bed of Rattlesnake Creek (C.S. Magirl).

In contrast to the pattern in Sabino Canyon, slope failures in Rattlesnake Canyon (fig. 2) coalesced into a large debris flow (fig. 19). Although smaller debris flows can be traced to their initiation points in individual slope failures, the larger combined debris flow has an indefinite start point but traveled at least 2.4 mi to Sabino Creek from the most downstream slope failures. This debris flow filled a box culvert and then overtopped and destroyed the Sabino Road; farther downstream, it destroyed a pedestrian bridge built in the 1930s by the Civilian Conservation Corps (fig. 20). The large flood in Sabino Creek quickly diluted the incoming Rattlesnake debris flow and prevented movement further downstream, but local deposition in the channel was substantial, especially downstream from the juncture with Rattlesnake Canyon (fig. 20*D*).

The net result of debris flows and streamflow floods in Sabino Creek is that as much as 15-20 ft of deposition occurred within Sabino Creek from Rattlesnake Canyon to Sabino Dam (figs. 21 and 22). Because little sediment deposition occurred upstream from Rattlesnake Canyon (fig. 18), we believe that the Rattlesnake Canyon debris flow, its runout facies, and reworking by the record flood in Sabino Creek contributed most of this sediment. The snout of the Rattlesnake Canyon debris flow was reworked by the record flood in Sabino Creek but can still be identified on aerial photography (fig. 20D). The debris flow also left a significant volume of sand and gravel in its wake within Rattlesnake Creek, causing aggradation in the bed and on channel margins (fig. 23; also see *http://wwwpaztcn.wr.usgs.gov/Santa_Catalina_Debris_Flows.pdf*, slides 48-51, accessed June 3, 2008).

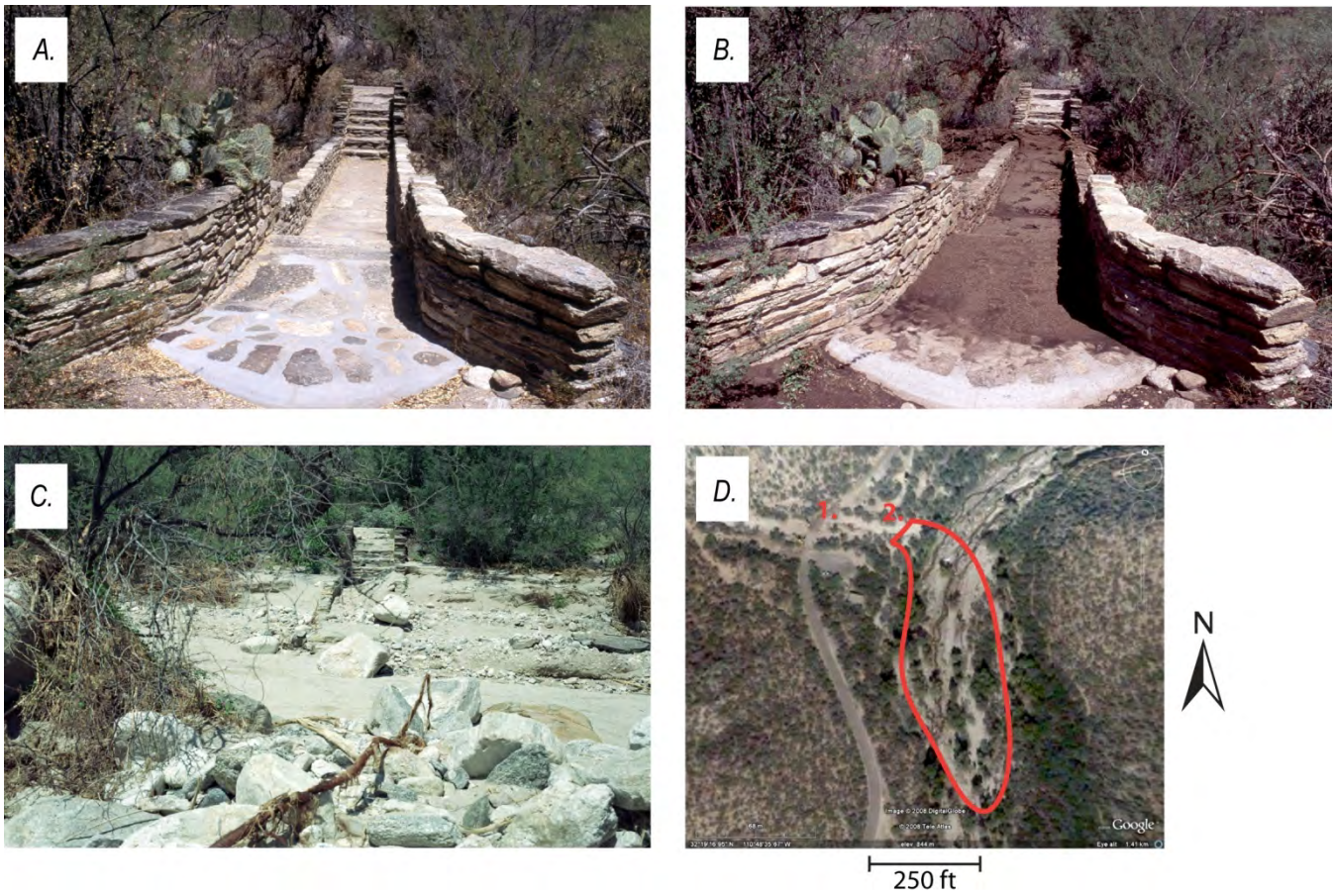

Figure 20. Photographs of a Civilian Conservation Corps (CCC) footbridge across Rattlesnake Creek, Sabino Canyon Recreation Area. *A*, (July 9, 2003) In 1934 or 1935, the CCC constructed this footbridge across Rattlesnake Creek just above its confluence with Sabino Canyon. David Lazaroff established this camera station at the southern end of the bridge in order to document conditions around the time of the Aspen Fire (photograph courtesy of D.W. Lazaroff, PR817-27). *B*, (August 23, 2003) On August 23, 2003, the largest flood of the summer occurred in Sabino Creek, with a smaller flood occurring along Rattlesnake Creek. Water from Sabino Creek backed up into Rattlesnake Creek, overtopping the footbridge and depositing ash-laden sediment (D.W. Lazaroff, PR825-10). *C*, (September 1, 2006) The 2006 debris flow down Rattlesnake Canyon destroyed the footbridge, leaving only the stone steps on the north end. A debris-flow levee obscures what remains of the bridge in the foreground (R.M. Turner, Stake 3268). *D*, (2008) The debris flow from Rattlesnake Canyon cut through the Sabino Canyon Road (1), destroyed the CCC Bridge (2), turned downstream on Sabino Creek, then flowed about 100 yards before stopping. The red outline is the approximate perimeter of the debris-flow snout (Google Earth Image).

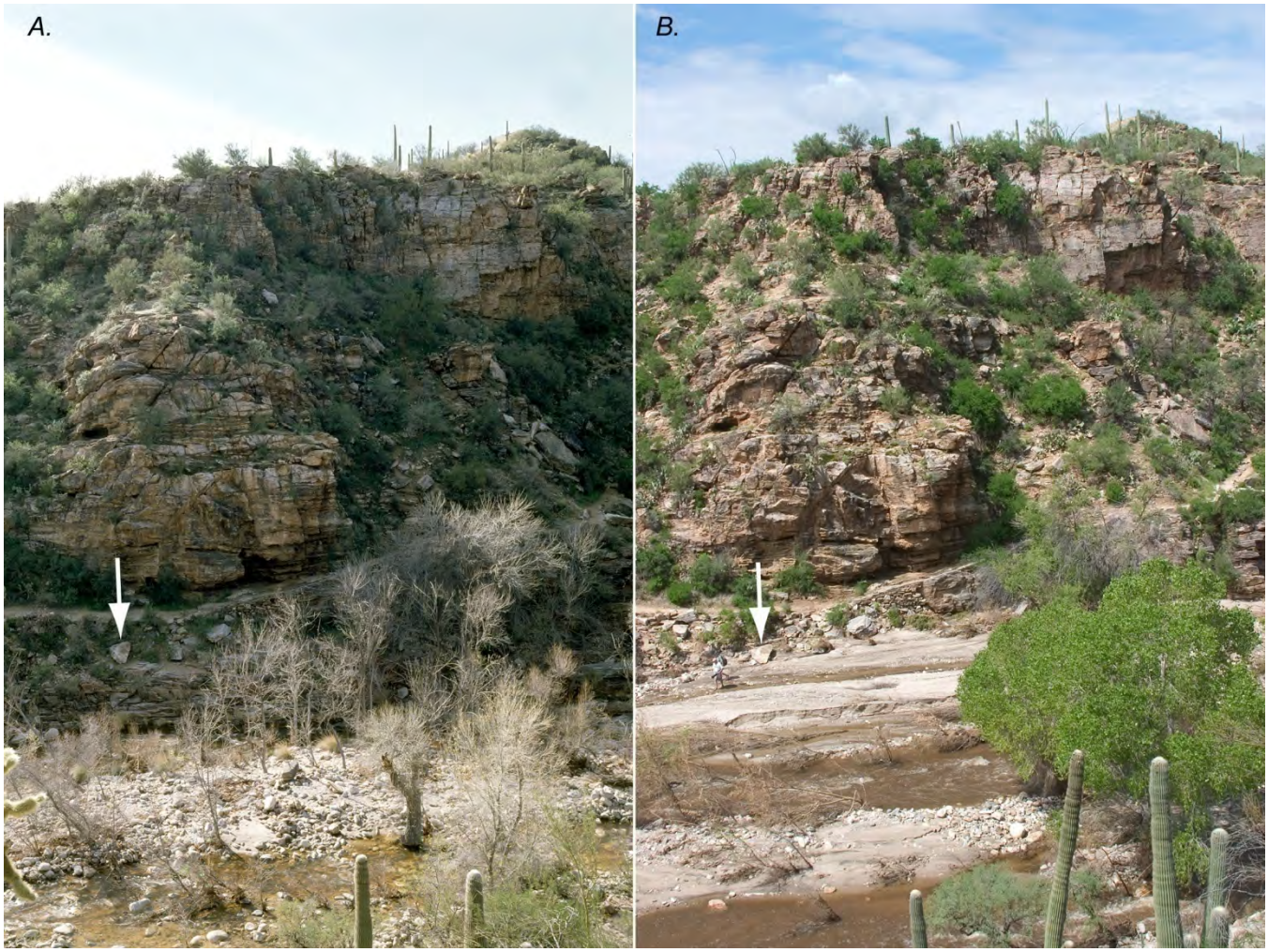

Figure 21. Repeat photographs of Sabino Creek upstream from Sabino Lake and downstream from Sabino Canyon. *A*, (December 28, 1994) This view across Sabino Creek shows the Bluff Trail along Sabino Canyon at a point approximately 1,000 ft upstream from Sabino Dam; the view is southwest. Note the triangular-shaped rock below the trail at left center (white arrow). The trees in the channel are leafless in the winter season but are mostly cottonwood (*Populus fremontii*). This is the third match of a photograph originally taken by George Roskruge in 1890; little channel change is evident in the first 104 years of this photographic record other than changes in the riparian vegetation (D.P. Oldershaw, Stake 243). *B*, (August 15, 2006) The 2006 debris flow from Rattlesnake Canyon deposited a significant amount of coarse-grained sediment in this reach of Sabino Creek. The tip of the triangular-shaped boulder (white arrow) is at about the current streambed elevation in this view, and we estimated that approximately 20 ft of sediment have been deposited in the creek bed. Much of the channel vegetation has been scoured or buried, although one cottonwood has leafed out at lower right (D.E. Boyer, Stake 243).

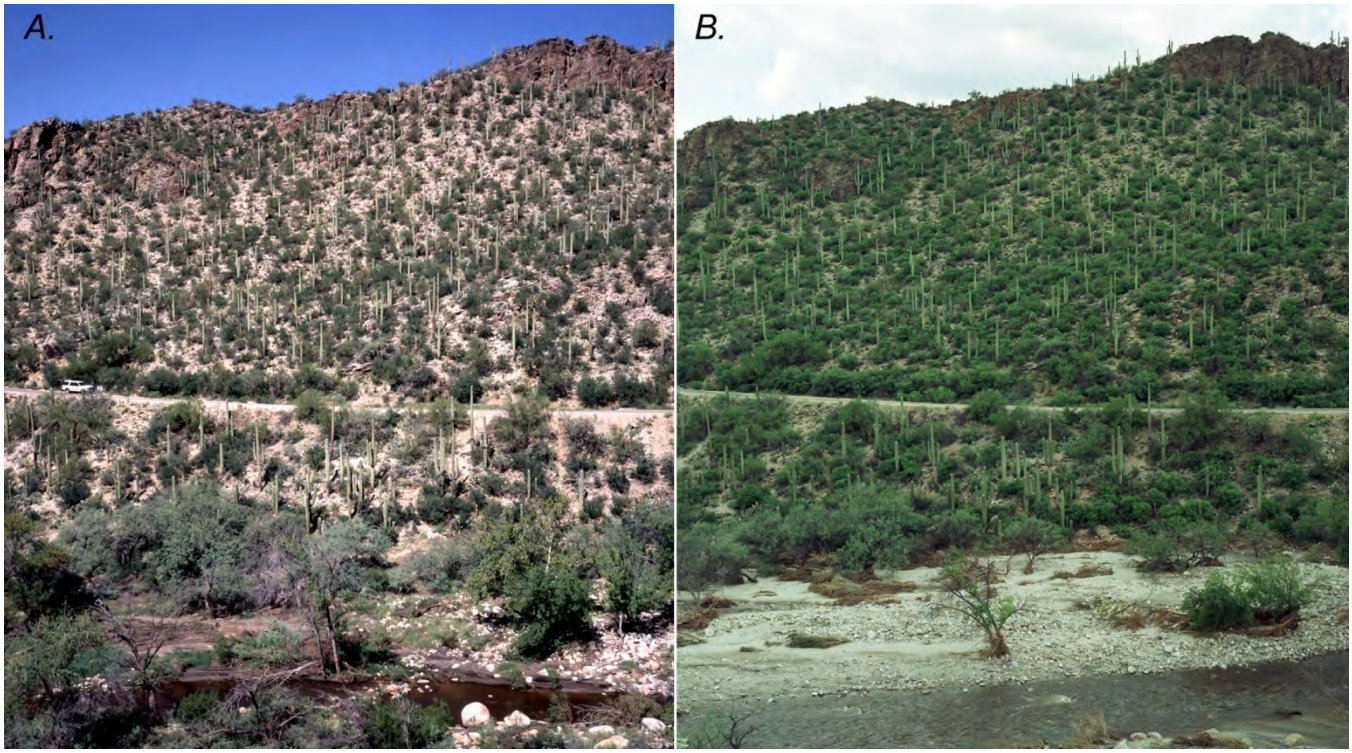

Figure 22. Repeat photographs of Sabino Creek downstream from Rattlesnake Canyon in Sabino Canyon Recreation Area. *A*, (September 26, 2003) This northwesterly view of Sabino Canyon was taken from a point about half a mile upstream of the lower dam and near where the Sabino Canyon Road first enters Sabino Canyon. Sabino Creek flows from right to left, and Rattlesnake Canyon enters Sabino Creek less than a half mile upstream. The trees in and near the channel, which include velvet ash (*Fraxinus velutina*) and mesquite (*Prosopis* sp.), show moderate damage from floods in the summer of 2003 following the Aspen Fire. Dark-colored sediments on the floodplain at bottom left contain a large quantity of ash. This view is part of a series of photographs originally taken in 1890 of Sabino Creek (Turner and others, 2003, p. 188-191), although this view has not been previously published (R.H. Webb, Stake 186G). *B*, (August 15, 2006) Sediments carried during the July 31, 2006, flood, which included coarse-grained sediment reworked from the snout of the Rattlesnake Canyon debris-flow deposit just upstream, deposited considerable amounts of sediment in the channel of Sabino Creek. Most of the channel vegetation has been scoured out and/or buried. Few reliable markers can be used to estimate the magnitude of deposition, but the appearance of the trees in the foreground suggests perhaps 5-20 feet of deposition (R.M. Turner, Stake 186G).

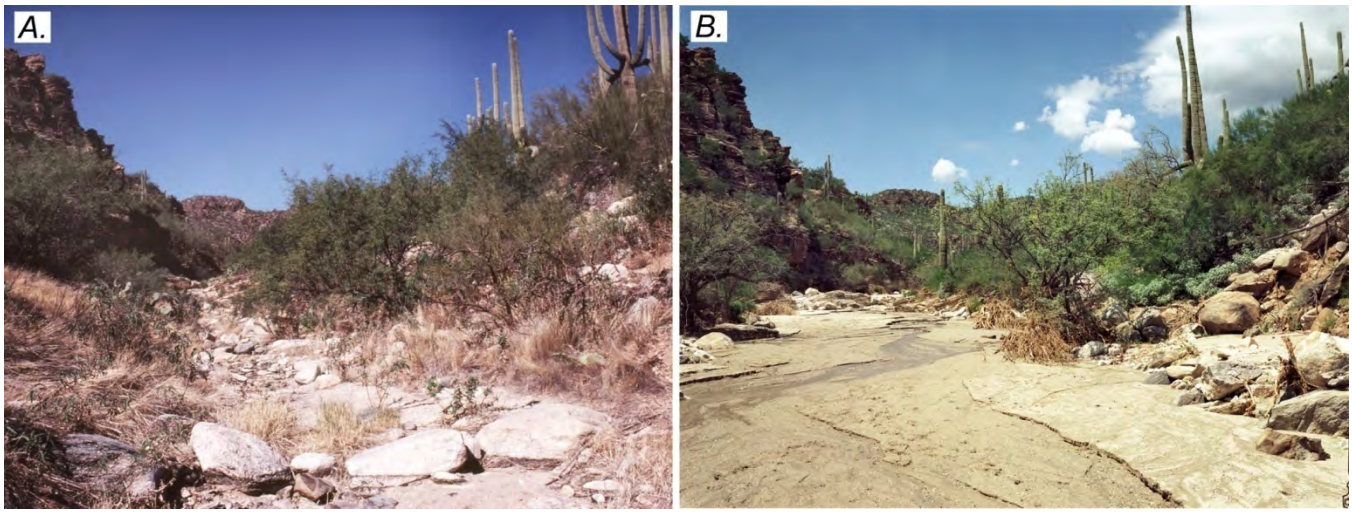

Figure 23. Repeat photographs near the mouth of Rattlesnake Creek. *A*, (October 28, 1980) This view is west northwest up Rattlesnake Canyon, about 100 yards upstream from the Sabino Canyon road bridge. Mesquites (*Prosopis* sp.) line the channel, and many saguaros (*Carnegia gigantea*) are visible in the view (D.W. Lazaroff, KR-07). *B*, (September 1, 2006) The creek bed is filled with sediment from the debris flow of July 31, 2006, which destroyed the bridge behind the camera station. The boulders prominent in the earlier view are now either gone or covered with fine-grained sediment deposited in the recession of the flood. Although debris-flow levees are not visible here, they are present upstream and downstream from this site. Many of the mesquites in the earlier view are still present, albeit reduced in size by flood damage. Some of the saguaros present 26 years earlier have died off, whereas others are now visible through the shorter and less-dense mesquites. The camera station is not precise owing to the changes in the channel bed (R.H. Webb, Stake 4913).

Figure 24. (August 18, 2006) Aerial photograph showing numerous slope failures on the west slope (east-facing slope) of a tributary of Soldier Creek. A total of 56 slope failures were mapped in the Soldier Creek watershed. This slope appears in the repeat photography pair shown in Figure 25 (R.H. Webb).

In four other canyons (Bird, Bear, "Gibbon", and Soldier), all with smaller drainage areas and no antecedent floods, debris flows coalesced in the main channels and traveled several miles towards the mountain front. Two of these debris flows exited the mountain front and deposited coarse-grained sediment on or near the apices of alluvial fans. For example, a debris flow exited the mountain front from an unnamed drainage below Gibbon Mountain; this debris flow may have traveled 0.7 mi into a residential neighborhood near the intersection of Snyder and Houghton Roads and appears on maps in Youberg and others (2008) as a "latest Holocene to modern" deposit.

In Soldier Canyon, 4 mi east of Sabino Canyon (fig. 2), 56 failures occurred during the July 31 storm (fig. 24). Repeat photography in the headwaters of this canyon suggests that slope failures in at least part of the watershed heavily affected by this storm are unprecedented historically (fig. 25). Sediment and water from these failures and other runoff within the watershed coalesced into at least one pulse of debris flow that scoured vegetation but otherwise caused little channel change upstream from the Catalina Highway (fig. 26). These views also indicate that this reach was a zone of transport; the zone of deposition started downstream, probably below the culvert on the Catalina Highway. Near the snout of this debris flow, between a private road and the Mount Lemmon Short Road (fig. 27), there is no indication of debris-flow deposition between 1915 and 2006, underscoring the absence of a historical precedence for this event.

Figure 25. Repeat photographs of the headwaters of Soldier Canyon. *A*, (September 1910) This westerly view of Soldier Canyon in the Santa Catalina Mountains was taken about one-half mile south of the Gordon Hirabayashi Picnic Area along a section of trail that has since been rerouted. A portion of the Tucson basin, largely barren of human development in 1910, is visible at left center (D.T. MacDougal or F. Shreve, B3-27). *B*, (August 29, 2007) At least 18 slope failures (red arrows) that occurred during the July 2006 floods are visible on the slopes opposite the canyon from the camera station (also see fig. 12). The amount of recovery from the 2003 Aspen Fire is visible in part of this view by comparing the left (unburned) and right (burned) halves of the foreground. Numerous structures and roads are now present in the Tucson basin in the left distance (D.E. Boyer, Stake 3150).

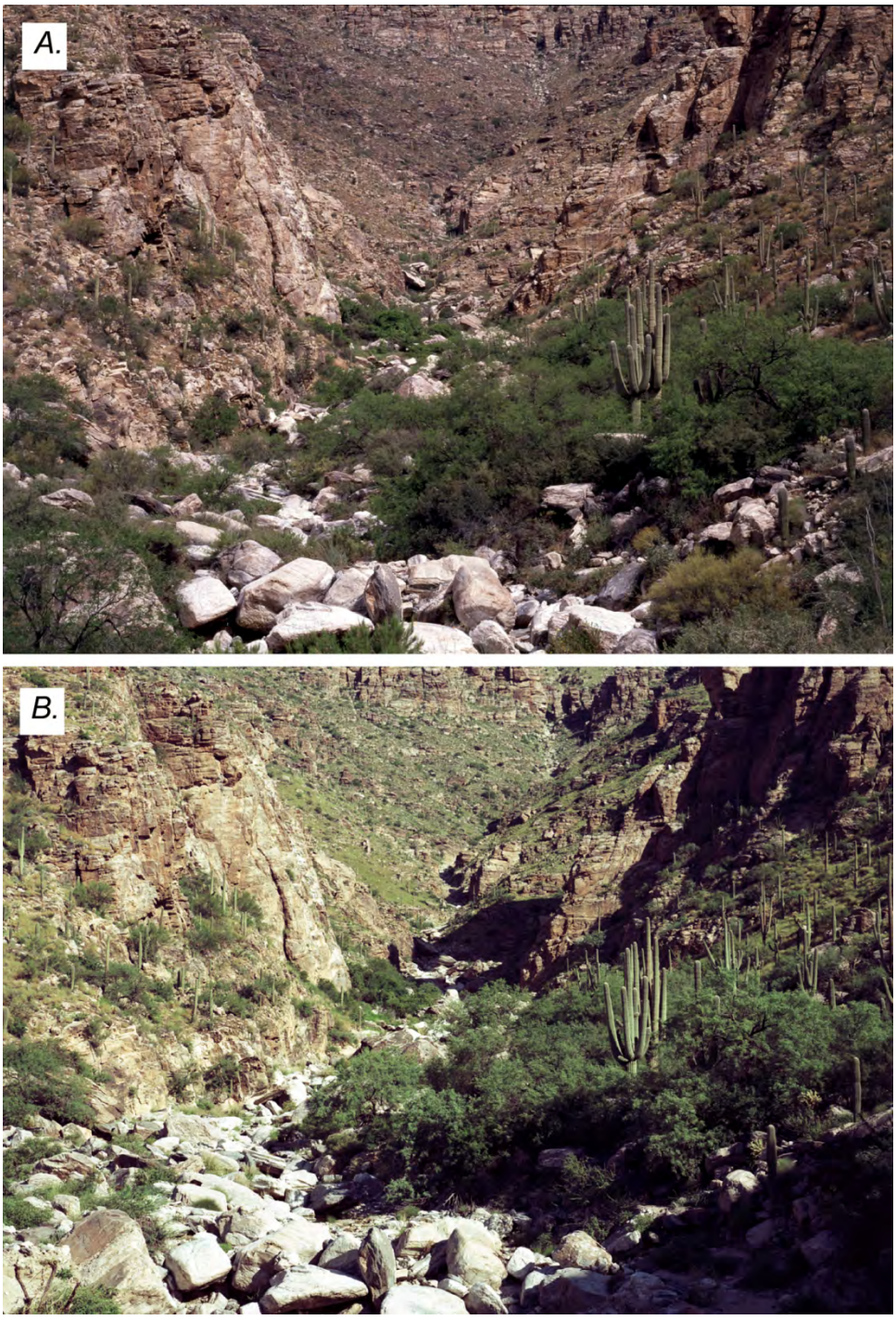

Figure 26. Repeat photographs of Soldier Canyon. *A*, (April 27, 1995) This view looks northeast up Soldier Canyon from a hairpin turn along the Catalina Highway, which is behind the photographer (D.W. Lazaroff, courtesy of the photographer). *B*, (August 29, 2007) The debris flow and subsequent floods of July 31, 2006, in Soldier Creek scoured vegetation in the channel, but the large boulders are mostly in the same locations as they were 12 years earlier (R.M. Turner, Stake 4962).

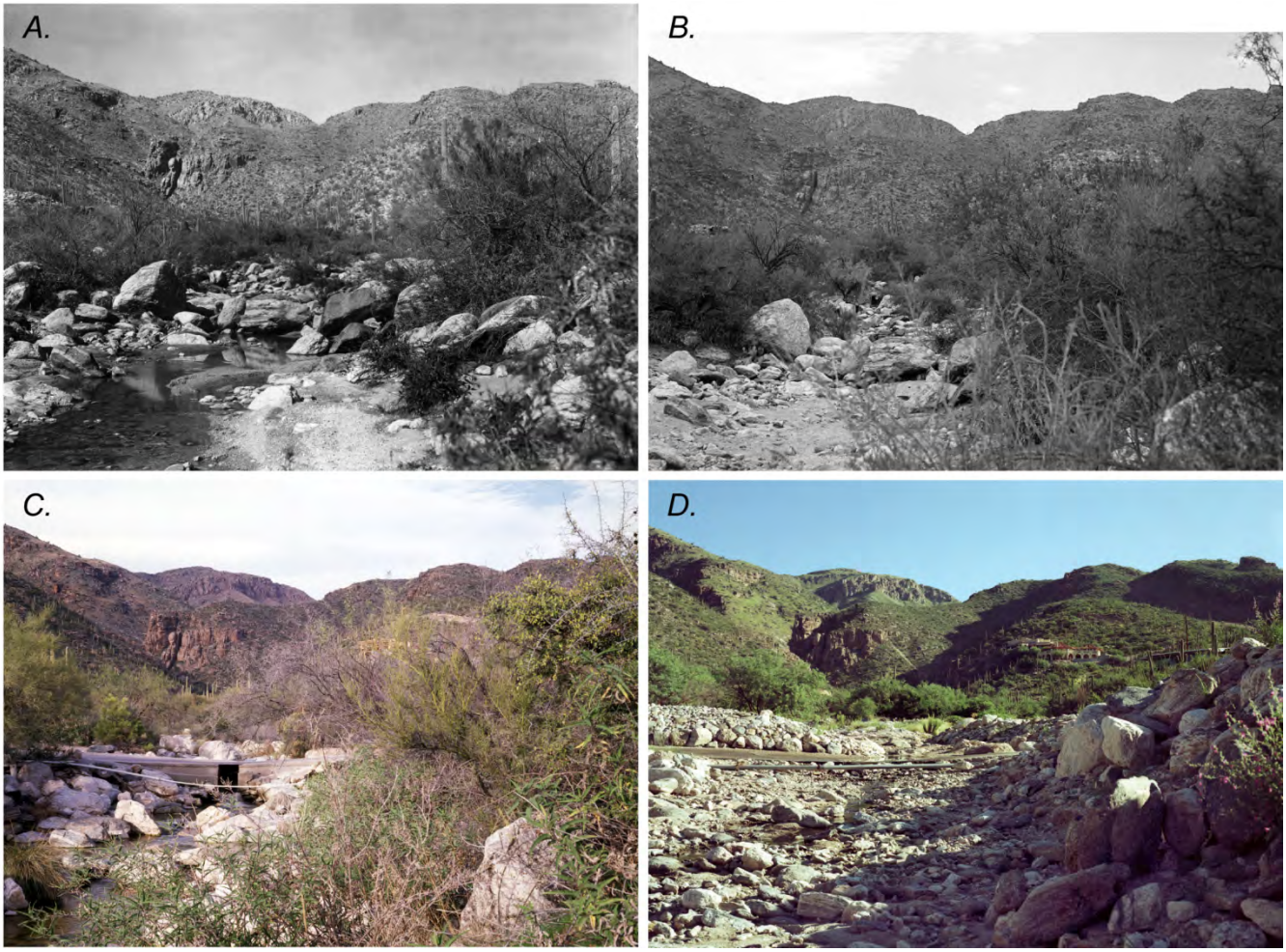

Figure 27. Repeat photographs of Soldier Creek upstream from the Mount Lemmon Short Road. *A*, (March 28, 1915) This view looks northeast up Soldier Canyon at the base of the Santa Catalina Mountains near Tucson. The immediate area was then largely undeveloped (D.T. MacDougal, B1-20). *B*, (July 6, 1960) Forty-five years later, the large boulders visible in the channel are still in approximately the same positions, while the density of the channel vegetation, mostly mesquite (*Prosopis* sp.) has increased. This photograph encompasses a slightly smaller field of view than the original and later matches (J.R. Hastings, Stake 3). *C*, (January 24, 1995) A private road crosses the center of the view, leading to houses out of view to the right. In constructing the ford crossing, nearly all of the large boulders present in the foreground were moved or buried (D.P. Oldershaw, Stake 3). *D*, (August 29, 2007) The debris flow of July 31, 2006, damaged the concrete ford across Soldier Creek, and debris-flow deposits were dredged from the channel before this photograph was taken. Some of the dredged material appears on the right (R.H. Webb, Stake 3).

Geologic Deposits

Youberg and others (2008) mapped debris-flow deposits along channels and on alluvial-fan surfaces on the southern and southwestern side of the Santa Catalina Mountains. Using standard techniques for relative age discrimination of surficial deposits, they found that most debris-flow deposits in this area are of Pleistocene age and occurred during a climatic regime quite different than today. They also used ^{10}Be cosmogenic dating (Gosse and Phillips, 2001) on selected geomorphic surfaces emanating from Finger Rock, Pima, and Soldier Canyons (appendix 1) and verified the relative ages in general, although the cosmogenic dating had considerable problems when applied to debris flows in this region.

Holocene debris-flow deposits were readily observed at lower elevations in canyons cut through the Pleistocene deposits. They also report relatively young radiocarbon dates for debris flows, including one small deposit in Finger Rock Canyon dated at 550 years before present and an even smaller deposit in Pima Canyon that dates from the 1950s; however, the magnitude of these debris flows, as implied from the heights of deposits above the current channel, suggest that they were small events.

In general, the surficial geologic evidence suggests that the likely recurrence interval of debris flows reaching the apices of alluvial fans on the southern fringe of the Santa Catalina Mountains is probably on the order of thousands of years, and the largest debris flows that are documented in the geologic record occurred during the Pleistocene, more than 11,000 years ago. Although Holocene debris-flow deposits are abundant, they appear to represent much smaller events that did not extend long distances beyond the mountain front and may be thousands of years old.

Event Recurrence Interval

The floods and debris flows of July 31 clearly resulted from a meteorological event that was synoptic in scale with an extremely long recurrence interval. From the precipitation data recorded at rainfall gages closest to the most heavily impacted area in the southern Santa Catalina Mountains, recurrence-interval estimates exceed 100 years and, in one case, the 3-day precipitation exceeded 1,000 years (fig. 7). From the weather-radar data, the average recurrence interval for rainfall in grid cells encompassing slope failures exceeded 100 years with recurrence interval in several cells ranging beyond 1,000 years (fig. 9). Streamflow flooding recorded at long-term gaging stations was record breaking and flood frequency ranged from about >200 to 500 years at two stations. The number of slope failures in these watersheds is unprecedented, and repeat photography suggests that few slope failures occurred in this area during the 20th century; channel change, while localized in the case of Sabino Creek, was substantial during the July 31 floods. Finally, geologic maps (Youberg and others, 2008) suggest that the majority of debris-flow deposits by area are of Pleistocene age (>11,000 years) with only smaller debris-flow deposits identified as Holocene events.

Debris Flows at Coronado National Memorial

The storm of July 31, 2006, swept through southeastern Arizona and had large local effects at the southern end of the Huachuca Mountains (Pearthree and Youberg, 2006; Youberg and others, 2006). Debris flows had previously occurred in response to fire in this area in 1977 and again in 1988 (Wohl and Pearthree, 1991). At Coronado National Memorial, just north of the U.S.-Mexico border in Cochise County (fig. 1), an area of 333 acres within the park (2,000 acres total area) had burned in the 103 Fire of June 2006, leaving it highly vulnerable to erosion during the summer monsoon. Rainfall data are sparse for this area, but Youberg (unpublished data, 2008) reported that 8.50 in. of rainfall occurred in 24 hours at the Visitor Center of the National Memorial and 3.31 in. was recorded by the Agricultural

Research Service just east of the Memorial. From the precipitation-frequency relations for this area, 8.50 in. of rainfall in 24 hours has a recurrence interval of much greater than 1,000 years.

Although runoff from watersheds within Coronado National Memorial is unknown, the flood on July 31 was 14,200 ft^3/s at the gaging station San Pedro River at Palominas, AZ (09470500), which is the 5th highest annual peak discharge in a 69-year record. A. Youberg (written commun., 2008) reports that 113 slope failures occurred during the storm, of which 60 percent were from unburned areas. A total of 66 identifiable debris flows resulted from these slope failures in the southern Huachuca Mountains during this storm, but only about a third of these came from burned areas and others came from areas that have not burned recently, including Montezuma Peak (fig. 28).

Figure 28. (February 2007) Slope failures at the southern end of the Huachuca Mountains, Coronado National Memorial. This view shows several failures beneath granite outcrops from an area not recently burned on the east face of Montezuma Peak (R.H. Webb).

Floods and Debris Flows in Aravaipa Canyon

Aravaipa Creek (figs. 1 and 29) has a long history of large floods, including one in October 1983 (fig. 3*A*) that was part of the widespread flooding associated with Tropical Storm Octave (Roeske and others, 1989). In 2006, record flooding generated mostly within the Galiuro Mountains (fig. 29) resulted from the late July-early August 2006 storm, and these storms also caused numerous debris flows, which were not reported for the 1983 event. The record flood in Aravaipa Creek occurred on August 1 (fig. 4*B*), a day later than at other sites in southeastern Arizona. Unlike other affected areas, there is some uncertainty as to when debris flows occurred in this canyon.

Aravaipa Canyon is a wilderness area administered by the Bureau of Land Management (BLM), and The Nature Conservancy (TNC) owns small parcels at the east and west ends of the canyon. Observations of personnel from BLM (Patrick O'Neill, Bureau of Land Management, oral commun., 2007) and TNC (Mark Haberstich, The Nature Conservancy, oral commun., 2007) provided data and eye-witness accounts to the flooding and its aftermath in this remote area.

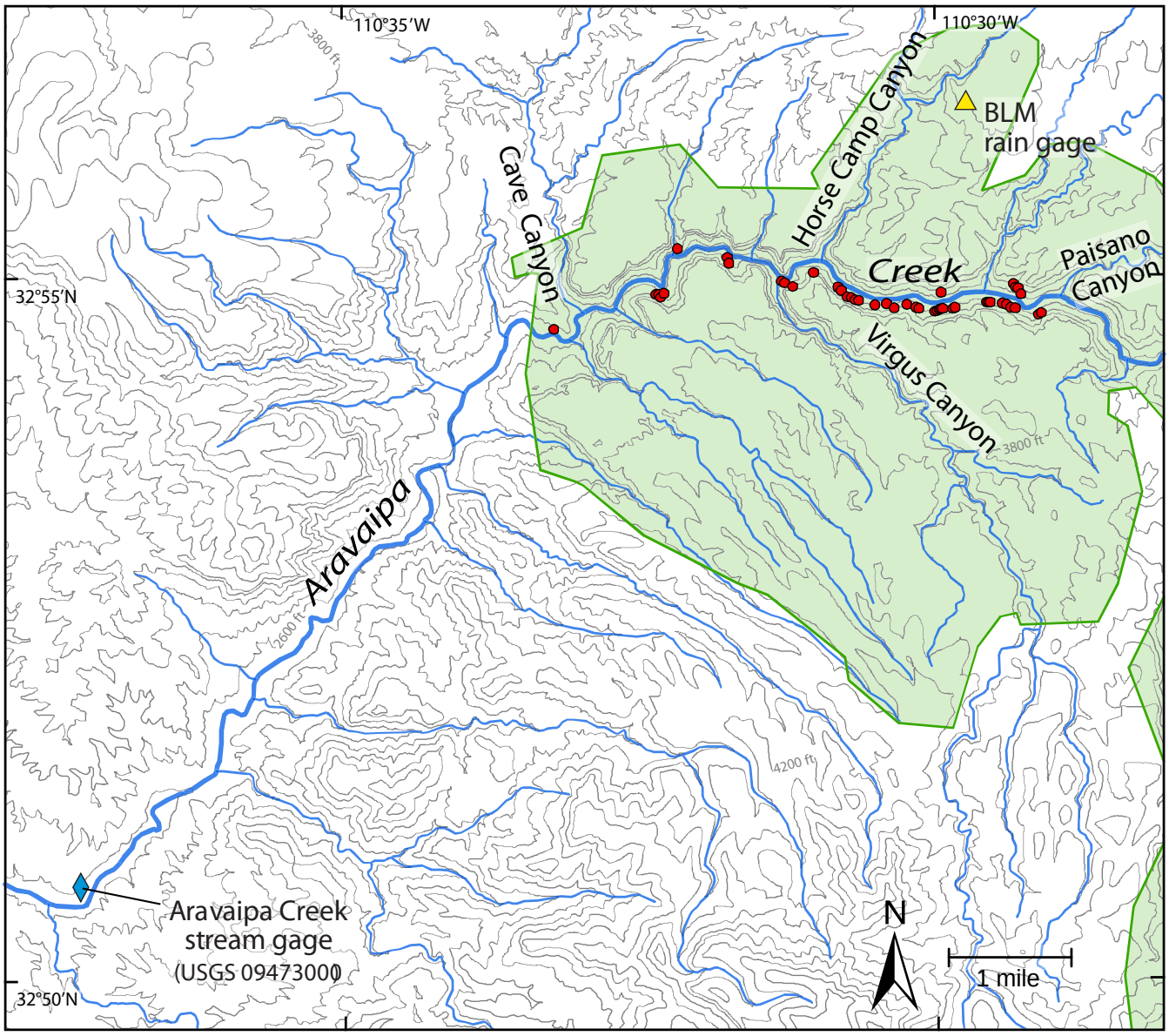

Figure 29. Map showing the spatial extent of the 45 slope failures (red dots) in the western part of the Aravaipa Creek watershed in Aravaipa Canyon. Most were between Virgus and Paisano Canyons. Aravaipa Canyon Wilderness is shown in green. Contour interval is 200 feet.

Rainfall

During the last week of July 2006 at TNC offices, located at the eastern end of Aravaipa Canyon, more than 10 in. of rain fell during the 5-day period from July 27–31 (table 2; M. Haberstich, The Nature Conservancy, written commun., 2008). At the gaging station at the western end of the canyon, a total of 9.99 in. was recorded from July 27 through August 1, and the BLM rainfall gage at Horse Camp Canyon, located in the middle of Aravaipa Canyon and north of Aravaipa Creek, recorded a total of 9.18 in. from July 27 through August 1, with a one-day total on August 1 of 4.56 in. falling in less than 4 hours. The daily rainfall data for these stations appears in table 2.

Table 2. Precipitation from July 27 through August 1 at three rainfall gages in the vicinity of Aravaipa Creek.

	DAILY PRECIPITATION (in.)		
Date	Aravaipa Creek at Mammoth, AZ (9473000)	Horse Creek [1]	The Nature Conservancy Headquarters[2]
Relative Location	West End	Canyon Center	East End
July 27	1.06	0.2	0.2
July 28	2.09	0.93	1.4
July 29	5.36	2.58	3.7
July 30	0.52	0.76	2.1
July 31	0.69	0.15	0.1
August 1	0.27	4.56	2.9
Maximum 4-day total	9.03	8.05	8.8
NOAA 4-day Recurrence interval[3]	>1,000	>1,000	>1,000

[1] Bureau of Land Management RAWS data, from *http://www.raws.dri.edu/cgi-bin/rawMAIN.pl?azAHOR*, accessed June 12, 2008.

[2] Data courtesy of M. Haberstich, The Nature Conservancy, written commun., 2008.

[3] Analyses were performed using *http://hdsc.nws.noaa.gov/hdsc/pfds/sa/az_pfds.html*, accessed June 3, 2008.

On the basis of National Weather Service regional frequency relations, the maximum 4-day rainfall totals for all three precipitation records have a recurrence interval in excess of 1,000 years (table 2). Based on rainfall data from surrounding climate stations outside of Aravaipa Canyon, the high rainfall of August 1 appears to have been within the Galiuro Mountains; rainfall at the few climate stations upstream from Aravaipa Canyon recorded insignificant rainfall on July 31 and August 1. The intense rainfall of August 1 fell on already saturated soils and generated the record flooding in the Aravaipa Creek watershed (fig. 4*B*), even though it appears to have been restricted to a relatively small part of this 537 mi^2 watershed.

Streamflow Flooding

Like Sabino Creek, the series of daily floods was extraordinary, with peak discharges of 23,100, 10,500, 10,300, and 28,000 ft^3/s occurring from July 29 through August 1 (fig. 4*B*). The stage on August 1 was higher than the stage recorded in October 1983, and a step-backwater model yielded the peak discharge on this date to be significantly lower than the peak discharge of 70,800 ft^3/s estimated for the October 1983 flood (Roeske and others, 1989). Roeske and others (1989) used a slope-area measurement to estimate the 1983 discharge, and many reviewers thought that this discharge was excessive despite the fact that it helped explain the extremely high discharge in the lower San Pedro and Gila Rivers downstream from Aravaipa Creek.

We estimated the recurrence interval for the August 1, 2006, flood using the USGS gaging station record for Aravaipa Creek near Mammoth, AZ (09473000), which has annual peak-discharge data for 1919-21, 1931-41, and 1965-2006 (56 years of record, fig. 3A). One problem with flood-frequency analysis is choice of a peak discharge for the 1983 flood. Roberts (1986) used a step-backwater model of floodplain deposits, termed “slackwater deposits,” to retrospectively estimate a

peak discharge for the 1983 flood of 26,500 ft^3/s. This better matches the flood record of Aravaipa Creek because it is slightly lower than the August 1, 2006, peak discharge, which had a higher peak stage. Using a lower discharge for the 1983 flood, the 2006 flood has a recurrence interval of slightly less than the 100-year flood.

The 2006 flood in Aravaipa Canyon created significant changes to the vegetation and geomorphology along the river corridor (fig. 30). In the Narrows, just below Cave Canyon, trunks of cottonwood trees (*Populus fremontii*) were deposited 25-30 ft above the creek bed. Flood stages were also high in tributary canyons, including Painted Cave and Virgus Canyons. Removal of riparian vegetation just below the Narrows is well documented using repeat photography (O'Neill, 2006). Similarly, we matched a photograph taken by Josef Muench (ca. 1950-1970) showing some cottonwood trees removed in the intervening years (fig. 30), and these observations match the general observation of riparian vegetation removal throughout the canyon. One observer believed that the reduction in riparian vegetation during the 2006 flood was of similar magnitude to that of the 1983 flood (Patrick O'Neill, BLM, oral commun., 2007). As would be expected for a large flood, local scour and fill was significant as large boulders were transported downstream, particularly below tributaries yielding debris flows during the event, and large alluvial bars were deposited along the channel margins.

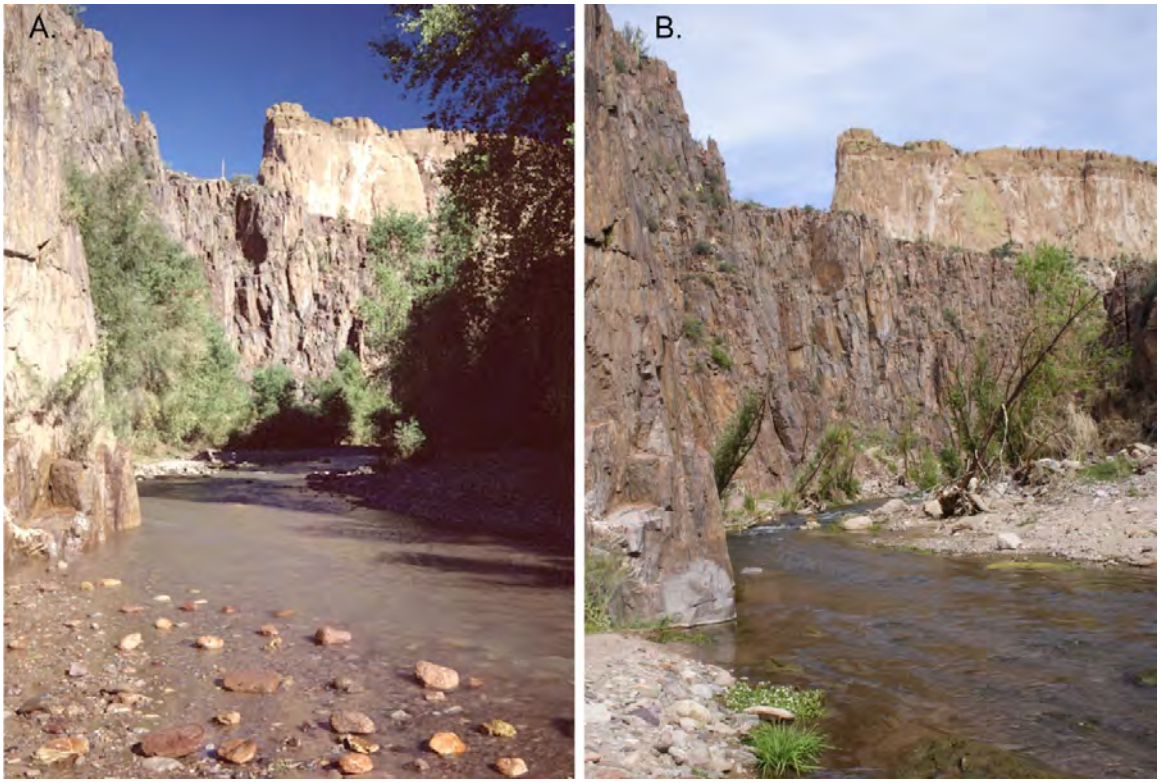

Figure 30. Repeat photographs of Aravaipa Creek in Aravaipa Canyon. *A*, (between 1950 and 1970) This view of Aravaipa Creek in Aravaipa Canyon is 300 ft upstream from Painted Cave Canyon and upstream from the Narrows. Scattered cottonwood (*Populus fremontii*) and sycamores (*Platanus racemosa*) line the channel (Josef Muench, Cline Library, Northern Arizona University, NAU.PH.2003.11.50.6.M-4769). *B*, (March 26, 2007). The riparian vegetation—particularly the cottonwood trees—has been significantly damaged or removed by the record flood of 2006. Considerable sediment that once lined the left foreground has been scoured to a depth of about 4 ft, and the point bar in the right midground is more prominent and may have aggraded (D.E. Boyer, Stake 4875).

Slope Failures and Debris Flows

The debris flows observed in Aravaipa Canyon probably resulted from the intense, heavy rainfall on August 1, though heavy rainfall on July 31 may have also caused some failures. Many small slope failures were visible on the talus slopes of the canyon walls throughout Aravaipa Canyon. Some of these slope failures mobilized into debris flows that traveled to Aravaipa Creek; between Paisano Canyon and the western entrance of the wilderness area, we counted 45 slope failures that mobilized into debris flows. East of Paisano Canyon, Mark Haberstich (The Nature Conservancy, oral commun., 2007) observed many slope failures but did not count them or record their locations. The highest concentration of debris flows in western Aravaipa Canyon occurred in the reach between Paisano and Virgus Canyons (fig. 29). Within the first mile of Virgus and Cave Canyons upstream from Aravaipa Creek, we observed no debris flows or evidence of debris flows coming down the tributaries; slope failures, however, may have occurred on the talus slopes in the larger side canyons.

Most of the slope failures we observed came from the south side of Aravaipa Canyon at an elevation around 3,000 ft (fig. 29), and 60 percent of the observed failures had volumes less than about 130 yd^3. Thirteen debris flows had a volume estimated to be between 130-370 yd^3, and five of the observed debris flows had estimated volumes larger than 370 yd^3 (fig. 31). The largest failure occurred just upstream of Virgus Canyon with an estimated volume of 1,300 yd^3.

Figure 31. (March 28, 2007) A representative debris-flow deposit in Aravaipa Canyon from the 2006 event. This debris flow occurred across from the mouth of Horse Canyon at an elevation of 3,000 feet and had a volume estimated to be about 370 yd^3 (D.E. Boyer).

Debris Flows in the Vicinity of Bowie Mountain

Several days of heavy rainfall affected the mountains to the south of Fort Bowie National Historic Site (fig. 1) during the final week of July 2006. Fort Bowie was built in the 1860s at the northern end of the Chiricahua Mountains to protect water sources and passage through Apache Pass (Greene, 1980), a route between the Chiricahua and Dos Cabezas Mountains. The National Historic Site is at an elevation of 5,000 ft and is north of Bowie Mountain, the highest topographic point in the area with an elevation of 6,931 ft (fig. 32). Fort Bowie has a semiarid climate with annual precipitation of about 15 inches. Larry Ludwig (National Park Service, oral commun., 2007) reported that the most recent fire to affect this area was in the 1920s.

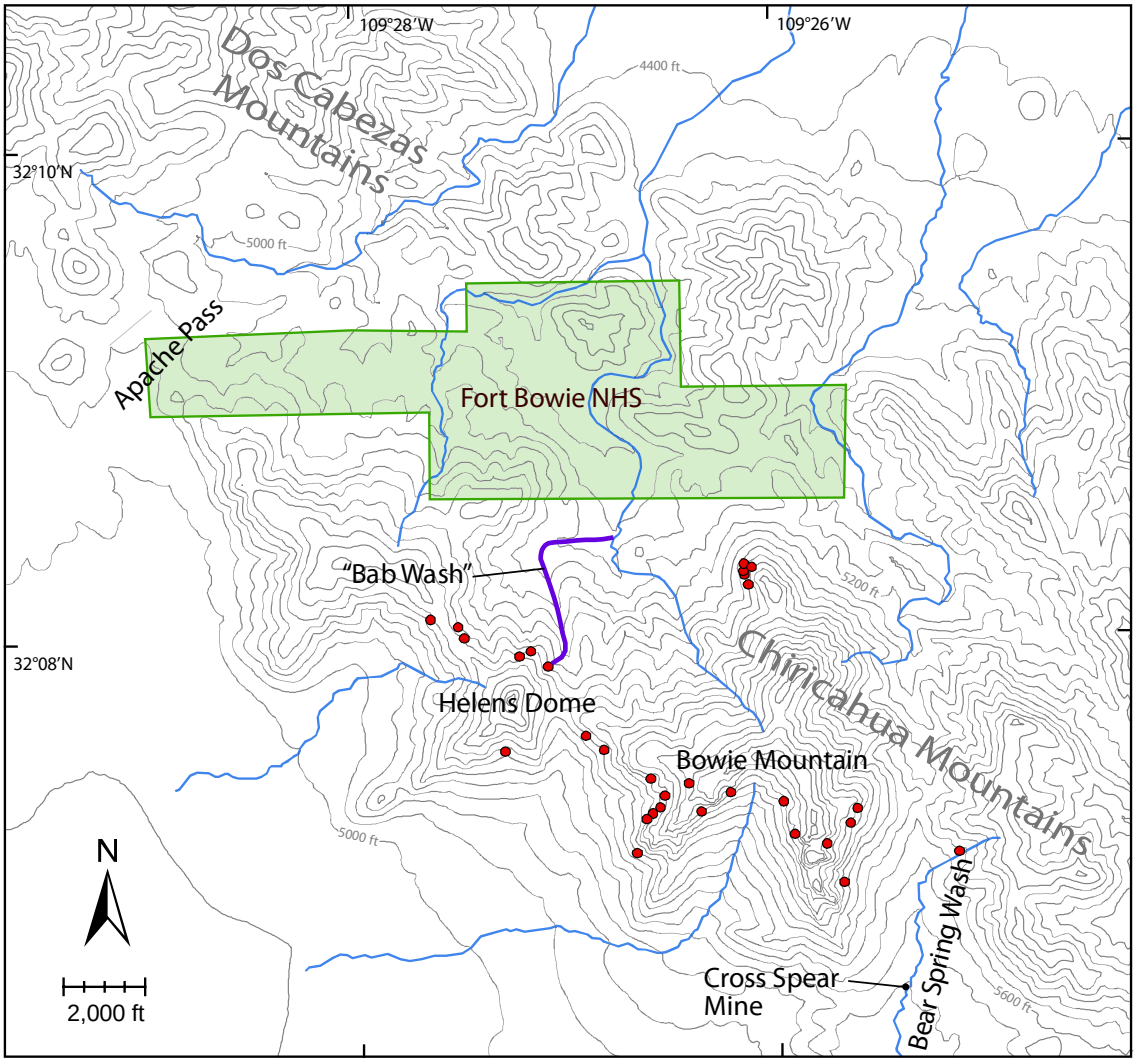

Figure 32. Map of 30 slope failures (red dots) in the vicinity of Bowie Mountain and Fort Bowie National Historic Site (shown in green), southeastern Arizona, that occurred on July 31, 2006. Contour interval is 100 feet.

In late July, the same synoptic weather pattern that affected the Santa Catalina Mountains produced rainfall near Fort Bowie. On July 31, heavy rain fell after dawn on the range of hills to the south and southwest of Fort Bowie. Ludwig (National Park Service, oral commun., 2007) measured 3.98 in. of rainfall on July 30 (reading was made on the morning of July 31 before the heaviest rain) and

another 3.30 in. on July 31. This amount of rainfall—7.28 in. in 48 hours—exceeds the 1,000-year rainfall event for this area (*http://hdsc.nws.noaa.gov/hdsc/pfds/sa/az_pfds.html*, accessed June 1, 2008). Rainfall measured at a BLM gage in Apache Pass, about 2.5 mi northwest of the epicenter of debris-flow activity, was 4.17 in. for July 31, an amount with a recurrence interval of 200-500 years. Reports from workers at the Cross Spear Mine on the southeastern side of Bowie Mountain indicate that maximum rainfall locally may have been as high as 9 in. on July 31, although we believe this measurement is unreliable.

NWS weather radar estimated that rainfall ranged from 3 to 5 in. over the general Fort Bowie area for the morning of July 31; this 6-hour rainfall has an estimated recurrence interval of 100 to greater than 1,000 years. The abundance of atmospheric moisture and the lack of cold-top thunderstorms (cloud tops did not cool lower than -67° C) suggest the potential for local underestimation of rainfall estimates from weather radar and that precipitation may have been closer to 9 in. on Bowie Mountain; if so, this amount of precipitation far exceeds the 1,000-year recurrence interval rainfall for this area.

Major washes draining Bowie Mountain had large but unmeasured streamflow floods that caused local damage. On the surrounding rangeland, a number of roads were washed out, fences were destroyed, and stock tanks were filled with sand. No streamflow gaging stations record discharge in this area, and the magnitude and recurrence interval of these floods is unknown.

In addition to damaging flash floods, the rainfall produced a number of slope failures, many of which coalesced into debris flows that traveled down washes scouring sediment and removing trees. The epicenter of activity was along a ridge to the south and southwest of Fort Bowie stretching from Bowie Mountain to Helens Dome (6,376 ft). At least 30 slope failures were identified on the flanks of these two mountains, and one of the largest failures, which scoured the colluvium to bedrock, occurred the northeast side of Helens Dome. The resulting debris flow, which occurred in an unnamed channel informally called Bab Wash by Ludwig, appeared to be one of the largest historic debris flows in Arizona. The debris flow had a volume of about 480 yd^3 and scoured a channel 2,000 ft long and as much as 60 ft wide. The depth of the flow locally was greater than 25 ft and the momentum of the flow removed a large strip of riparian vegetation, including a numerous large oak trees that were washed out and carried downstream. The debris flow transported and deposited large boulders downstream in an area that National Park Service Rangers previously drove through during their security operations (fig. 33). There is no record in the nearly 150 years of historical record in this area of this type of flood in the vicinity of Fort Bowie.

On the south side of Bowie Mountain, several large debris flows scoured slopes previously occupied by grasslands, depositing several feet of boulders and sand at their termini (fig. 34). The debris flows deposited boulders and voluminous quantities of sand, some of which entered Bear Spring Wash, an ephemeral channel that passes through the Cross Spear Mine, a limestone mining operation on the southeastern side of Bowie Mountain. The subsequent flooding damaged operations at the Cross Spear Mine, where employees at the mine reported that the flood pushed two 24 in. corrugated culverts out of an earthen bridge and destroyed the crossing.

Figure 33. (January 16, 2007) Large boulders now clog the channel of an unnamed wash, informally called Bab Wash, that drains the northeastern side of Bowie Mountain, southeastern Arizona. This area used to be a grassy channel that allowed passage of law-enforcement vehicles before July 2006 (R.H. Webb).

Figure 34. (January 16, 2007) Debris-flow deposits (left foreground) and erosion in an unnamed tributary to Bear Spring Wash, a drainage from the southeastern side of Bowie Mountain, southeastern Arizona. On exiting the cliffs in the left background, the debris flow cut across several channels, forming a new drainage network on the southeastern flank of Bowie Mountain (R.H. Webb).

Slope Failures and Sediment Yields in the Santa Catalina Mountains

Slope Failure Area and Density

Using aerial photography, we identified 435 slope failures in 10 watersheds that drain the Santa Catalina front range (fig. 35, table 3). Sabino Canyon had the most failures, with 213 overall. A total of 132 slope failures were identified in lower Sabino Canyon, 46 of which occurred in Rattlesnake Canyon (fig. 35). We digitized the area of slope failures from the high-resolution aerial photography; measurements of failure area have an estimated error of ±10 percent. Sabino Canyon had the largest composite failure surface area (101 acres), most of which was in lower Sabino Canyon (79.0 acres). Lower Sabino Canyon also had the largest density of failures (12.0 acres/mi^2), followed by Soldier Canyon (4.8 acres/mi^2) and Bird Canyon (3.8 acres/mi^2).

Table 3. Slope-failure density and sediment yield for watersheds in the southern Santa Catalina Mountains.

Drainage Basin	Drainage Area (mi^2)	Slope Failures (n)	Surface Area of Failures[2] (acre)	Density of Failures (acre/mi^3)	Volume of Failed Sediment[3] (1000 yd^3)	Mass of Failed Sediment[4] (1000 ton)
Unnamed - west	0.65	1	2.12	3.3	8.97	15.1
Ventana	3.9	4	1.51	0.4	6.39	10.8
Esperero	3.5	14	6.85	2.0	29.0	48.9
Bird	2.3	22	8.91	3.8	37.7	63.6
Sabino	35	213	101.2	2.9	428	722
Upper Sabino[1]	28	81	22.2	0.8	93.8	158
Lower Sabino[1]	6.6	132	79.0	12.0	335	564
Rattlesnake[1]	2.7	46	23.8	8.7	101	170
Bear	16.8	95	53.7	3.2	227	380
“Gibbon”	1.2	13	3.86	3.3	16.4	27.6
Soldier	3.9	56	18.7	4.8	79.3	134
Unnamed – east	0.94	2	1.28	1.4	5.42	9.1
Molino	7.0	15	8.91	1.3	37.8	63.6
Total	75	435	207	2.8	877	1,480

Note: All failure area estimates are ±20 percent. All volume and mass estimates have a precision of ±54 percent.

[1]Upper and Lower Sabino are sub-basins of Sabino and Rattlesnake is a sub-basin of Lower Sabino.

[2] Surface area is measured as the total exposed area of slope failures within each drainage basin.

[3] Volume of failed sediment was calculated by multiplying surface area of failures by a mean failure depth of 2.6 ft.

[4] Mass of failed sediment assumes a bulk density for debris flow material of 1.69 tons/yd^3.

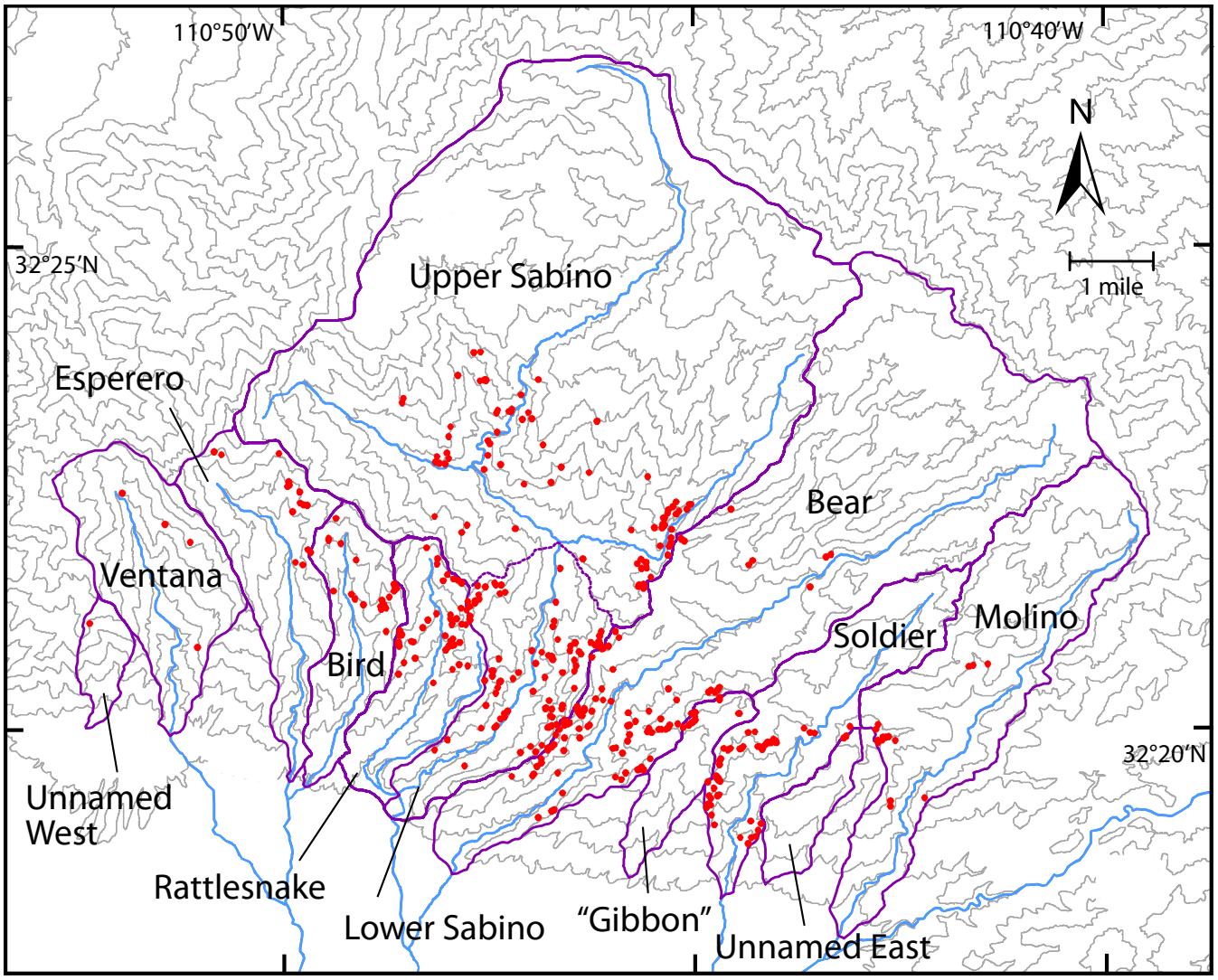

Figure 35. Map of 435 slope failures (red dots) that occurred on July 31, 2006, in 10 drainages of the southern Santa Catalina Mountains.

Failure Type and Depth

We documented two types of slope failure that occurred in July 2006. Most failures follow an existing topographic hollow, however subtle, that guides them to an existing stream channel at the canyon bottom (fig. 36A). These failures remain narrow (< 15 ft wide) throughout their length. A small percentage of failures crossed flatter areas and, unconstrained by topography, eroded a much wider swath of hillside (fig. 36B). Both types of failure, however, consistently stripped the colluvium down to bedrock; consequently, the depth of slope failures is relatively constant across the study area and linked directly to the depth of colluvium. Direct measurement of this depth is problematic owing to the difficulty of accessing many failures, particularly ones on high, steep-angle slopes. For the lower angle (<45º) failures that we have investigated, uneven bedrock results in failure depths ranging from <1 ft to about 5 ft, even in small (<1,000 ft^2) areas. An accurate estimate of mean failure depth by direct measurement would require measurement at hundreds of locations, a task well beyond the scope of this project.

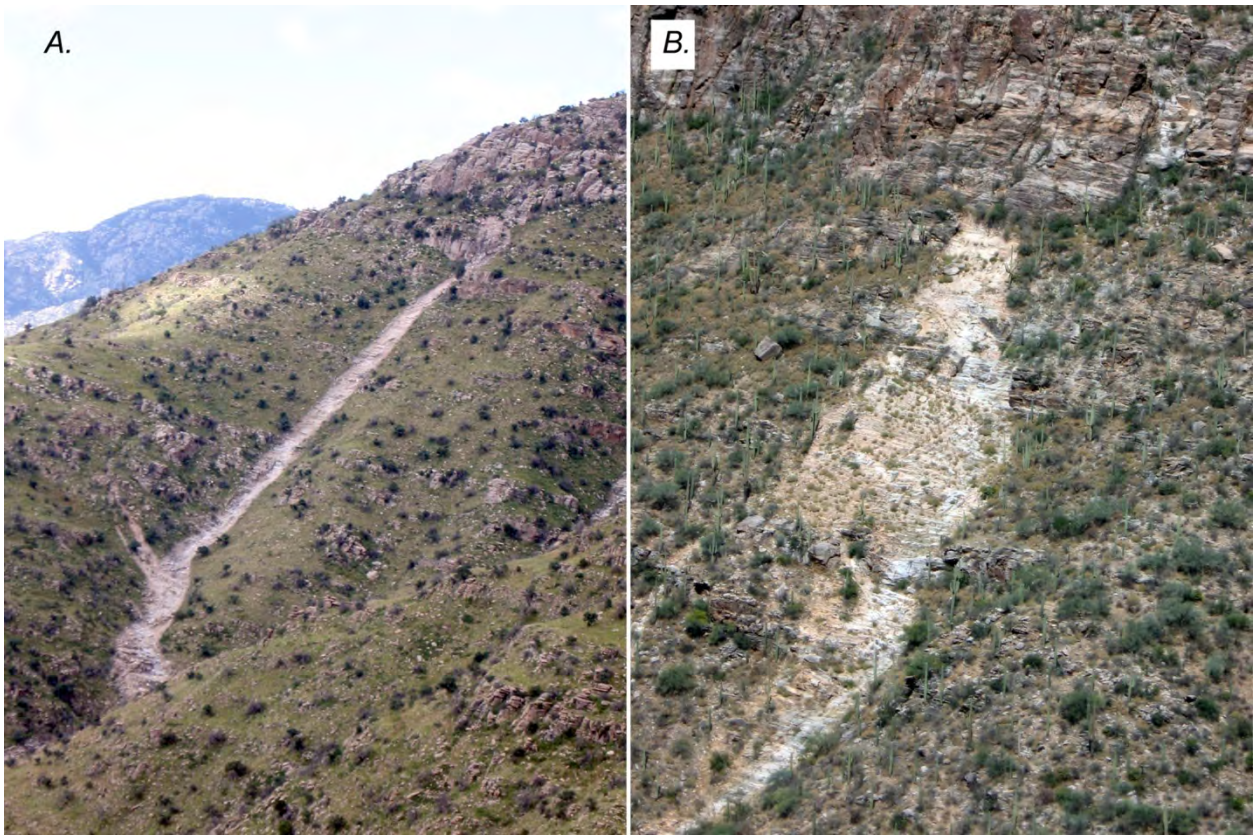

Figure 36. Two types of slope failure in the Santa Catalina Mountains that occurred on July 31, 2006. Both failure types scour colluvial slopes down to bedrock. *A*, (September 14, 2006) Most failures follow existing hollows in the landscape and are relatively narrow (Molino Canyon, P.G. Griffiths). *B*, (May 1, 2008) Where slope failures cross flat surfaces, much wider sections of bedrock are exposed (Sabino Canyon, P.G. Griffiths).

We attempted to measure failure depths by analyzing the difference between 2005 and 2007 LIDAR data collected over parts of the study area. These efforts were unsuccessful; the failure depth was lost in the general noise present in the two data sets, likely owing mostly to the inherent difficulty of measuring such rugged terrain as well as the presence of, and change in, riparian and hillslope vegetation. However, for the dozen failures we investigated in their entirety (in Esperero, Bird, Rattlesnake, Sabino, and Soldier Canyons), average failure depth is consistently about 2.5 ft, though typical failure depths ranged from 1.3 to 4.6 ft (± 50 percent of mean value). Although colluvium is deeper on lower-angle slopes, slope failures have typically joined with existing topographic hollows from which most of the colluvium already has been removed by previous geomorphic processes. New debris flows scoured these channels to bedrock, removing about as much colluvium as they did on the higher-angle slopes. We therefore elected to use a mean failure depth of 2.6 ± 1.3ft (50 percent) across the study area.

Debris-Flow and Streamflow Particle-Size Distributions

Abundant evidence of reworked debris-flow deposits associated with the 2006 events remains in the Santa Catalina Mountains (figs. 10-13, 19-20, 24, 27). Complete particle-size profiles of the sediment released by slope failures and debris flows were difficult to acquire because so few complete debris-flow deposits are preserved. Because of subsequent streamflow flood reworking, extant deposits

usually contain only the coarser particles of gravel, cobbles, and boulders; the finer material, or matrix, flowed downstream once the larger particles came to rest. Where matrix deposits were occasionally found preserved in a debris-flow levee perched above peak flood stage, there was usually insufficient deposit for measurement of a representative particle-size distribution. As a result, both point counts and sieve data were collected and integrated from debris-flow deposits at only five locations: along three debris-flow levees in Soldier Creek below Catalina Highway, along the debris-flow deposit plugging the Sabino Canyon road culvert in Rattlesnake Canyon above the confluence with Sabino Creek, and from a complete debris fan at the base of a single failure in the headwaters of Esperero Creek.

The Esperero Creek debris fan is unique in the Santa Catalina Mountains because it is a complete debris-flow deposit trapped along a 200-ft reach of stream channel in a grove of large trees. There is no indication that debris-flow matrix was lost during deposition or that the overall deposit was reworked by subsequent streamflow (fig. 37). The Rattlesnake Creek deposit plugging the Sabino Road culvert is nearly as complete, differing only in the absence of the largest boulders. The three Soldier Creek deposits, in contrast, show the effects of reworking by streamflow, with the potential addition of gravel and finer particles (<64 mm) following the debris flow (fig. 38). We chose to use the mean of particle-size data from the two best-preserved deposits, those at Esperero and Rattlesnake, as representative of the colluvial material released by the slope failures (table 4).

Table 4. Average particle-size distribution for 2 debris-flow and 15 streamflow deposits measured in the southern Santa Catalina Mountains (see text for methods of measurements).

Particle-Size Class	b-Axis (mm)	Weight Percent (percent)
Boulders	> 256	20.8
Cobbles	64 to 256	43.6
Gravel	2 to 64	26.8
Sand	0. 0625 to 2	8.6
Silt and Clay	< 0.0625	0.2
Streamflow[1]	< 64	35.6

[1] Size-class entrainable by streamflow from the Santa Catalina Mountains (for example, less than gravel size).

Streamflow deposits representative of the sediment size transported out from the Santa Catalina Mountains were collected at 13 locations on three washes: Soldier Creek (6 samples), Bear Creek (2 samples), and Sabino Creek (5 samples; fig. 37). These streamflow deposits, sampled in the summer of 2007, represent an amalgamation of sediment deposited by runoff, including during the July 2006 floods. The resulting data are presented in appendix 2. For our purposes, the critical value is the largest particle-size class delivered by typical streamflow, which was 32 mm. We therefore calculated sediment with potential for streamflow entrainment and transport out of the mountains as all particles < 64 mm (gravel and finer).

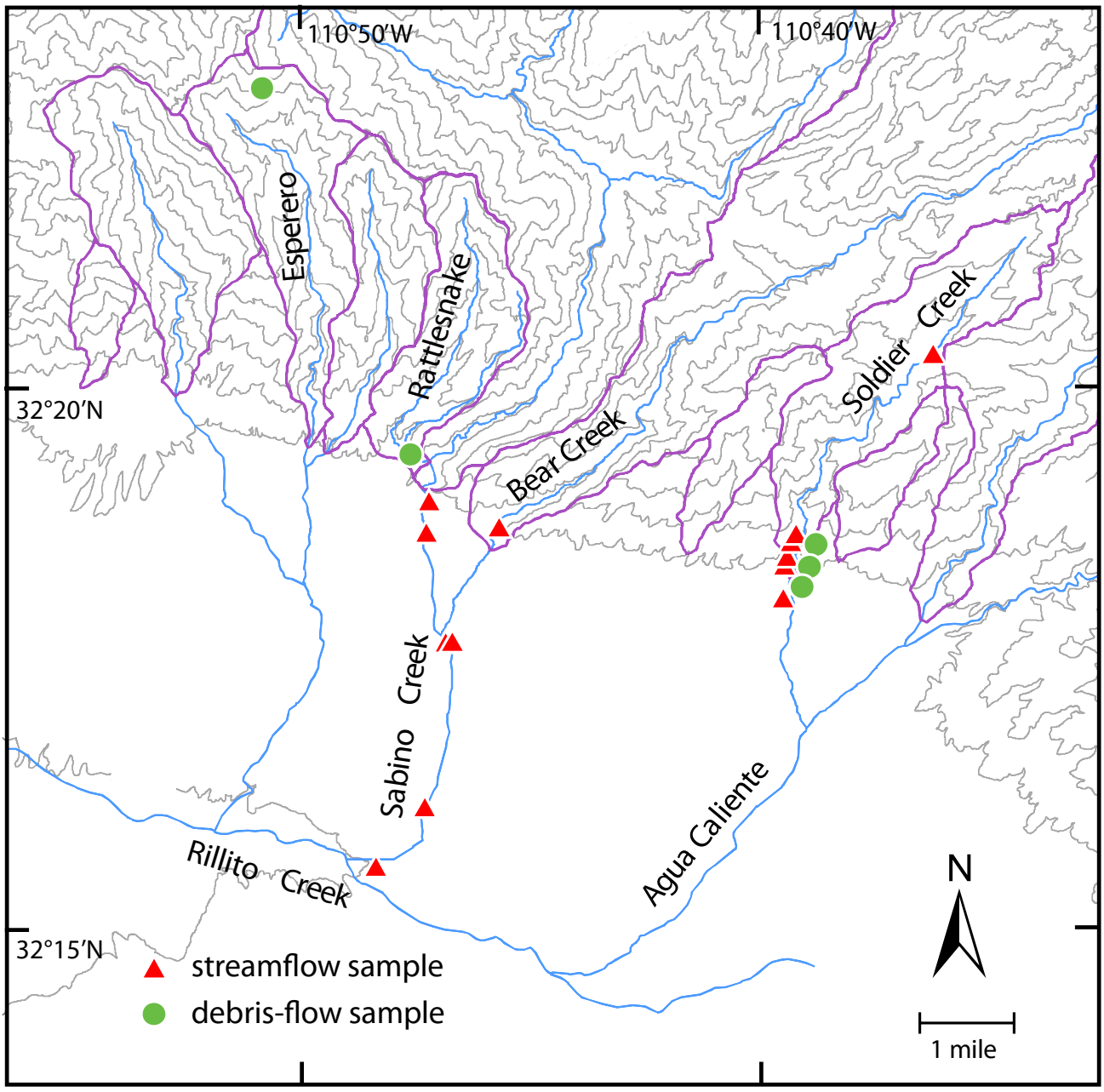

Figure 37. Map of sediment samples collected for debris-flow and streamflow particle size distributions in the southern Santa Catalina Mountains.

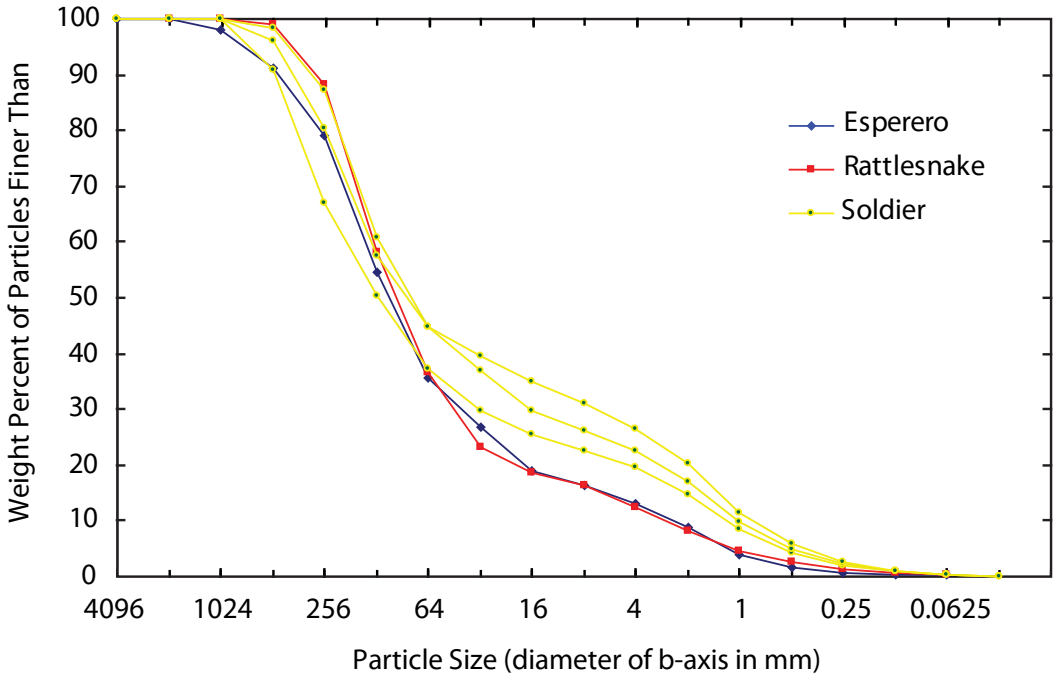

Figure 38. Plot of distribution of sediment particle size by weight from five samples of debris flow sediment deposited on July 31, 2006. The increased percentage of finer particle sizes (0.5 mm < b-axis < 64 mm) in the three samples from Soldier Creek indicates that sediment in this size range may have been added by streamflow after the debris flow occurred and before we collected the samples.

Sediment Yield

The total volume of sediment released by slope failures and debris flow was estimated to be 877,000 yd^3 in the southern Santa Catalina Mountains. Converting volume to mass with a bulk density of 1.69 tons/yd^3 (Webb and others, 2000) resulted in total sediment yield of 1.5 million tons of all particle sizes from 10 drainage basins (table 5). Nearly half of this sediment (722,000 tons) was generated in Sabino Canyon, followed by 380,000 tons in Bear Canyon and 134,000 tons in Soldier Canyon. Of the total sediment yield from all ten drainages, particles with a b-axis of <64 mm comprise 527,000 tons (about 36 percent) of the total sediment volume, and this mass has the potential to be entrained by typical streamflow discharges and transported beyond the mountain front. This sediment volume includes 127,000 tons of sand and 3,380 tons of silt and clay. Taking into consideration the estimated variability of slope-failure depths and areas of ±50 percent and ±20 percent, respectively, we place a precision on estimates of sediment volume and mass of ±54 percent.

If one were to assume that all 527,000 tons of <64 mm sediment (312,300 yds^3) were transported to and deposited in Rillito Creek, the effect on decreasing cross-sectional areas within the soil-cemented banks could be estimated. Assuming an average channel width of 330 ft between the soil-cemented banks of Rillito Creek, this amount of sediment, spread uniformly, would raise the bed elevation of Rillito Creek by an average of 4.6 in. along the 12.5 mi stretch between Agua Caliente Wash and the Santa Cruz River. However, this sediment is not likely to be delivered in a single pulse, nor will it be spread evenly along the bottom of the channel. If the sediment were to debouch en mass in the reach of Tanque Verde Creek between the confluences with the affected channels (from Agua Caliente Wash to Craycroft Road, average width = 348 ft), the average deposition in this 3.1 mi reach would reach a depth of about 1.5 ft.

Table 5. Estimates of sediment released by slope failure by particle-size class in the southern Santa Catalina Mountains.

Drainage Basin	Drainage Area (mi^2)	Volume of Failed Sediment (1000 yd^3)	Mass of Failed Sediment (1000 tons)	Boulders > 256 mm (1000 ton)	Cobbles 64 to 256mm (1000 tons)	Gravel 2 to 64 mm (1000 tons)	Sand 0.063 to 2mm (1000 tons)	Silt + Clay < 0.063 mm (ton)	Streamflow Sediment[2] < 64 mm (1000 tons)
Unnamed – west	0.65	8.97	15.1	3.14	6.58	4.05	1.30	34.5	5.39
Ventana Canyon	3.9	6.39	10.8	2.24	4.69	2.89	0.92	24.6	3.84
Esperero Canyon	3.5	29.0	48.9	10.2	21.3	13.1	4.20	112	17.4
Bird Canyon	2.3	37.7	63.6	13.2	27.7	17.1	5.46	145	22.7
Sabino Canyon	35	428	722	150	315	194	62.0	1650	257
Upper Sabino Canyon [1]	28	93.8	158	32.9	68.9	42.4	13.6	361	56.4
Lower Sabino Canyon [1]	6.6	335	564	117	246	151	48.4	1,290	201
Rattlesnake Canyon [1]	2.7	101	170	35.3	73.9	45.5	14.6	388	60.5
Bear Canyon	16.8	227	380	79.7	167	103	32.9	876	137
"Gibbon" Canyon	1.2	16.4	27.6	5.73	12.0	7.40	2.37	63.0	9.83
Soldier Canyon	3.9	79.3	134	27.8	58.2	35.9	11.5	305	47.6
Unnamed – east	0.94	5.42	9.14	1.90	3.98	2.45	0.78	20.9	3.26
Molino Canyon	7.0	37.8	63.6	13.2	27.7	17.1	5.46	145	22.7
Total	75	877	1,480	307	644	397	127	3,380	527

Note: All volume and mass estimates of a precision of ±54 percent.

[1]Upper and Lower Sabino are sub-basins of Sabino Canyon and Rattlesnake Canyon is a sub-basin of Lower Sabino Canyon.

[2] Streamflow sediment is defined as all sediment with a b-axis of <64 mm (gravel and finer).

Debris-Flow Mobility and Stochastic Modeling

Debris flows in the Santa Catalina Mountains can be conceived as moving through three general zones defined by the degree to which debris flows aggrade or deposit sediment: initiation, transport, and deposition. In initiation zones on the steep colluvial slopes, most debris flows had sufficient potential and kinetic energy to scour material from hillsides and channels, adding mass and momentum and increasing their destructive potential for structures and roadways below. In many cases, two or more debris flows coalesced into larger debris flows that turned downstream upon reaching the canyon bottom. Where the gradient was high and the channel narrow, debris flows continued on toward the mountain front, potentially coalescing with other debris flows entering the channel from other initiation points on canyon slopes. Where debris flows entered flooded streams like Sabino Creek, they quickly became diluted, dropping their coarse-sediment load and becoming reworked by the streamflow flood; the debris flow termed “Ocho Grande” (fig. 13) is a good example of this scenario. In the transport zone, net change in debris-flow volume is essentially minimal as sediment additions are offset by deposition. Where the grade decreased or the channel widened, debris flows quickly deposited the larger particles in levees and snouts; sediment aggradation can be substantial in this zone of deposition, most notably in Rattlesnake Canyon (fig. 39). For debris flows with sufficient energy, the final deposition zone began at the apex of alluvial fans where sediment losses over an unconfined surface exceeded the volume of the debris flow.

Figure 39. (August 18, 2006) Aerial photograph showing debris-flow levees (shaded in red) and channel sediments deposited on July 31, 2006, in Rattlesnake Canyon, southern Santa Catalina Mountains (R.H. Webb).

Field observations suggest that the larger debris flows consisted of multiple smaller pulses as has been described in many other areas (see Definitions section for a list of on-line videos). For example, in Rattlesnake Canyon, a large debris flow reached Sabino Creek (fig. 20) but snouts deposited in the channel upstream are indicative of other pulses that did not travel as far (fig. 19). This partly explains why the total cross-sectional area through which the debris flows passed in the transport zone was small in comparison to the total volume of material that was transported downstream: the total material was essentially attenuated in multiple pulses over time.

Along the southern flank of the Santa Catalina Mountains, debris flows had sufficient energy to approach or exit the mountain front in five canyons: Bird Canyon, Rattlesnake Canyon, Bear Canyon, Soldier Canyon, and an unnamed canyon between Soldier and Bear that drains a large catchment below Gibbon Mountain (figs. 2 and 35). Depending on the gradient and topography of the mainstem channels in these canyons, the ratio of the volume sediment deposited within the canyon to the volume that exited or nearly exited the mountain front was highly variable. Although it was difficult to precisely quantify the volume of the various deposits within the canyons, qualitative estimates of the general distribution of debris-flow material can be made by analyzing aerial photography and channel topography.

Figure 40 shows the characteristic deposits of the Rattlesnake debris flow upstream from its confluence with Sabino Creek. For the analysis, only two of the slope failures were plotted. The slope failure farthest from Sabino Creek originated near Rattlesnake Peak at an elevation of 5,500 ft (labeled "A" in fig. 40). This failure scoured a slope for a distance of about 0.4 mi before entering a steep reach of channel that was a transport zone. At about 0.8 mi from its source, this debris flow entered a wide, less steep section where it deposited sediment before entering another transport zone. A large failure on the west side of Rattlesnake Canyon (labeled "B" in fig. 40) entered the mainstem at 1.5 mi from the source of A, and this flow, combined with other local failures, deposited large volumes of boulders and cobbles in the channel at the juncture. Flows A and B likely were not coincident in time. After passing through another transport zone (fig. 40), the debris flow entered a relatively wide section of Rattlesnake Creek and deposited material on its way to Sabino Creek. Although the total volume of sediment released by slope failures in Rattlesnake Canyon was about 101,000 yd^3, an unknown but relatively large volume of that sediment remains deposited in discrete reaches along Rattlesnake Creek (fig. 19).

In Soldier Canyon, the total volume of mobilized sediment (about 79,300 yd^3) was slightly less than the volume of debris-flow sediment in Rattlesnake Canyon, but the topography of Soldier Canyon and the proximity of slope failures to the mountain front enabled much more material to flow onto the alluvial fan. Profiles of four failures within the catchment show that Soldier Creek effectively conveyed material downstream (fig. 41); for example, slope failures lettered "C" and "D" scoured considerable sediment before passage through a transport zone that extended to the culverts at Catalina Highway. Although some sediment was deposited in a relatively wide open area near failure "B," much of Soldier Creek between the upper sections of the watershed and the fan acted as a transport zone.

Other drainages were not as efficient at transporting debris flows. In Bird Canyon, some evidence of debris-flow deposits was observed near the mountain front, though it appeared that most of the debris-flow material was deposited within the upper watershed, relatively close to the slope failures. In Bear Canyon, many debris-flow pulses delivered copious sediment to the main channel where it was reworked by a large streamflow flood. Nevertheless, debris-flow sediments were still deposited close to the mountain front. The flow regime in Bear Creek probably fluctuated between debris flow, hyperconcentrated flow, and stream flood flooding throughout the morning of July 31 (see Melis and others, 1997), with large debris flows entering Bear Creek from local slope failures and some pulses reaching the mountain front.

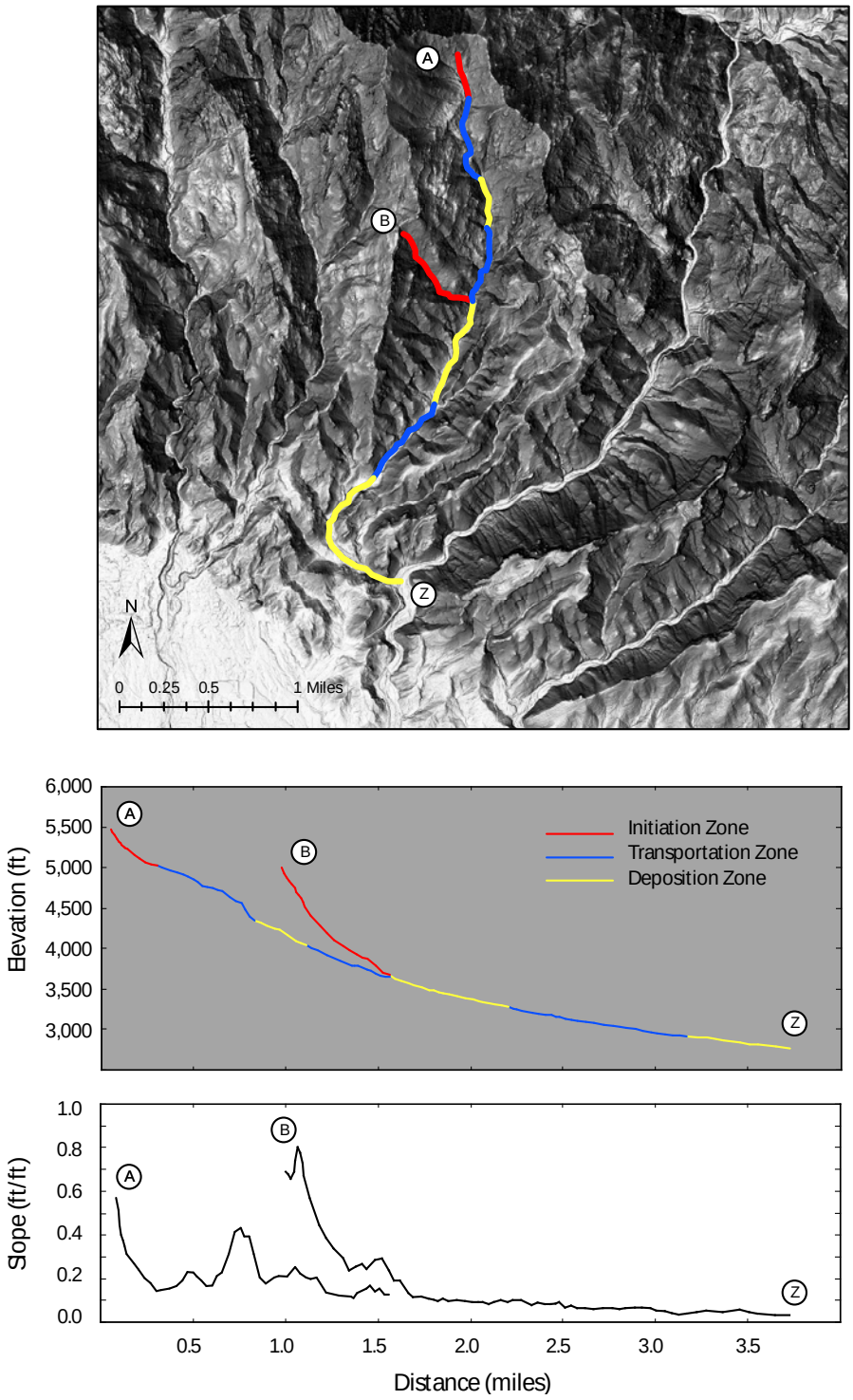

Figure 40. The travel path of debris flows from two initiation zones (A and B) that joined and traversed Rattlesnake Canyon. The two debris flows probably did not meet simultaneously, and their relative timing is not known. The flow path is shown in plan view as well as profile and the slope of the channel is included for comparison. Qualitative estimates of zones of initiation, transition, and deposition are included. In Rattlesnake Canyon, the debris flow deposited sizeable quantities of material along the main channel.

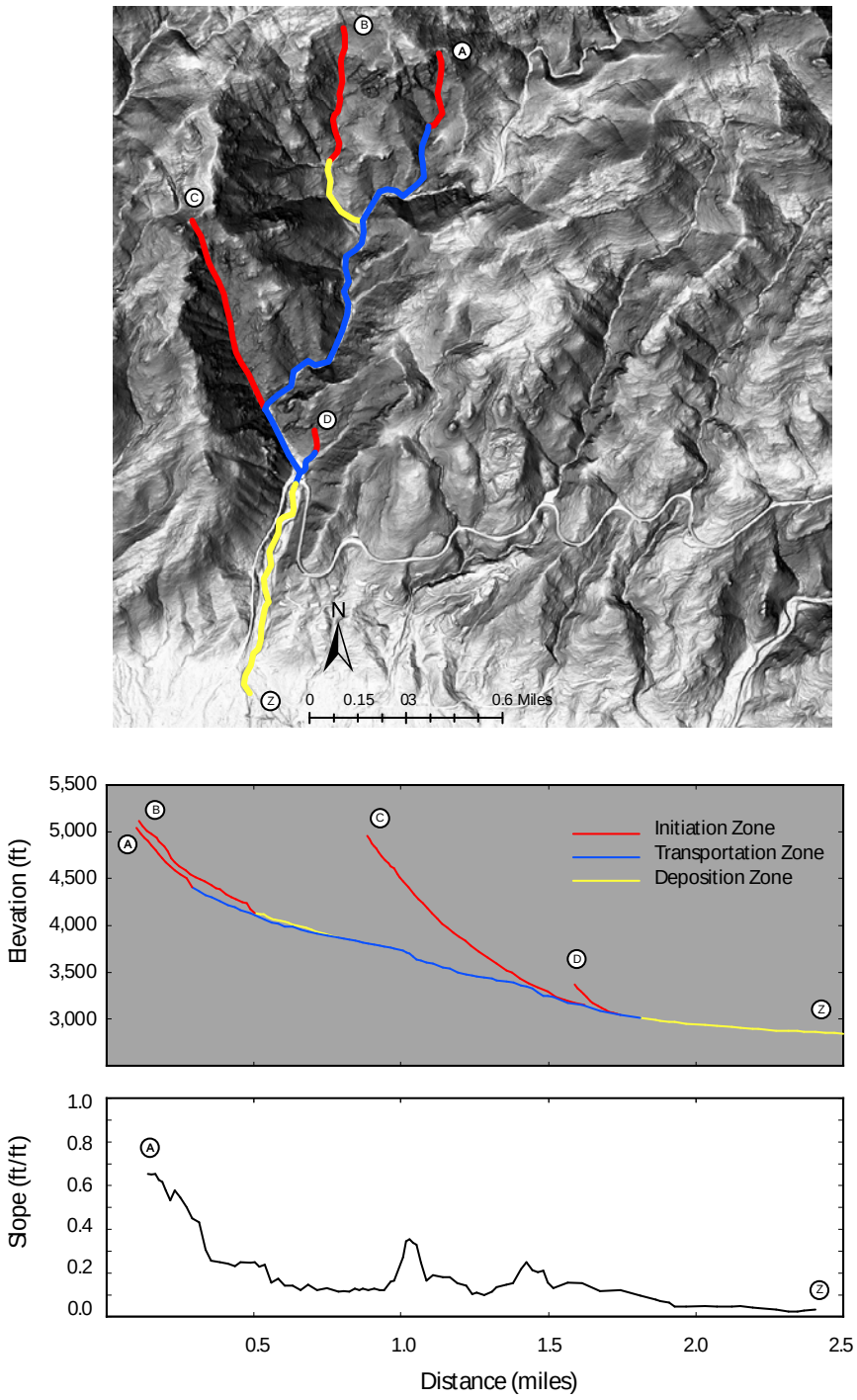

Figure 41. The travel path of debris flows from four initiation zones in Soldier Canyon. Although it is highly improbable that the debris flows joined simultaneously, the relative timing of each debris flow with respect to the others is unknown. Zones of initiation were significant in each branch and the mainstem effectively transported material to the mountain front. The relative proximity of many of the slope failures to the alluvial fan meant that much of the eroded sediment traveled to the relatively modest slope of the alluvial fan.

Finally, a debris-flow snout was observed about 0.5 mi from the mountain front in a unnamed wash draining Gibbon Mountain. This snout was small and contained only a few small boulders and cobbles. Although it was unmistakably a debris-flow snout, evidence of the debris flow was mostly removed by streamflow flooding, and the remaining evidence of the debris flow event is most recognizable in the channel upstream from the mountain front. Youberg and others (2008) map the snout we observed as a Holocene debris-flow deposit (they did not differentiate 2006 deposits from older ones on this alluvial fan).

Stochastic Modeling with LAHARZ

In order to evaluate the suitability of the LAHARZ proportionality coefficients for southeastern Arizona, we measured the volume, cross-sectional area, and planimetric area for six 2006 debris flows in southeastern Arizona representing a range of debris-flow volumes (table 6). For the large debris flow at Bab Wash near Fort Bowie, no topographic data pre-dating the 2006 event were available, so the volume of this debris flow was estimated by analyzing cross sections along the course of the debris flow and estimating the depth of material scoured during the event. For the debris flow in Esperero Canyon, volumes and cross-sectional areas were estimated with greater accuracy by detailed field study. One small debris flow in the Soldier Creek drainage, as well as Ocho Grande in Sabino Canyon, were also measured directly. The volume and area measurements of each of these four debris flows represented a single slope failure or closely spaced multiple slope failures that coalesced on the hillside into a single debris flow. To represent larger debris flows from entire catchments, the volumes of slope failures calculated using aerial orthophotography and LIDAR data were used to estimate the total volume of material transported by the Soldier Creek and Rattlesnake debris flows. These two debris flows resulted from the congregation of multiple slope failures and multiple debris flows distributed across the water shed, rather than a single slope failure and debris flow.

Table 6. Estimated values of debris-flow volume, cross-sectional area, and planimetric area measured for six debris flows in southeastern Arizona that occurred on July 31, 2006.

Name of Event/ Location	Flow Volume (yd^3) V	Maximum Inundated Cross-sectional Area (ft^2) A	Total Inundated Planimetric Area (ft^2) B
Bab Wash, Bowie Mountain	6,600	680	130,000
Esperero Canyon, Santa Catalina Mountains	2,600	570	48,000
Ocho Grande, Santa Catalina Mountains	35,000	210	260,000
Small DF in Soldier Canyon[1]	390	100	15,000
Soldier Canyon, Santa Catalina Mountains	79,000	410	1,300,000
Rattlesnake Canyon, Santa Catalina Mountains	101,000	430	1,200,000

[1] This resulted from a highly visible slope failure near the Catalina Highway at the base of the Santa Catalina Mountains.

Figure 42 shows these data from southeastern Arizona compared to debris-flow data assembled by Griswold and Iverson (2008). The largest cross-sectional areas of the Arizona debris flows are comparable to the world-wide debris-flow data and use of the $c_1 = 0.1$ coefficient proposed by Griswold and Iverson (2008) is appropriate. When comparing planimetric area, however, the southeast Arizona

data plot at the upper range of the world-wide data. In other words, for a given flow volume, a debris flow in southeastern Arizona during the 2006 storm tended to cover a larger area than debris flows elsewhere. This difference may reflect the relatively water-rich and clay-poor properties of the Arizona debris flows; with more water and less clay, the southeastern Arizona debris flows appear to have been more mobile than typical lahars. Based on a linear regression of the southeastern Arizona data, $c_2 = 40$ coefficient is the best fit for debris flows in southeastern Arizona, and this value was used in the subsequent modeling.

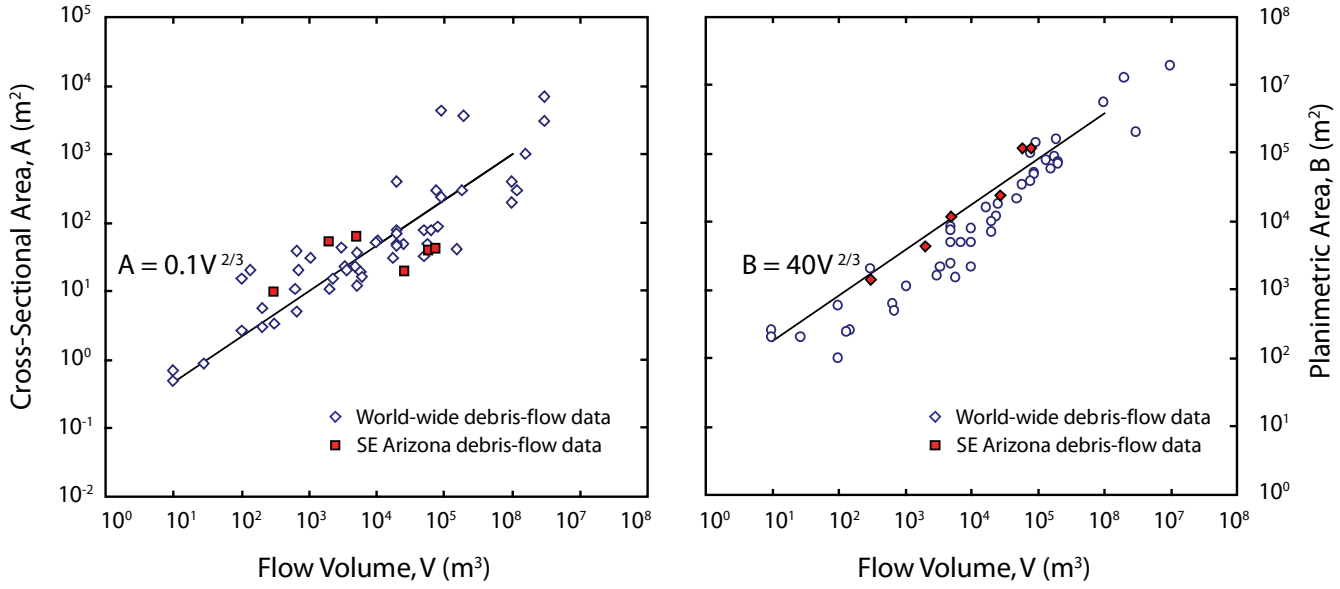

Figure 42. Debris-flow data comparing flow volume with the cross-sectional area, *A*, and the planimetric area, *B*, of the flow. Worldwide data supplied by Griswold and Iverson (2008) are used for LAHARZ. The southeastern Arizona data compare well with the worldwide data for cross-sectional area. For planimetric area, the data from southeastern Arizona suggest that these debris flows tend to cover slightly more area per given flow volume than debris flows elsewhere.

LAHARZ Results

The depositional zones of the five debris flows that approached the front of the Santa Catalina Mountains were modeled with LAHARZ using the failure volumes estimated in this report (table 3), 1-meter digital topography derived from the 2007 LIDAR data, and best-judgment estimates of the start of zones of deposition. For debris flows that exited the mountain front, model start points were set at the mountain front. For the debris flow in Rattlesnake Canyon, the start point was set where the canyon widened significantly and the first large debris-flow deposits were observed. For the debris flow in Bear Canyon, because deposition was widespread, the start point was set just downstream from the last large slope failure. The volume of the debris flow modeled with LAHARZ was chosen to represent the best approximation of the total volume of material mobilized in each catchment. Additional model predictions were also made for each canyon using slightly larger and smaller volumes.

In general, the deposition zones generated by LAHARZ were reasonable. Where debris flows entered onto alluvial fans, they did not travel more than a half mile from the mountain front. Model results most closely matched the extent of deposition in 2006 when the start of the deposition zone

could be clearly determined. In Soldier Canyon, for example, the starting point of the depositional zone was set just downstream from the Catalina Highway culvert, and LAHARZ accurately modeled the existing extent of the depositional zone, predicting that the debris flow would reach and almost cover the Mount Lemmon Short Road (figs. 43 and 44, yellow shading). A larger debris flow would not travel that much further downstream, spreading its volume more evenly across the alluvial fan from this point (fig. 43). Where the starting point of the deposition zone was more ambiguous, LAHARZ results tended to fall short of the known extent of the 2006 debris flows. For Rattlesnake Canyon, LAHARZ under-predicted the extent of the depositional zone, stopping about 1,000 ft short of the confluence with Sabino Creek (fig. 45). As mentioned above, Rattlesnake Canyon is known to have a complex arrangement of deposition and transport zones along its entire length.

For both Bear Canyon and the unnamed canyon draining Gibbon Mountain, the LAHARZ zones of deposition fell short of the last observed deposits of debris-flow material (figs. 46 and 47). In both cases, discrete, disconnected debris-flow deposits were observed along the lower channels of these washes, suggestive of disturbance and reworking by following streamflow floods, a flow mechanism that LAHARZ cannot account for. In addition, the LAHARZ model tended to simulate a much deeper and wider depositional zone than we observed in the field. The debris-flow deposits appear to have been reworked by streamflow at and near the mountain front, obscuring any field evidence. We believe a different set of proportionality coefficients more typical of a lahar might better predict the depositional area of this debris flow, but we do not have sufficient evidence to justify this change.

Bird Canyon was perhaps the most difficult canyon to model. Field evidence suggests that the depositional zone of the debris flow in Bird Canyon was primarily in the upper-half of the drainage, with only a few discrete debris-flow deposits near the mountain front. Using a model start point where the canyon first widens notably, the LAHARZ simulation greatly over predicted the travel length of the debris flow and the resulting area of the depositional zone (fig. 48).

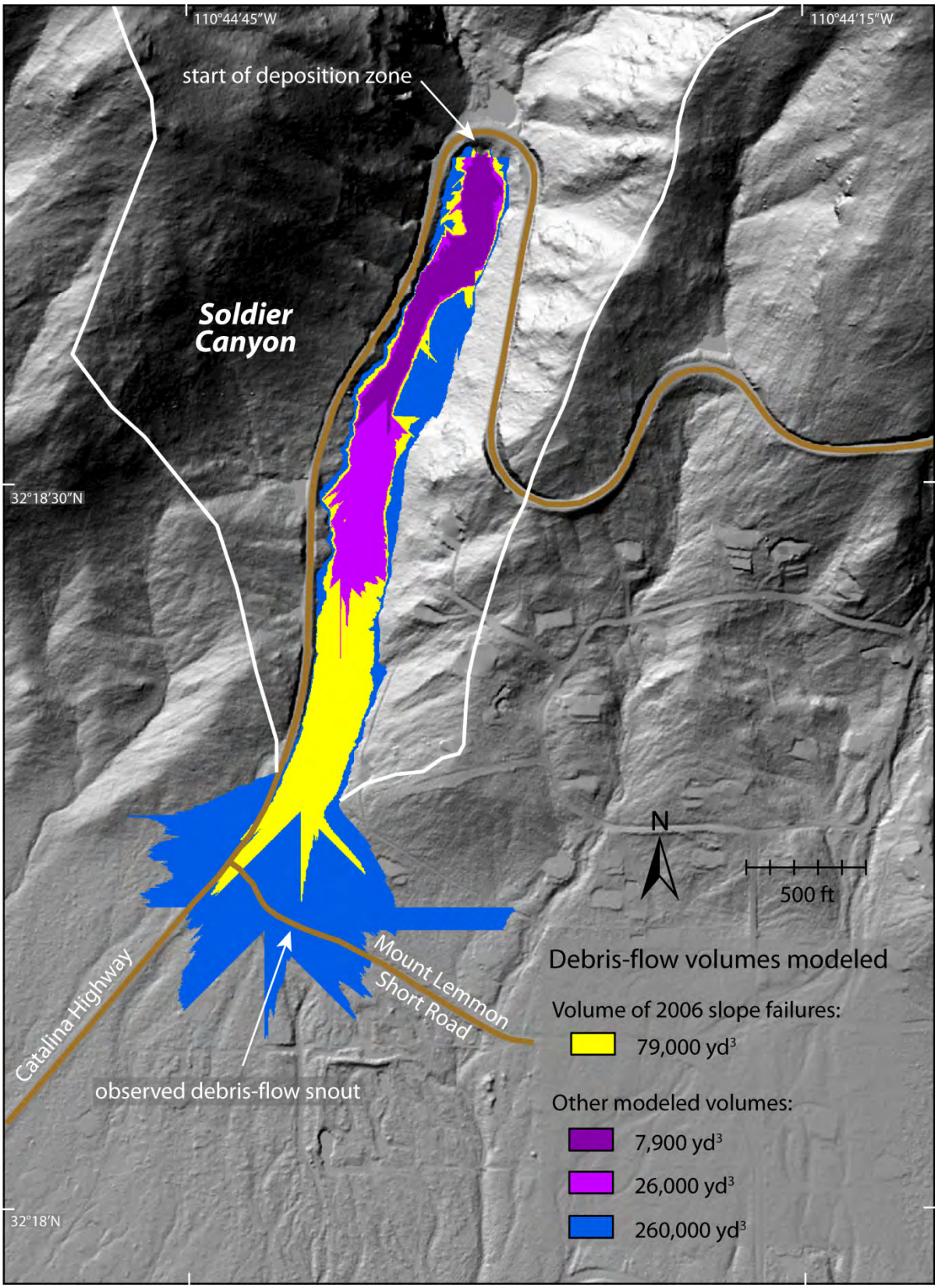

Figure 43. Results of the LAHARZ simulation superimposed on the DEM at Soldier Canyon. The volume of material mobilized from slope failures in Soldier Canyon on July 31, 2006, was about 78,000 yd³ (yellow shading). LAHARZ predicted this size of debris flow would just approach the Mount Lemmon Short Road; the 2006 debris flow actually stopped just beyond this road (see fig. 2).

Figure 44. (September 13, 2006) This oblique aerial photograph of the snout of the Soldier Canyon debris flow shows that debris-flow deposits filled the culvert at the bend in the Mount Lemmon Short Road (upper center), and streamflow deposits related to the debris flow surrounded the house at lower left (C.S. Magirl).

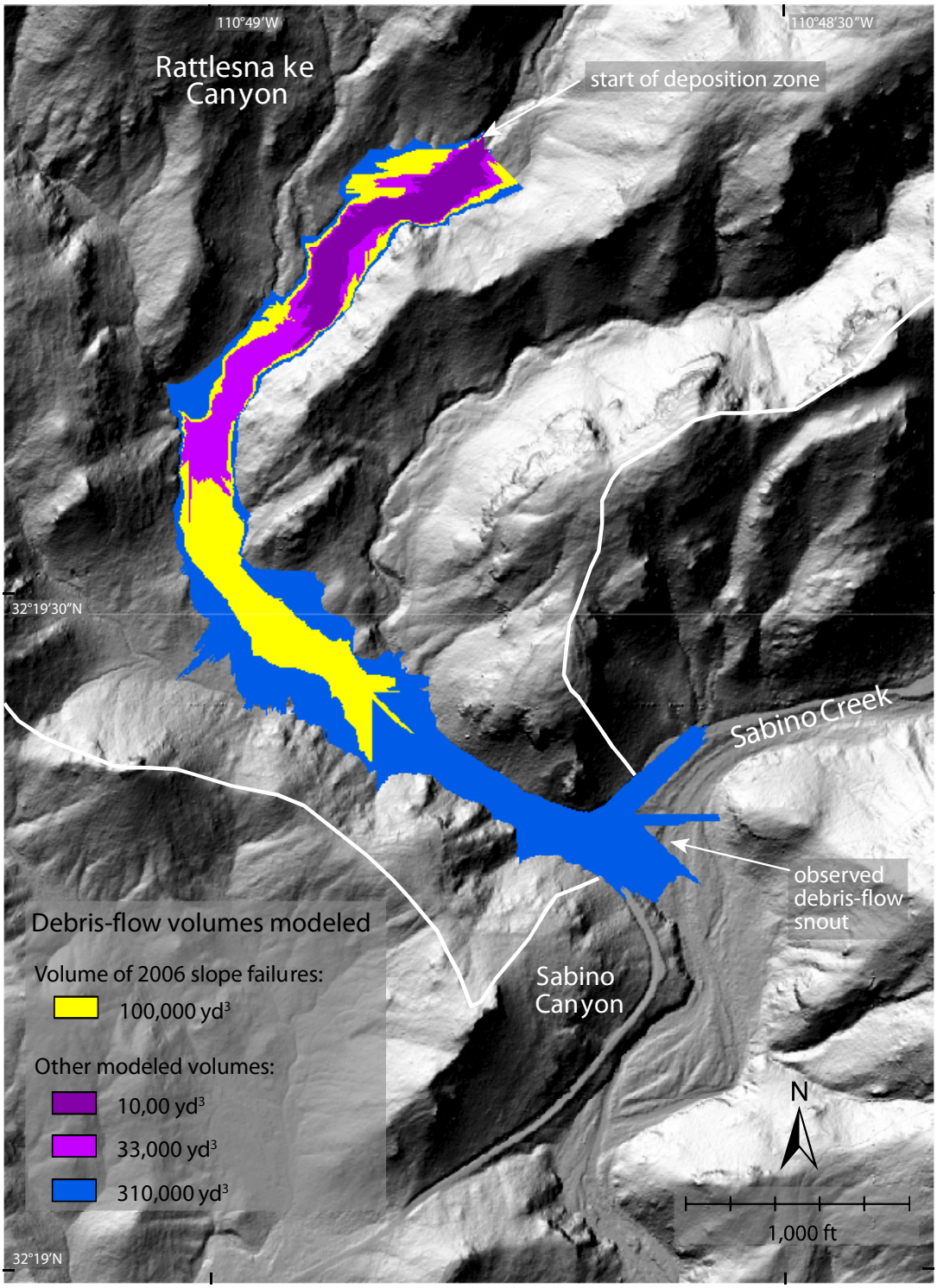

Figure 45. Results of the LAHARZ simulation superimposed on the DEM at Rattlesnake Canyon. The estimated volume of material mobilized in the Rattlesnake watershed on July 31, 2006, was about 100,000 yd³ (yellow shading), but some of that sediment was deposited in lateral levees along the channel. LAHARZ predicted that a much larger debris flow of about 310,000 yd³ (blue shading) would be needed to reach Sabino Creek despite the fact that the 2006 event did indeed reach the channel (see fig. 2).

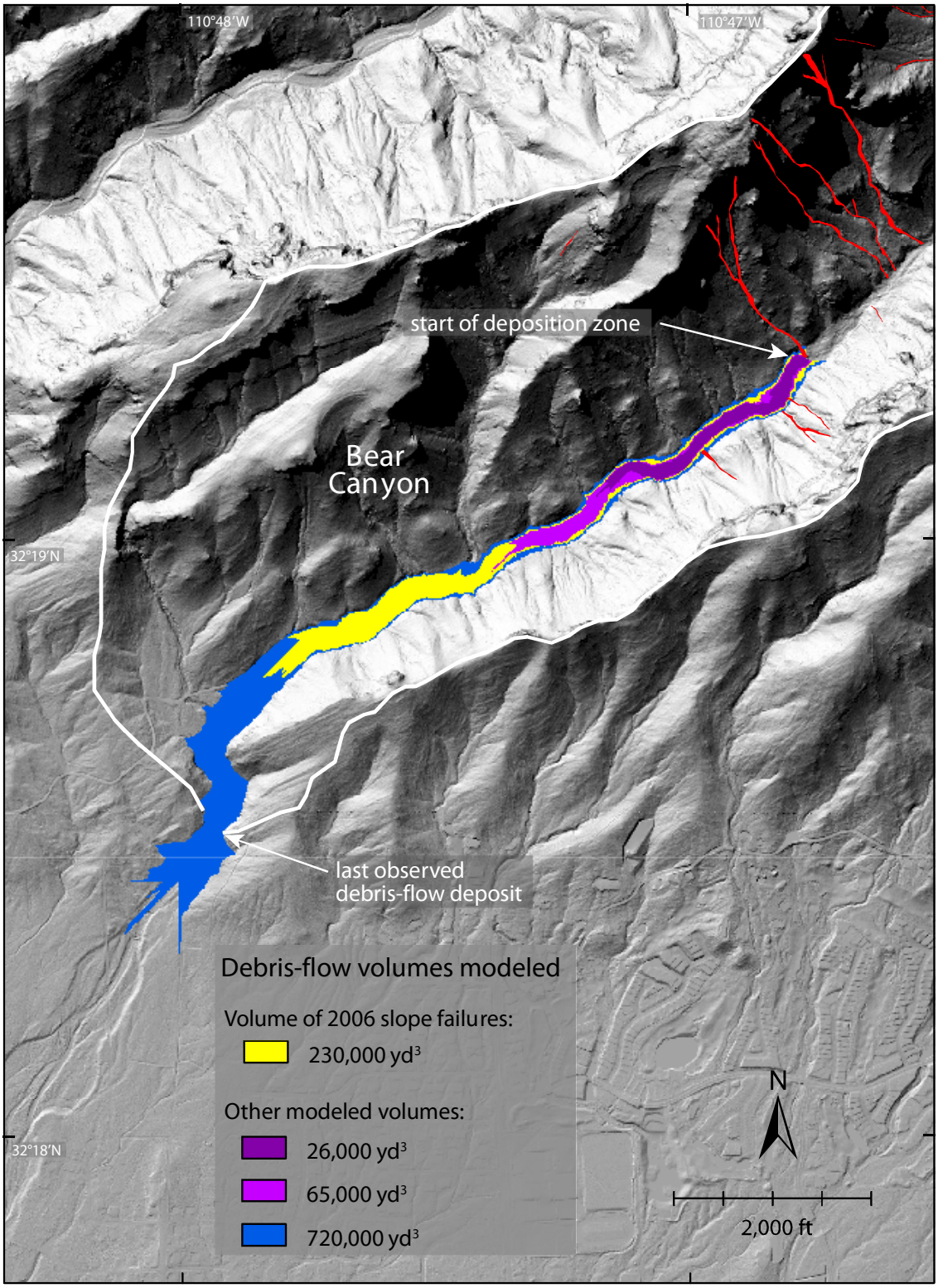

Figure 46. Results of the LAHARZ simulation superimposed on the DEM at Bear Canyon; the slope failures in the Bear Canyon watershed are shown in red. The volume of material mobilized from slope failures in this watershed on July 31, 2006, was about 230,000 yd³ (yellow shading). Field evidence showed the debris flow moved to near the mountain front (see fig. 2).

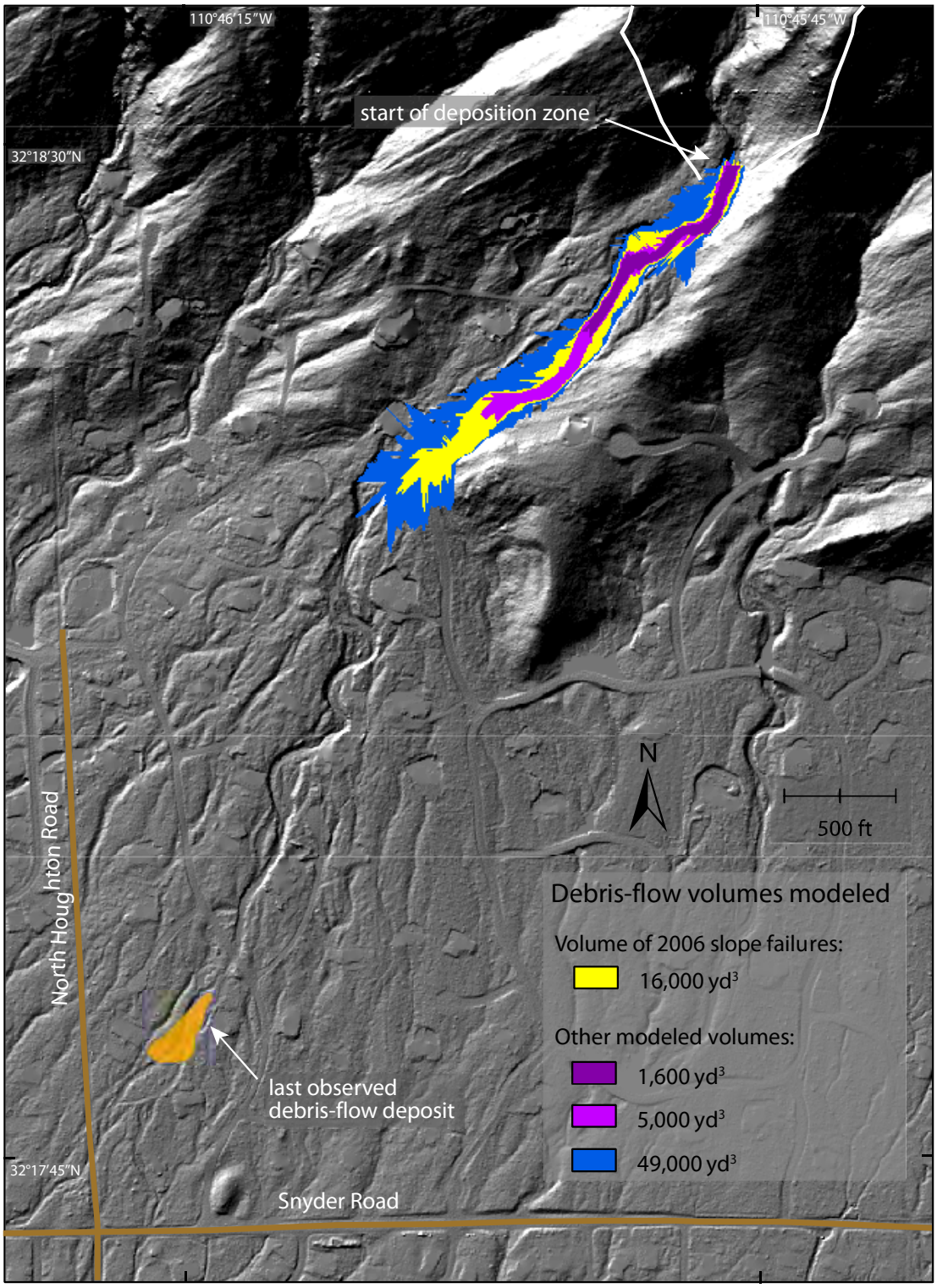

Figure 47. Results of the LAHARZ simulation superimposed on the DEM at the unnamed canyon draining the region below Gibbon Mountain. The volume of material mobilized from slope failures in this watershed on July 31, 2006, was about 13,000 yd³ (yellow shading). We located a fresh debris-flow deposit about 0.5 mile from the mountain front (orange shading), much farther out on the debris fan than LAHARZ predicts.

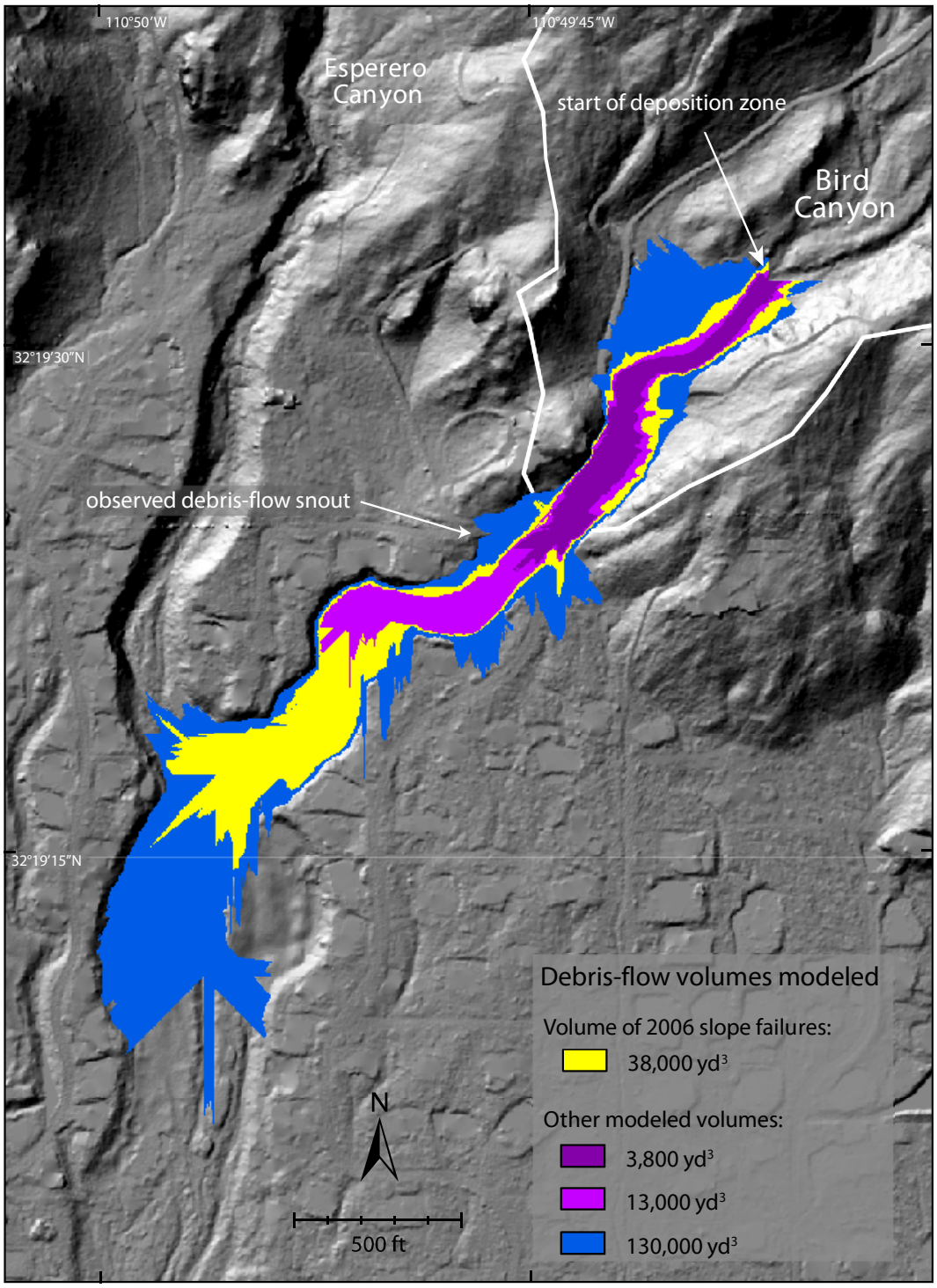

Figure 48. Results of the LAHARZ simulation superimposed on the DEM at Bird Canyon. The volume of material mobilized from slope failures in the Bird watershed on July 31, 2006, was about 39,000 yd³ (yellow shading), but most of that sediment was deposited in the upper half of the watershed. Had that total volume of material arrived at the mountain front, LAHARZ predictions suggest that the area of inundation would have been much larger.

Discussion and Conclusions

Relation to Precipitation Magnitude and Frequency

The ensemble of available hydrologic data indicates that the spate of slope failures and debris flows that occurred on July 31 and August 1, 2006, in southeastern Arizona was caused by extreme precipitation of historically unprecedented proportions for this region. The spate of debris flows in southeastern Arizona in July 2006 followed extreme, multiday precipitation. Some precipitation intensity and daily totals on July 31 and August 1 were unusual for southeastern Arizona during the North American Monsoon; the 24-hr total at Coronado National Memorial of 8.50 in. is exceptional. The Arizona state 24-hour precipitation record is 10.99 in. at Workman Creek 1 in central Arizona during Tropical Storm Norma (Kangieser, 1972), and the highest one-day total during the October 1983 floods was 5.10 in. for Mount Lemmon (Roeske and others, 1989).

Rainfall on July 31 and August 1 fell on nearly saturated soils. Multiday storm totals, which reflect antecedent conditions and amount of soil saturation (Griffiths and others, in press), had recurrence intervals exceeding 1,000 years at several sites, both for measurements made in rainfall gages and rainfall spatially averaged by weather radar. Record floods were generated from watersheds subjected to this magnitude of precipitation; in several cases, long-term gaging stations had record floods that equaled or exceeded the 100-year recurrence interval.

For future assessments of debris-flow hazard in this region, it is desirable to know what combination of rainfall intensity and storm duration is required to initiate widespread slope failures. Shallow landslides and associated debris flows induced by rainfall can result from intense, short-lived events or from less-intense but longer-duration rainfall. Many researchers have proposed intensity-duration thresholds as a predictive tool to estimate likelihood of slope failures and debris flows (Wieczorek and Glade, 2005). In areas with relatively frequent debris-flow activity in Arizona, such as Grand Canyon (Webb and others, 2000; Griffiths and others, 2004), insufficient meteorological data are available to assess an intensity-duration threshold.

One of the early attempts at establishing a threshold was made by Caine (1980), who used shallow landslide data to generate a linear threshold relating rainfall intensity, I (in/h), and rainfall duration, D (h),

$$I = 0.58D^{-0.39}. \qquad (3)$$

For a given duration of rainfall, equation (3) defines the rainfall intensity above which shallow slope failures are likely. The equation was constructed using data gathered worldwide and reflects a wide range of climate, soil types, and precipitation regimes that may differ significantly from conditions in Arizona. Because the Santa Catalina Mountains were well instrumented in July 2006, the opportunity exists to estimate an intensity-duration threshold that better models the conditions particular to southeastern Arizona. The results are plotted with the Caine (1980) threshold in figure 49.

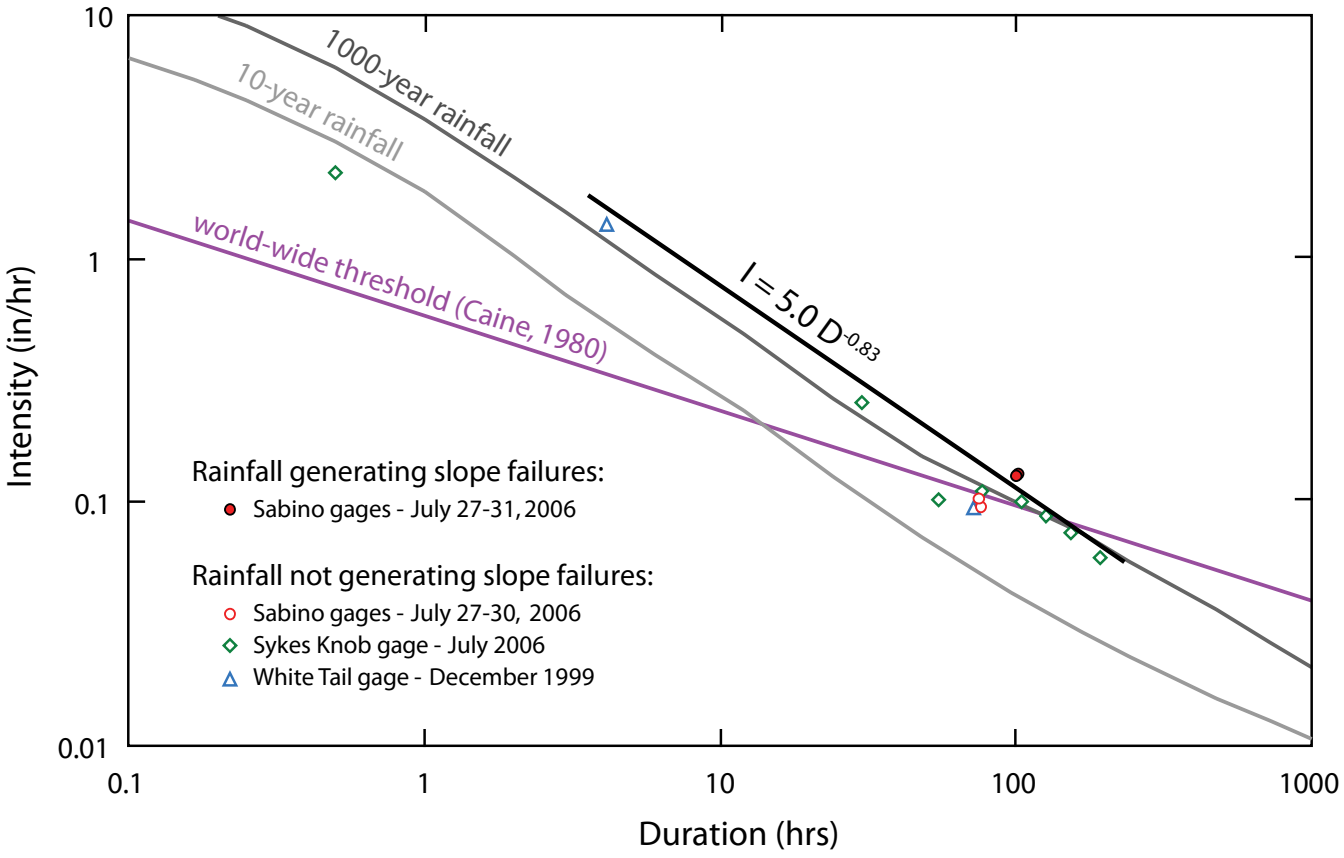

Figure 49. A intensity-duration relation for three locations for the final week of July 2006 and one location for a storm in December 1999 in the Santa Catalina Mountains. Multiple slope failures occurred in the vicinity of the Sabino gages (Middle and Upper) after five days of rainfall ending on July 31. Slope failures did not occur at all in the vicinity of Sykes Knob, a gage location near Mount Lemmon, during the July 2006 storms, nor at White Tail during short-duration, high-intensity rain in December 1999. The rainfall intensities for both the 1999 and 2006 storms at all sites are generally above Caine's (1980) intensity-duration threshold for shallow landslides worldwide, but the 10-year rainfall-recurrence curve for 5,000 ft elevation in the Santa Catalina Mountains (from *http://hdsc.nws.noaa.gov/hdsc/pfds/sa/az_pfds.html*, accessed June 15, 2008) indicates that high-intensity, short-duration storms are commonplace in the monsoon-dominant climate of southeastern Arizona. Based on the precipitation data collected near slope failures, a minimum rainfall intensity-duration threshold of $I = 5.0\ D^{-0.83}$ was generated for slope failures in the Santa Catalina Mountains.

Of the available rainfall gages in the Santa Catalina Mountains, only two (Middle Sabino and Upper Sabino; see fig. 2) recorded rainfall within the area of the slope failures. From July 27 through July 31, 13.54 in. of rain fell at the Middle Sabino gage and 12.80 in. of rain fell at the Upper Sabino gage, resulting in rainfall intensities of 0.13 in/hr over 102 hours and 0.13 in/hr over 104 hours, respectively. These are the only two data representing rainfall that triggered slope failures on July 31 in the Santa Catalina Mountains (fig. 49).

To bracket the local slope-failure threshold as closely as possible, we also plotted the highest recorded rainfalls that did not generate slope failures. Because slope failures did not occur until July 31, rainfall at the two Sabino gages over the four days from July 27 through July 30 (0.10 in/hr over 76 hours and 0.094 in/hr over 77 hours) represent rainfall that falls beneath the slope-failure threshold (fig. 49). Of the other gages outside the region of slope failures, the gage at Sykes Knob (near Mount

Lemmon at an elevation of 7,812 ft; see fig. 2), recorded the highest levels of rainfall from July 27 through July 31: 11.11 in. over 126.5 hours for an intensity of 0.088 in/hr (fig. 49). For this gage, we also include the peak intensity recorded over this time period for a variety of durations, none of which resulted in slope failures. We also include data from another intense thunderstorm that did not generate slope failures in the Santa Catalina Mountains. In the early morning hours of July 15, 1999, 5.79 in. of rain fell over 4.2 hours at a Pima County Alert rainfall gage located at White Mountain (fig. 2) for an intensity of 1.39 in/hr (fig. 49). This was the final storm in a series of storms over 72 hours that dropped a total of 6.81 in. at the White Tail gage (0.095 in/hr).

To analyze how extreme the intensity of rainfall was for these two gages during July 2006, intensity-duration data were assembled using NOAA statistics for return frequency of rainfall (*http://hdsc.nws.noaa.gov/hdsc/pfds/sa/az_pfds.html*, accessed June 26, 2008). Calculating the NOAA recurrence interval for the Santa Catalina Mountains at 5,000 ft near Thimble Peak, the intensity-duration curves for both 10- and 1,000-year events were plotted directly on figure 49. As previously discussed, the highest recorded rainfall intensities for the 2006 storm were significantly higher than the intensity expected for a 1,000-year storm for durations longer than 50 hours. The 1999 storm, in contrast, was very intense and short lived, producing a rainfall intensity that was on the order of a 1,000-year recurrence interval for a one-day event.

Plotting the intensity-duration threshold proposed by Caine (1980) directly on figure 49 suggests not only that rainfall as measured at the Middle and Upper Sabino gages should produce slope failures (which it did), but that rainfall at both Sykes Knob in 2006 and White Mountain in 1999 should have also produced slope failures (which did not happen). The Caine (1980) threshold does not accurately predict slope failures in southeastern Arizona, in part because thunderstorms are common in the Santa Catalina Mountains and hillslopes may have adjusted to the regular occurrence of intense precipitation. We hypothesize that colluvial hillslopes in the Santa Catalina Mountains may be stable at higher rainfall intensities than the average case worldwide (Caine, 1980). As the NOAA magnitude-frequency data indicate, long duration, heavy rainfall is rare in southeastern Arizona, and our comparison of the NOAA data and the Caine (1980) threshold for durations >100 hours supports this observation.

Using the data available from the 2006 and 1999 storms, a unique slope-failure threshold was constructed for climatic, topographic, and geomorphic characteristic of southeastern Arizona. We separated the rainfall intensities in areas with slope failures from intensities where failures did not occur during 2006, and the threshold relation is given by

$$I = 5.0D^{-0.83}. \qquad (4)$$

This threshold (fig. 49) applies to rainfall durations between 4 and 200 hours. It should be stressed, however, that the data for actual slope-failure occurrence are extremely limited, and this relation should be considered a rough first estimate. It is important to note the threshold portrayed in equation (4) closely follows the intensity-duration curve for a 1,000-year storm in the Santa Catalina Mountains.

Relation to Wildland Fires

Considered as a group, the slope failures and debris flows that occurred on July 31, 2006, were not related to wildland fire, although burned areas enhanced the occurrence of slope failures locally. Cannon and Gartner (2005) found enhanced debris-flow potential on hill slopes affected by forest fires decreases to pre-fire levels in about two years; they also found the great majority of post-fire debris flows initiate through the process of progressive sediment bulking rather than discrete slope failures, which is the dominant failure mode observed in southeastern Arizona.

In 2003, the Aspen Fire, the largest historical wildfire in the Santa Catalina Mountains, burned 85,000 acres of forest and shrubland on a mountain range spanning 3,000-8,000 ft in elevation. Fire severity was highest near the top of the range (fig. 50). Three years after the fire, 89 percent of the slope failures were either in unburned or low-severity-burned areas. Although a 2006 fire in Coronado National Memorial occurred almost two months before the late July storms, only about a third of the debris flows here originated from slope failures in burned areas (A. Youberg, written commun., 2008). Other areas with large numbers of slope failures had not burned recently. For example, the most recent fire on Bowie Mountain was in the 1920s (Larry Ludwig, National Park Service, oral commun., 2007). Likewise, the area of slope failures in Aravaipa Canyon had not burned for an indeterminate number of years; moreover, the vegetation zone in this canyon, located in the Arizona Upland subdivision of the Sonoran Desert (Turner and Brown, 1994), is rarely affected by rangeland fires.

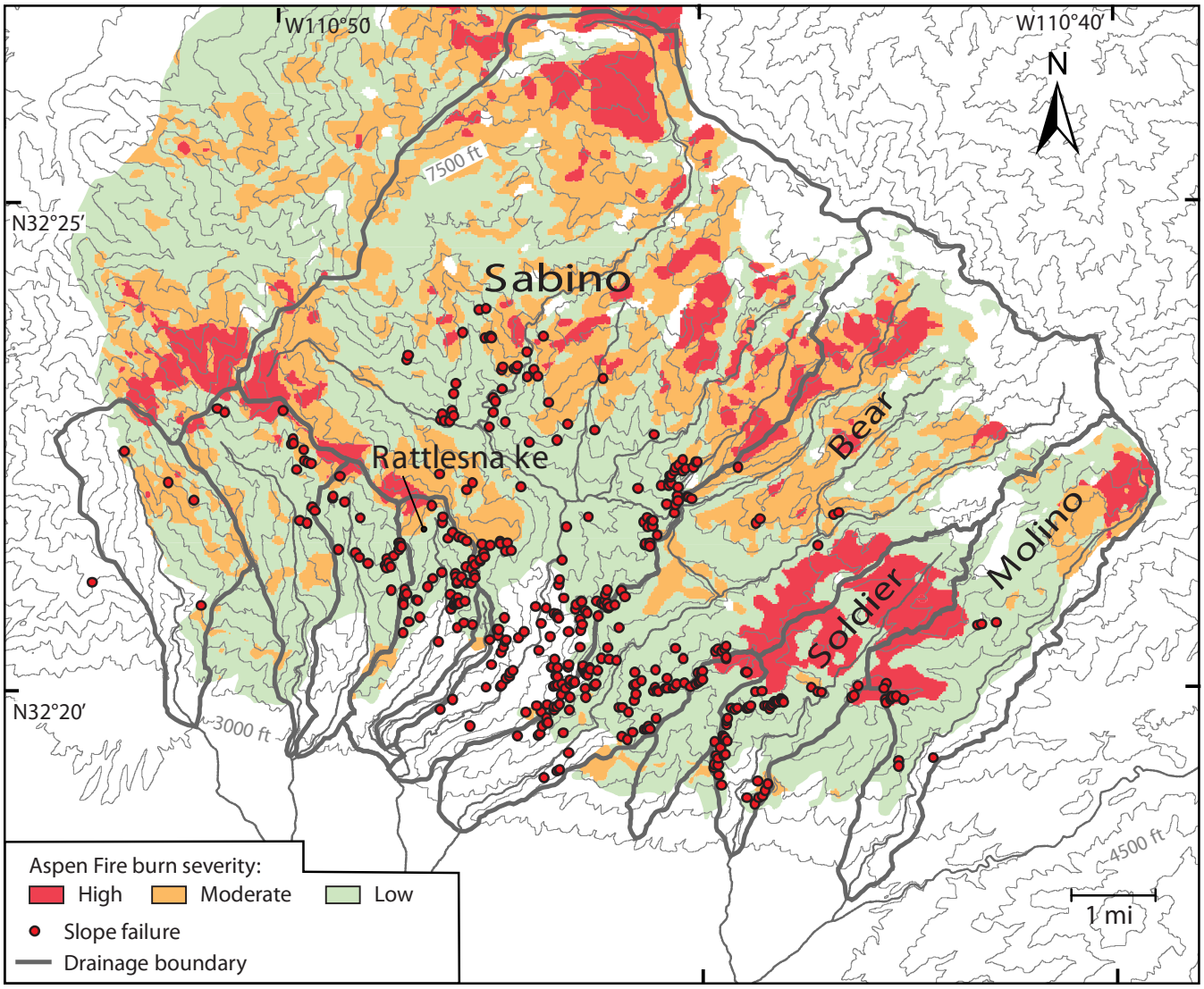

Figure 50. Relation of 435 slope failures to the intensity of the 2003 Aspen Fire in the southern Santa Catalina Mountains. Only the area of the Aspen Fire in which slope failures occurred during July 2006 is shown. Only 11 percent of the mapped failures were within high- or moderate-intensity regions of the Aspen Fire.

Sediment Yield from Slope Failures and Debris Flows

Analysis of aerial and satellite imagery reveals that 435 slope failures occurred in 10 drainage basins of the southern Santa Catalina Mountains during late July 2006. These failures typically initiated where the wedges of colluvium that thinly blanket the canyon give way to steep walls of bedrock toward the top of drainage divides (figs. 5, 7, and 35). In almost every case, these narrow failures eroded through the colluvium and down to bedrock, delivering a collective estimate of 1.5 million tons of very poorly sorted sediment to the canyon bottoms in the form of debris flows, including 0.72 million tons in Sabino Canyon alone. Although some of this material was transported out of the watersheds as debris flows, most still remains as deposits along stream channels. The debris-flow deposits are very coarse, consisting of only 0.3 percent silt and clay and 64 percent cobbles and boulders (b-axis >64 mm) by weight. Assuming cobbles and boulders are unlikely to be entrained by normal streamflow, only 36 percent, or 527,000 tons of sediment (gravel, sand, silt and clay) has the potential of exiting the Santa Catalina Mountains and moving into Agua Caliente and Rillito Creek.

Figure 51. (September 14, 2006) Deposition in the headwaters of Soldier Creek caused by the combination of the 2003 Aspen Fire and the 2006 debris flows in the watershed filled the channel, eliminating the usefulness of the pedestrian bridge (left center) in the Gordon Hirabayashi Picnic Area (C.S. Magirl).

This unconsolidated sediment potentially poses a hazard to fixed-conveyance floodplain structures in Rillito Creek. However, our analyses suggest that deposition in the channel would be modest, even in the unlikely event that all the sediment displaced in the 2006 slope failures were to arrive in the channel simultaneously. It should be noted that sediment from the 2006 debris flows are not the only source of additional sediment from the Sana Catalina Mountains; denudation of hillslopes during the Aspen Fire in 2003 also contributed to increased sedimentation of fine particles, much of which is still stored in stream channels in the canyons and available for entrainment by future floods (fig. 51).

Acknowledgments

Numerous individuals, groups, and agencies helped with the collection of observational and quantitative data on floods and debris flows in southeastern Arizona during the summer of 2006. The

U.S. Forest Service helped provide access to Sabino Canyon, and Salek Shafiqullah, a hydrologist with Coronado National Forest, was extremely helpful and encouraging. David Lazaroff and James Klein generously provided historical photographs of Sabino Creek and other canyons in the southern Santa Catalina Mountains. Some rainfall and runoff data were provided by Pima County Regional Flood Control District as part of their ALERT program. The BLM ranger at Aravaipa, Patrick O'Neill, was kind enough to accompany us for a distance into the western end of the canyon during our visit there, and Larry Ludwig, Unit Manager at Fort Bowie National Historic Site, escorted us to Bab Wash and provided data on rainfall amounts at the park and near Bowie Mountain. Melissa Amentt of the Bureau of Land Management provided rainfall data for Apache Pass. Jeff Balmat and Colleen Filippone of the National Park Service provided additional precipitation and hydrologic data for Fort Bowie, and Colleen Filippone provided post-event photos that were used to analyze the failure near Bowie Mountain. Julie Griswold, Steve Schilling, and Dick Iverson supplied debris-flow data and provided training and support for the LAHARZ software. Evan Canfield, Mark Krieski, Fazle Karim and Akitsu Kimoto, from the Pima County Regional Flood Control District, reviewed the manuscript.

References Cited

Adams, D.K., and Comrie, A.C., 1997, The North American Monsoon: Bulletin of the American Meteorological Society, v. 78, p. 2197-2213.

Betancourt, J.L., 1990, Tucson's Santa Cruz River and the arroyo legacy: Tucson, Arizona, University of Arizona, unpublished Ph.D dissertation, 232 p.

Bonnin, G.M., Martin, D., Lin, B., Parzybok, T., Yekta, M., and Riley, D., 2006, Precipitation-frequency atlas of the United States, volume 1 version 4.0—Semiarid Southwest (Arizona, southeast California, Nevada, New Mexico, Utah): Silver Springs, Maryland, National Oceanic and Atmospheric Administration, NOAA Atlas 14, 261 p.

Caine, N., 1980, The rainfall intensity–duration control of shallow landslides and debris flows: Geografiska Annaler, v. 62, series A, issues 1-2, p. 23-27.

Cannon, S.H., and Gartner, J.E., 2005, Wildfire-related debris flow from a hazards perspective, *in* Hungr, O. and M. Jacob, eds., Debris-Flow Hazards and Related Phenomena: Springer-Praxis Books in Geophysical Sciences, p. 321-344.

Cooke, R., Warren, A., and Goudie, A. 1993, Desert geomorphology: London, University College London Press, 526 p.

Costa, J.E., 1988, Rheologic, geomorphic, and sedimentologic differentiation of water floods, hyperconcentrated flows, and debris flows, *in* Baker, V.R., Kochel, R. C., and Patton, P.C., eds., Flood Geomorphology: John Wiley and Sons, New York, p. 113-122

Costa, J.E., and Williams, G.P., 1984, Debris-flow dynamics: U.S. Geological Survey Open File Report 84-606, 1 VHS videotape, *http://pubs.er.usgs.gov/usgspubs/ofr/ofr84606*, accessed June 20, 2008.

Desilets, S.L.E., Nijssen, B., Ekwurzel, B., and Ferré, T.P.A., 2007, Post-wildfire changes in suspended sediment rating curves: Sabino Canyon, Arizona: Hydrological Processes, v. 21, p. 1413-1423. doi: 10.1002/hyp.6352.

Douglas, M.W., 1995, The summertime low-level jet over the Gulf of California: Monthly Weather Review, v. 123, p. 2334-2347.

Folk, R.L., 1974, Petrology of sedimentary rocks: Austin, Texas, Hemphill Publishing, 182 p.

Force, E.R., 1997, Geology and mineral resources of the Santa Catalina Mountains, southeastern Arizona: Tucson, Arizona, Center for Mineral Resources, Monograph of Mineral Resources Science, No. 1, 135 p.

Gosse, J.C., and Phillips, F.M., 2001, Terrestrial in situ cosmogenic nuclides: theory and application: Quaternary Science Reviews, v. 20, p. 1475-1560.
Greene, J.A., 1980, Historic structure report, Historical data section, Fort Bowie: Its physical evolution, 1862-1894, Fort Bowie National Historic Site, Arizona: Denver, Colorado, National Park Service, Branch of Historic Preservation, 520 p.
Griffiths, P.G., Webb, R.H., and Melis, T.S., 2004, Initiation and frequency of debris flows in Grand Canyon, Arizona: Journal of Geophysical Research, Surface Processes, v. 109, F04002, doi:10.1029/2003JF000077, 14 p.
Griffiths, P.G., Magirl, C.S., Webb, R.H., Pytlak, E., and Lyon, S., in press, Spatial precipitation frequency of an extreme event: the July 2006 mesoscale convective complexes and floods in southeastern Arizona: Water Resources Research.
Griswold, J.P., and Iverson, R.M., 2008, Mobility statistics and automated hazard mapping for debris flows and rock avalanches: U.S. Geological Survey Scientific Investigations Report 2007-5276, 59 p.
Hales, J.E., Jr., 1975, A severe Southwest desert thunderstorm: 19 August 1973: Monthly Weather Review, v. 103, p. 344-351.
Iverson, R.M., 1997, The physics of debris flows: Reviews of Geophysics, v. 35, no. 3, p. 245-296.
Iverson, R.M., and Vallance, J.W., 2001, New views of granular mass flows: Geology; v. 29, p. 115–118.
Iverson, R.M., Schilling, S.P., and Vallance, J.W., 1998, Objective delineation of lahar-inundation hazard zones: Geological Society of America Bulletin, v. 110, p. 972-984.
Kangieser, P.C., 1972, Unusually heavy 24-hour rainfall at Workman Creek 1, Arizona: Monthly Weather Review, v. 100, p. 206-207.Kellerhals, R., and Bray, D.K., 1971, Sampling procedures for coarse fluvial sediments: American Society of Civil Engineers, Journal of the Hydraulics Division, v. 97, p. 1165-1180.
Landel, G., Smith, J.A., Baeck, M.L., Steiner, M., and Ogden, F.L., 1999, Radar studies of heavy convective rainfall in mountainous terrain: Journal of Geophysical Research, Atmospheres, v. 104(D24), p. 31,451-31,465.
Larsen, M.C., 2008, Rainfall-triggered landslides, anthropogenic hazards, and mitigation strategies: Advances in Geosciences, v. 14, p. 147-153.
Maddox, R.A., Chappell, D.F., and Hoxit, L.R., 1979, Synoptic and meso-α scale aspects of flash flood events: Bulletin of the American Meteorological Society, v. 60, p. 115-123.
Maddox, R.A., McCollum, D.M., and Howard, K.W., 1995, Large-scale patterns associated with severe summertime thunderstorms over central Arizona: Weather Forecasting, v. 10, p. 763-778.
Magirl, C.S., Webb, R.H., Schaffner, M., Lyon, S.W., Griffiths, P.G., Shoemaker, C., Unkrich, C.L., Yatheendradas, S., Troch, P.A., Pytlak, E., Goodrich, D.C., Desilets, S.L.E., Youberg, A., and Pearthree, P.A., 2007, Impact of recent extreme Arizona storms: EOS, v. 88, no. 17, p. 191, 193.
McCollum, D.M., Maddox, R.A., and Howard, K.W., 1995, Case study of a severe mesoscale convective system in central Arizona: Weather Forecasting, v. 10, p. 643-665.
Melis, T.S., Webb, R.H., and Griffiths, P.G., 1997, Debris flows in Grand Canyon National Park: Peak discharges, flow transformations, and hydrographs, *in* Chen, Cheng-lung, ed., Debris-flow hazards mitigation: Mechanics, prediction, and assessment: New York, American Society of Civil Engineers, p. 727-736.
O'Neill, P., 2006, Photo journal: Southwest Hydrology, v. 5, p. 35.
Osterkamp, W.R., 2008, Annotated definitions of selected geomorphic terms and related terms of hydrology, sedimentology, soil science and ecology: U.S. Geological Survey Open File Report 2008-1217, 49 p.

Pearthree, P.A., and Youberg, A., 2006, Recent debris flows and floods in southern Arizona: Arizona Geology, v. 36, 6 p.
Pierson, T.C., and Costa, J.E., 1987, A rheologic classification of subaerial sediment-water flows: Geological Society of America, Reviews in Engineering Geology, v. VII, p. 1-12.
Pierson, T.C., and Scott, K.M., 1985, Downstream dilution of a lahar: transition from debris flow to hyperconcentrated streamflow: Water Resources Research, v. 21, no. 10, p. 1511-1524.
Pytlak, E., Goering, M., and Bennett, A., 2005, Upper tropospheric troughs and their interaction with the North American Monsoon: paper presented at the 19th Conference on Hydrology, 85th Annual Meeting of the American Meteorological Society, CD-ROM, JP2.3, American Meteorological Society, San Diego, California.
Rice, S., and Church, M., 1996, Sampling surficial fluvial gravels—The precision of size distribution percentile estimates: Journal of Sedimentary Research, v. 66, p. 654-665.
Roberts, L. K., 1986, Paleohydrologic reconstruction, hydraulics, and frequency-magnitude relationships of large flood events along Aravaipa Creek, Arizona: Tucson, Arizona, University of Arizona, unpublished M.S. thesis, 63 p.
Roeske, R.H., Garrett, J.M., and Eychaner, J.H., 1989, Floods of October 1983 in southeastern Arizona: U.S. Geological Survey Water-Resources Investigations Report 85-4225-C, 77 p.
Schilling, S.P., 1998, LAHARZ: GIS programs for automated mapping of lahar-inundation hazard zones: U.S. Geological Survey Open-File Report 98-638, 80 p.
Turner, R.M., and Brown, D.E., 1994, Sonoran Desertscrub, *in* Brown, D.E., ed., Biotic communities, southwestern United States and northwestern Mexico: Salt Lake City, University of Utah Press, p.181-222.
Turner, R.M., Webb, R.H., Bowers, J.E., and Hastings, J.R., 2003, The changing mile revisited: Tucson, Arizona, University of Arizona Press, 334 p.
U.S. Water Resources Council, 1981, Guidelines for determining flood flow frequency: Washington, D.C., U.S. Interagency Advisory Committee on Water Data, Hydrology Subcommittee, Bulletin 17B, 28 p. plus appendices.
Webb, R.H., Griffiths, P.G., Melis, T.S., and Hartley, D.R., 2000, Sediment delivery by ungaged tributaries of the Colorado River in Grand Canyon: U.S. Geological Survey Water Resources Investigations Report 00-4055, 67 p.
Webb, R.H., Boyer, D.E., and Turner, R.M., 2007a, The Desert Laboratory Repeat Photography Collection—An invaluable archive documenting landscape change: U.S. Geological Survey Fact Sheet 2007-3046, 4 p.
Webb, R.H., Leake, S.A., and Turner, R.M., 2007b, The ribbon of green—Change in riparian vegetation in the southwestern United States: Tucson, University of Arizona Press, 462 p.
Wells, S.G., and Harvey, A.M., 1987, Sedimentologic and geomorphic variations in storm-generated alluvial fans: Geological Society of America Bulletin, v. 98, p. 182-198.
Wieczorek, G.F., and Glade, T., 2005, Climatic factors influencing occurrence of debris flows, *in* M. Jakob and O. Hungr, eds., Debris-flow Hazards and Related Phenomena: Springer, New York, p. 325-362.
Wohl, E.E., and Pearthree, P.A., 1991, Debris flows as geomorphic agents in the Huachuca Mountains of southeastern Arizona: Geomorphology, v. 4, p. 273-292.
Wolman, M.G., 1954, A method of sampling coarse-river-bed material: Transactions of the American Geophysical Union, v. 35, no. 6, p. 951-956.
Youberg, A., Pearthree, P.A., and Baker, V.R., 2006, Comparison of debris flows generated in adjacent unburned and recently-burned areas, Coronado National Memorial, Arizona: San Francisco,

California, American Geophysical Union, Fall Conference, Abstract No 12661, Paper No H53D-0661.
Youberg, A., Cline, M.L., Cook, J.P., and Pearthree, P.A., 2008, Geologic mapping of debris flow deposits in the Santa Catalina Mountains, Pima County, Arizona: Arizona Geological Survey Open-File Report 08-06.

Glossary

This glossary uses the authors' experiences in the southwestern United States, as well as numerous references, to provide definitions of terms used in this report. For other information, perhaps counterpoint to these definitions, readers should refer to Pierson and Costa (1987), Cooke and others (1993), and Osterkamp (2008).

Alluvial Fan Here we use a geomorphic definition that has no legal flood-hazard designation. An alluvial fan is a depositional surface emanating from a channel that debouches from a mountain range or other incised/confined drainage or channel system. Alluvial fans are constructed from fluvially transported sediment (for example, streamflow and (or) debris-flow deposits) and may contain a small amount of colluvium derived from rock avalanches or rockfalls that occur near their apices. This definition does not distinguish between alluvial fans with fan-head entrenchment or fully incised channels and those with little or no channel definition (or distributary channels) that are more common in more tectonically active areas than southern Arizona.

Annual Flood Series A time series of the annual peak discharges for a streamflow gaging station that is used in flood-frequency analysis.

Atmospheric Deformation Zone Region of atmospheric divergence and instability that promotes convection, particularly mesoscale convective systems.

Avulsion An abrupt shift in channel position, caused either by erosion across a floodplain terrace or by deposition within the main channel, that occurs during a flood. Avulsions occur in debris flows and streamflow floods alike but have different signature effects on the landscape.

b-Axis Diameter If a particle is assumed to be an elliptical solid, the b-axis is the intermediate-axis dimension, as opposed to the long-axis or short-axis, used to describe the size of the particle.

Bedrock Failure Collapse of a bedrock outcrop, typically either in zones of deep weathering or along joints created by geologic stress. When dry, bedrock failures typically cause rockfalls or rock avalanches. When sufficient moisture is present, these failures can create or contribute to debris flows.

Boulder Train A group of boulders that may be deposited during a debris flow upstream or downstream from a flow obstruction. Typically, flow obstructions include large immobile boulders and trees. Boulder trains that form downstream from flow obstructions tend to be deposited by streamflow, while boulder trains that form upstream from flow obstructions tend to be deposited by debris flows.

Channel Conveyance Channel conveyance is a measure of the carrying capacity of a channel based on uniform flow in the channel. The discharge in such a channel can be expressed as

$$Q = K \cdot S^{0.5}, \quad (5)$$

where Q = discharge, S = slope, and K = conveyance. K is defined using

$$K = 1.49\, A \cdot R^{0.667}/n, \quad (6)$$

where A = cross sectional area, R = the hydraulic radius, and n = Manning's n value. R is calculated as

$$R = A/P \text{ , (7)}$$

where P = the wetted perimeter. Sediment deposition in a soil-cemented reach could increase the potential for overbank flooding by decreasing the cross-sectional area, A, thus decreasing channel conveyance.

Cold-Top Thunderstorm A convection cell with sufficient lifting to create very low cloud-top temperatures (for example, the 2006 cold-top thunderstorms were -74°C). Cold-top thunderstorms often produce hail and generally have higher rainfall intensities and larger rainfall droplets than warm-top thunderstorms.

Colluvium Poorly sorted sediment that accumulates on hillslopes from rockfall or rock-avalanche sources. Colluvium may accumulate during discrete rockfalls or rock avalanches or may accrue over long periods of time from episodic additions.

Colluvium Failure Collapse and mobilization of unconsolidated sediments on steep slopes that typically accumulated through rockfall contributions.

Contributing Area The partial drainage area generating runoff or debris flows during a flood.

Cosmogenic Dating The use of isotopic extraction and measurement techniques to estimate the age of particles at the Earth's surface from the natural rate of accumulation of certain isotopes generated through spallation processes caused by cosmic-ray bombardment. Cosmogenic dating directly dates particles in a geologic deposit, but uncertainties may arise from prior exposure to cosmic radiation (for example, the particle moved from a position on the Earth's surface to a different exposed position) or through erosion. Cosmogenic ^{10}Be dating, summarized here, theoretically can be used to date deposits millions of years old but in practice is limited by the erosion rate of particles and their deposits.

Debris Flow A two-phase fluid of less than 40 percent water and more than 60 percent sediment by weight, generally poorly sorted, that typically results from saturated slope failures in the desert Southwest. Debris flows are considered to be non-Newtonian flows that are dominated by particle-particle friction.

Debris-Flow Deposit Typically, a poorly-sorted deposit of particles along a watercourse, either within the margins of a channel (for example, levees) or in an unconfined setting (for example, snout). Debris-flow deposits can be difficult to distinguish from streamflow deposits or colluvium, but several characteristics can be definitive: (1) the presence of poorly-sorted sediment with a surface subparallel to a channel, (2) the general lack of strongly imbricated particles in the deposit, (3) the presence of boulder trains extending upstream from an obstruction, (4) large particles (for example, boulders) resting on a bed of fine-grained sediment and not in contact with other large particles within a deposit, (5) the general lack of stratification in deposits. Many of these characteristics may also be present in hyperconcentrated-flow deposits.

Debris-Flow Matrix A two-phase mixture of water and sediment, typically particles less than about 8 mm in diameter and decreasing to clay-sized particles, that enables debris-flow movement. Because the water and sediment interact as a slurry, the amalgamation is considered to behave as a single phase with specific hydraulic properties.

Debris-Flow Scars Debris-flow scars are the highly visible landscape reminders of where slope failures occurred. In southeastern Arizona, debris-flow scars may be from 2006 or at earlier times (for example, 2003; see fig. 14*C*).

Depositional Zone During debris-flow events, this zone is where net deposition occurs and typically the debris flow loses enough mass to stop. Depositional forms in this zone include debris-flow snouts, push-out deposits, channel-constraining levees, boulder trains, and debris fans.

Digital-Elevation Model (DEM) A raster file of elevations at specific spatial dimensions. For example, a 3-ft DEM provides the elevation for every 3 ft x 3 ft pixel in the model.

Distributary Channels Typically occurring on alluvial fan heads, but also present in areas of confined but broad channels, this landform allows the shifting of flows among a series of channels whose beds differ by only small elevations. Distributary channel networks tend to be controlled by high sediment load in streamflow floods or debris flows, where deposition of levees or general channel aggradation may cause flow to abruptly switch channels. Avulsions, particularly through mid-channel islands or marginal floodplains, are common in distributary channels.

Head Scarps Vertical or near-vertical surfaces at the upslope (head) of hillslope failures. Head scarps may be associated with any type of failure, ranging from large landslides to small rotational slumps.

Hillshade Model A three-dimensional surface portrayed as if light were shined on it from a specific direction. Hillshade models are used only to illustrate topography.

Holocene In the southwestern United States, the Holocene generally is considered to be the past 11,000 years of geologic time.

Hydrometeors Any solid or liquid water in the atmosphere (for example, raindrops, hail, snow).

Hyperconcentrated Flow In our usage, this fluvial process results from pulses of debris flows and (or) runout facies downstream from debris flows. Hyperconcentrated flow may also result from sediment-laden flash-floods unrelated to debris flows. Sediment concentration in hyperconcentrated flow generally is in the 40-60 percent range by weight. Insufficient research has been done to know whether this poorly understood type of flow is Newtonian, non-Newtonian, or another type of two-phase media.

Hyperconcentrated-Flow Deposits The deposit left from a hyperconcentrated flow. When associated with debris flows, hyperconcentrated-flow deposits have a characteristic arrangement of stratigraphic layers, which can be relatively thin, showing deposition of poorly sorted sediment (but with smaller particles) interbedded with relatively well sorted sand or gravel lenses.

Imbrication Three-dimensional arrangement of large particles in a sedimentary deposit that indicates either streamflow deposition or reworking by streamflow. Imbricated deposits may appear to be flat-lying and overlapping as if tiled, and the orientation of the tiling points to the flow direction. Reworked debris-flow deposits can exhibit weak imbrication.

Initiation Zone During debris-flow events, the initiation zone is where sediment and water are mixed in high-energy settings, typically on steep slopes and involving hillslope failures or landslides. In the broadest sense, this is the zone where debris flows “bulk up” by adding sediment from hillslope failures, channel-bed entrainment, and (or) channel-bank failures.

LAHARZ A stochastic debris-flow hazards prediction model created by the USGS Cascades Volcanic Observatory. This model uses average debris-flow properties gleaned from events worldwide to estimate flow distances from initiation points.

Landslide This term is somewhat ambiguous when applied to desert environments. In more humid environments, a landslide is a deep-seated slope failure of large spatial extent that typically moves along a saturated failure plane fed by ground water; the overlying sediments may or may not be saturated. To avoid confusion, we typically refer to the saturated shallow failures that occurred in July 2006 in southeastern Arizona, as well as most initiation points for debris flows in the southwestern United States, using the generic “slope failure” term.

Levee In this case, a debris-flow deposit along the margin or center of a channel that has a characteristic form and poorly sorted particles. Boulders generally are the most obvious particles in a debris-flow levee. Lateral levees typically form along the margins of channels; medial levees typically occur in the center of channels.

LIDAR, Airborne Aircraft based Light Detection and Ranging instrument that uses a laser to image land surfaces in three dimensions, enabling the construction of digital-elevation models.

Matrix Deposits Debris-flow matrix deposits represent a reasonably intact sample of the range of fine particles transported during a debris flow, at least at the time of deposition during the event. The debris-flow matrix is difficult to define in terms of particle-size distribution but generally consists of all transported particles <2 mm to about 8 mm with no rigid definition.

Mesoscale Convective System Once referred to as mesoscale convective complexes, mesoscale convective systems are closely spaced groups of thunderstorms that can cover areas of about 100 to 500 mi^2. In the Southwest, mesoscale convective systems typically occur during the North American Monsoon when large-scale atmospheric steering mechanisms cause atmospheric divergence under conditions of high relative humidity and low vertical wind shear.

Mudflow A specific type of debris flow with a high (typically >40 percent) content of fine-grained sediment. Mudflows seldom occur in Arizona and none occurred during the 2006 event.

Newtonian Flow A Newtonian fluid deforms continuously under the application of a shear stress such that rate of deformation is directly proportional to the applied shear stress through a constant, known as absolute viscosity. Newtonian flow obeys Newton's law of shear, which is expressed by

$$\tau = \mu \, \partial v/\partial z \qquad (8),$$

where τ = shear stress, μ = the viscosity coefficient, v = velocity, and z = vertical dimension. Streamflow follows this relation and is considered to be Newtonian flow. Debris flows have different types of relations to handle internal shearing and are considered to be non-Newtonian flows.

Non-Newtonian Flows Fluids that do not deform proportionally to applied shear but follow some non-linear relationship are known as non-Newtonian fluids. Debris flows and hyperconcentrated flows are non-Newtonian; readers should see the references in this paper for more detailed information on the procedures used to mathematically model debris flows.

North American Monsoon A term of relatively recent origin that describes the meteorology of the summer thunderstorm season in Arizona scaled to hemispheric dimensions. Previous terms in common usage include the Arizona monsoon and the Mexican monsoon.

Particle-Size Distribution A relation that describes the range of particles in a deposit, traditionally measured in millimeters. Size is based on a b-axis diameter, which reflects the space in a sieve through which the particle can pass. Poorly sorted deposits, such as debris-flow deposits, have a range in particle size from clay through boulders. Streamflow deposits tend to be well sorted, typically containing sand-size particles or sand and small gravel.

Pleistocene The Pleistocene represents the period of geologic time from 2 million to 11,000 years before present. The latest Pleistocene is 22,000 to 11,000 years before present in our usage.

Push-Out Deposits This type of deposit generally results from failure of preexisting or new levees in the depositional zone and a channel avulsion. Push-out deposits may be considered debris-flow snouts, potentially for secondary debris-flow pulses, or they may be cross-cutting deposits across previously deposited levees.

Quaternary The Quaternary period of geologic time is the last 2 million years and includes the Pleistocene and the Holocene.

Radiocarbon (or ^{14}C) Dating Carbon 14 (^{14}C) is a radioactive isotope with a half-life of 5,200 years that is created by cosmogenic bombardment of nitrogen atoms in the upper atmosphere. Plants and animals accrue ^{14}C in proportion to its concentration in the atmosphere, and after death, ^{14}C decays in organic material, providing a time interval between accrual and the present used to determine an age. ^{14}C measured in geologic deposits has an uncertain association that may create errors in dating.

Rainfall Gage A device that measures rainfall. During the July 2006 storms, several types of rainfall gages were in operation in southeastern Arizona. Storage gages are read manually and report rainfall totals between readings; most storage gages are read at 24-hour intervals in the early daylight hours. Tipping-bucket rainfall gages typically record the frequency of volume increments (usually 0.01 in. of rainfall), either using data loggers or telemetry to transmit data to a base station, and rainfall may be aggregated into specific time intervals (for example, 15 minutes). A Belfort Storage Gage, which uses a strip-chart recorder, was used by the Bureau of Land Management in Apache Pass. Automated rainfall gages record volumes in specific time intervals on data loggers.

Rawinsonde A meteorological sensor carried upwards into the atmosphere following ground release. Rawinsondes carry a transponding GPS and typically measure temperature, humidity, and wind speed in a vertical gradient through the lower atmosphere.

Recurrence Interval This statistical term, also called a return period, refers to how often, on average, an expected observation will occur in the future. Although this term is used for hazard prediction, and technically the 100-year flood is an event with a 1:100 probability of occurring in the next year, recurrence interval is also used to describe a recent event in terms of its past rate of occurrence and is useful in describing the magnitude and frequency of meteorological and hydrological events.

Reworking Alteration in the particle size and form of a deposit after its deposition. Recessional streamflow that follows a debris flow may entrain fine-grained sediment and alter the geometric arrangement of larger particles, and these changes may obscure the original deposition mechanism.

Rill Linear depression on hillslope that fills with overland flow during rainfall and conveys the water down to the watershed stream network. A rill is considered an erosional landform.

Rill Failure Relatively small additions of sediment to debris flows along the margins of rills on steep hillslopes. Although the individual failures tend to be small, considerable sediment can be added to flow in rills on long hillslopes, potentially resulting in the controversial concept of debris flow "bulking up."

Rock Avalanche As used here, a failure in bedrock that results in a relatively large volume of material cascading down a steep or vertical slope at high velocity and as a one-phase media (solids). There is no quantitative distinction separating a rock avalanche from a rockfall on the basis of size, although a rock avalanche typically moves as a coherent mass while a rockfall travels as isolated particles.

Rockfall Typically a failure in bedrock of small spatial extent that rapidly travels downslope as isolated particles, not a coherent mass.

Rotational Slumps A type of deep-seated hillslope failure, typically in unconsolidated sediments but also potentially in bedrock, where movement occurs en mass along a saturated failure plane. Large rotational slumps are considered to be a special type of landslide. Rotational slumps may or may not mobilize into debris flows but typically result from deep saturation.

Slab Failure A special type of bedrock failure where a large consolidated piece of bedrock fails along a jointing plane or fault zone.

Slackwater Deposits Typically fine-grained sediment deposits left by flooding rivers in bays and alcoves away from the main current where flow decreases and sediment drops out of suspension. Such deposits can be used to forensically estimate the discharge of old floods.

Slope Failure A generic term that applies to a wide range of sediment delivery mechanisms from steep slopes to channels that usually involves rapid entrainment of relatively large amounts of sediment into water flow. Types of slope failures range from landslides, which are relatively slow moving, to rock avalanches and rockfalls, which move extremely quickly. Here, we typically refer to shallow-seated slope failures, which typically are of limited spatial extent and have thicknesses of less than 10 ft (typically less than 3 ft).

Snout Termination deposits of a debris flow that typically are poorly sorted and contain large boulders.

Streamflow Newtonian flow that typically contains less than 40 percent sediment.

Streamflow Flood Although any flow in an ephemeral channel during a rising stage might be considered a flood, here we consider a flood to be either the largest instantaneous streamflow that occurs in a year or a group of streamflows that are extremely high in the recorded history of a watercourse at a gaging station.

Streamflow Gaging Station Streamflow gaging stations typically measure the stage (or height) of streamflow passing the station, typically recorded at 15-minute intervals. Stage is converted to discharge using a stage-discharge relation developed from either direct measurement of discharge at a specific stage or by modeling flow using the channel geometry and roughness near the gaging station. Flood peak discharges represent instantaneous flow, which is manifested by the highest recorded stage.

Thalweg The deepest part of a channel.

Topographic Hollow On steep slopes, "channels" may be difficult to identify owing to the numerous mechanisms, mainly colluvial, that can create a path for downslope water and sediment movement. We refer to the areas on slopes where water accumulates as topographic hollows in an attempt to avoid confusion with larger channels at the bases of slopes.

Transport Zone During debris-flow events, debris flows typically pass from the initiation zone into a transport zone characterized by channels confined in bedrock chutes or canyons or within relatively resistant alluvium (for example, deposits cemented with calcium carbonate). In the transport zone, particles may be entrained, moved, or deposited but the net change in sediment volume is negligible.

Warm-Top Thunderstorm A convection cell with lower cloud-top elevations and temperatures (for example, the 2006 warm-top thunderstorms were -55°C). Warm-top thunderstorms generally produced more sustained and prolonged precipitation with small rainfall droplets at lower intensities than cold-top thunderstorms.

Appendix 1. Data for cosmogenic ^{10}Be dates on debris flows in Pima County

Table 1-1. Data input to CRONUS-Earth website (*http://hess.ess.washington.edu/math/al_be_stable/al_be_multiple.php*, accessed June 3, 2008) for calculating cosmogenic ages of debris-flow deposits in the southern Santa Catalina Mountains, Arizona.

Sample Name	Sample Number	Latitude	Longitude	Elev -ation (m)	Atmo -spheric Pressure	Thick -ness (cm)	Density (g/cm^3)	Topo- graphic Shielding Factor	Erosion Factor	^{10}Be Concen -tration (atoms/g)	^{10}Be Uncertainty (± atoms/g)
Finger Rock L1	070108-01	32.3392809	-110.9100319	965.5	std	4	2.65	0.9974	0	9.744E+04	4.053E+02
Finger Rock L1[1]	070108-02	32.3392809	-110.9100319	965.5	std	4	2.65	0.9974	0	1.062E+05	2.112E+03
Finger Rock L1[1]	070108-02	32.3392809	-110.9100319	965.5	std	4	2.65	0.9974	0	1.059E+05	4.984E+02
Finger Rock L1	070619-01	32.3392809	-110.9100319	965.5	std	4	2.65	0.9974	0	1.746E+05	9.808E+02
Finger Rock L2	070108-04	32.3392809	-110.9100319	961.0	std	4	2.65	0.9974	0	9.636E+04	4.692E+02
Finger Rock L2	070108-05	32.3392809	-110.9100319	959.2	std	4	2.65	0.9974	0	2.304E+05	8.101E+02
Finger Rock L2	070108-06	32.3392809	-110.9100319	956.8	std	4	2.65	0.9974	0	5.977E+04	2.203E+02
Finger Rock L2	070108-07	32.3392809	-110.9100319	958.6	std	4	2.65	0.9974	0	2.920E+05	7.850E+02
Finger Rock L3	070108-09	32.3392809	-110.9100319	953.9	std	4	2.65	0.9974	0	1.167E+05	4.296E+02
Finger Rock L3	070108-10	32.3392809	-110.9100319	954.2	std	3	2.65	0.9974	0	8.00E+04	2.988E+03
Finger Rock L3	070108-11	32.3392809	-110.9100319	956.1	std	6	2.65	0.9974	0	1.589E+05	5.181E+02
Finger Rock L4	070108-16	32.3392809	-110.9100319	950.4	std	4	2.65	0.9974	0	3.91E+04	2.158E+03
Finger Rock L4	070108-17	32.3392809	-110.9100319	950.8	std	4	2.65	0.9974	0	6.49E+04	3.357E+03
Finger Rock L4	070108-18	32.3392809	-110.9100319	950.2	std	4	2.65	0.9974	0	1.27E+05	5.128E+03
Pima L1[1]	070109-01	32.3525191	-110.94322985	911.6	std	4	2.65	0.9993	0	1.291E+05	4.317E+03
Pima L1[1]	070109-01	32.3525191	-110.94322985	911.6	std	5	2.65	0.9993	0	1.365E+05	4.405E+02
Pima L1[1]	070109-03	32.3525336	-110.94316037	911.6	std	4	2.65	0.9993	0	4.370E+05	8.286E+03
Pima L1[1]	070109-03	32.3525191	-110.94322985	911.6	std	2	2.65	0.9993	0	4.915E+05	1.207E+03
Pima L1	070109-04	32.3525191	-110.94322985	913.3	std	4	2.65	0.9993	0	2.428E+05	7.523E+02
Pima L2	070109-06	32.3525191	-110.94322985	910.0	std	5	2.65	0.9991	0	1.009E+05	4.769E+02
Pima L2	070109-07	32.3525191	-110.94322985	910.8	std	3	2.65	0.9991	0	1.044E+05	2.982E+02
Pima L3	070109-10	32.3525191	-110.94322985	917.1	std	4	2.65	0.9706	0	6.29E+04	2.816E+03
Pima L3	070109-11	32.3525191	-110.94322985	914.9	std	4	2.65	0.9706	0	2.28E+05	9.620E+03
Pima L3	070109-12	32.3525191	-110.94322985	915.9	std	6	2.65	0.9991	0	2.280E+05	3.121E+03
Pima L3	070109-14	32.3525191	-110.94322985	917.4	std	4	2.65	0.9706	0	7.22E+04	3.537E+03
Pima L3	070109-15	32.3525191	-110.94322985	916.2	std	4	2.65	0.9706	0	Low current[2]	
Sabino DF8[1]	070110-21	32.3377691	-110.78564402	963.0	std	4	2.65	0.9706	0	7.147E+04	1.402E+03
Sabino DF8[1]	070110-21	32.3377691	-110.78564402	963.0	std	4	2.65	0.9706	0	1.388E+05	1.854E+03
Sabino DF8	070110-23	32.3377691	-110.78564402	955.5	std	4	2.65	0.9232	0	2.108E+05	6.135E+02
Soldier L1	070111-01	32.3080977	-110.74366730	889.6	std	5	2.65	0.9958	0	2.222E+05	7.733E+02
Soldier L1	070111-03	32.3080977	-110.74366730	888.1	std	4	2.65	0.9962	0	4.886E+05	1.200E+03
Soldier L3	070111-08	32.3080977	-110.74366730	908.1	std	4	2.65	0.9962	0	2.401E+05	6.221E+02

Table 1.1 (continued)

Sample Name	Sample Number	Latitude	Longitude	Elev -ation (m)	Atmo -spheric Pressure	Thick -ness (cm)	Density (g/cm^3)	Topo- graphic Shielding Factor	Erosion Factor	^{10}Be Concen -tration (atoms/g)	^{10}Be Uncertainty (± atoms/g)
Soldier L3	070111-09	32.3080977	-110.74366730	908.9	std	4	2.65	0.9881	0	2.325E+05	6.112E+02
Soldier L3	070111-10	32.3080977	-110.74366730	906.6	std	4	2.65	0.9962	0	3.246E+05	5.022E+03
Soldier L5	070111-14	32.3080977	-110.74366730	911.5	std	4	2.65	0.9962	0	Low current[2]	
Soldier L5	070111-15	32.3080977	-110.74366730	909.3	std	4	2.65	0.9962	0	Low current[2]	
Soldier L5	070111-16	32.3080977	-110.74366730	912.2	std	4	2.65	0.9962	0	1.99E+05	8.865E+03
Soldier Amalgam	070111-22	32.3080977	-110.74366730	916.5	std	9	2.65	0.9962	0	1.736E+05	2.205E+03
Sabino Amalgam	070110-29	32.3377691	-110.78564402	952.5	std	10	2.65	0.9919	0	5.630E+06	2.856E+05

[1] Indicates these pairs of samples are duplicates used for quality assurance of method.
[2] Indicates that the sample yielded insufficient Be to make a measurement on the accelerator mass spectrometer (AMS).

Appendix 2. Particle-size distribution data for selected watercourses in northeastern Pima County

Table 2-1. Sediment size distribution of bedload in Sabino Creek at Cloud Road.

Particle size (mm)	Particle size (Phi units)	Cumulative Percent Finer—raw data
32	-5	100.0
16	-4	99.8
8	-3	99.4
4	-2	96.6
2	-1	84.1
1	0	53.9
0.5	1	22.7
0.25	2	4.3
0.125	3	0.4
0.063	4	0.1
Percent Finer	**Modeled particle size (Phi units)**	**Modeled particle size (mm)**
5	1.926	0.263
16	1.259	0.418
25	0.912	0.531
35	0.571	0.673
50	0.116	0.923
65	-0.319	1.248
75	-0.64	1.558
84	-1.002	2.002
90	-1.343	2.536
95	-1.782	3.439

Table 2-2. Sediment size distribution of bedload in Sabino Creek at Snyder Road.

Particle size (mm)	Particle size (Phi units)	Cumulative Percent Finer—raw data
32	-5	100.0
16	-4	99.6
8	-3	96.8
4	-2	90.1
2	-1	72.6
1	0	39.4
0.5	1	15.1
0.25	2	3.6
0.125	3	0.4
0.063	4	0.1
Percent Finer	**Modeled particle size (Phi units)**	**Modeled particle size (mm)**
5	1.799	0.287
16	0.958	0.515
25	0.531	0.692
35	0.153	0.9
50	-0.309	1.239
65	-0.752	1.684
75	-1.107	2.154
84	-1.581	2.992
90	-1.992	3.978
95	-2.633	6.205

Table 2-3. Sediment size distribution of bedload in Soldier Canyon at Kellis property.

Particle size (mm)	Particle size (Phi units)	Cumulative Percent Finer—raw data
32	-5	100.0
16	-4	99.9
8	-3	99.0
4	-2	95.8
2	-1	85.8
1	0	61.0
0.5	1	32.0
0.25	2	11.9
0.125	3	3.7
0.063	4	1.5
Percent Finer	**Modeled particle size (Phi units)**	**Modeled particle size (mm)**
5	2.767	0.147
16	1.747	0.298
25	1.29	0.409
35	0.89	0.54
50	0.374	0.772
65	-0.134	1.097
75	-0.499	1.413
84	-0.91	1.879
90	-1.321	2.498
95	-1.874	3.665

Table 2-4. Sediment size distribution of bedload in Soldier Canyon above Mount Lemmon Short Road, Site 1.

Particle size (mm)	Particle size (Phi units)	Cumulative Percent Finer—raw data
64	-6	100.0
32	-5	99.3
16	-4	97.4
8	-3	93.0
4	-2	75.9
2	-1	40.7
1	0	13.3
0.5	1	4.8
0.25	2	2.5
0.125	3	1.6
0.063	4	1.0
Percent Finer	**Modeled particle size (Phi units)**	**Modeled particle size (mm)**
5	0.964	0.513
16	-0.128	1.093
25	-0.499	1.414
35	-0.829	1.776
50	-1.251	2.38
65	-1.661	3.163
75	-1.969	3.916
84	-2.384	5.221
90	-2.749	6.724
95	-3.362	10.283

Table 2-5. Sediment size distribution of bedload in Soldier Canyon above Mount Lemmon Short Road, Site 2.

Particle size (mm)	Particle size (Phi units)	Cumulative Percent Finer—raw data
32	-5	100.0
16	-4	98.8
8	-3	85.9
4	-2	61.8
2	-1	35.6
1	0	16.4
0.5	1	8.4
0.25	2	4.5
0.125	3	2.5
0.063	4	1.4
Percent Finer	**Modeled particle size (Phi units)**	**Modeled particle size (mm)**
5	1.84	0.279
16	0.055	0.963
25	-0.499	1.413
35	-0.973	1.963
50	-1.551	2.931
65	-2.11	4.316
75	-2.482	5.588
84	-2.902	7.475
90	-3.174	9.028
95	-3.482	11.173

Table 2-6. Sediment size distribution of bedload in Soldier Canyon above Mount Lemmon Short Road, Site 3.

Particle size (mm)	Particle size (Phi units)	Cumulative Percent Finer—raw data
32	-5	100.0
16	-4	99.2
8	-3	92.9
4	-2	69.3
2	-1	35.5
1	0	12.1
0.5	1	4.4
0.25	2	2.1
0.125	3	1.2
0.063	4	0.6
Percent Finer	**Modeled particle size (Phi units)**	**Modeled particle size (mm)**
5	0.886	0.541
16	-0.213	1.159
25	-0.621	1.538
35	-0.983	1.977
50	-1.424	2.684
65	-1.864	3.641
75	-2.177	4.521
84	-2.514	5.713
90	-2.807	6.998
95	-3.188	9.112

Table 2-7. Sediment size distribution of bedload in Soldier Canyon below Catalina Highway.

Particle size (mm)	Particle size (Phi units)	Cumulative Percent Finer—raw data
32	-5	100.0
16	-4	99.8
8	-3	94.8
4	-2	73.1
2	-1	41.3
1	0	19.2
0.5	1	8.8
0.25	2	4.2
0.125	3	2.3
0.063	4	1.2
Percent Finer	**Modeled particle size (Phi units)**	**Modeled particle size (mm)**
5	1.779	0.291
16	0.268	0.83
25	-0.301	1.232
35	-0.745	1.677
50	-1.263	2.4
65	-1.724	3.304
75	-2.058	4.164
84	-2.38	5.207
90	-2.66	6.319
95	-3.015	8.086

Table 2-8. Sediment size distribution of bedload in Soldier Canyon at Prison Camp.

Particle size (mm)	Particle size (Phi units)	Cumulative Percent Finer—raw data
32	-5	100.0
16	-4	99.4
8	-3	95.7
4	-2	82.1
2	-1	54.0
1	0	27.3
0.5	1	11.6
0.25	2	4.2
0.125	3	1.1
0.063	4	0.3
Percent Finer	**Modeled particle size (Phi units)**	**Modeled particle size (mm)**
5	1.845	0.278
16	0.67	0.629
25	0.119	0.921
35	-0.31	1.24
50	-0.857	1.812
65	-1.348	2.546
75	-1.701	3.251
84	-2.101	4.291
90	-2.455	5.482
95	-2.91	7.516

Table 2-9. Sediment size distribution of bedload in Sabino Canyon 650 ft above confluence with Tanque Verde Wash.

Particle size (mm)	Particle size (Phi units)	Cumulative Percent Finer—raw data
16	-4	100.0
8	-3	99.9
4	-2	98.8
2	-1	95.1
1	0	82.6
0.5	1	54.3
0.25	2	13.8
0.125	3	1.9
0.063	4	0.7
Percent Finer	**Modeled particle size (Phi units)**	**Modeled particle size (mm)**
5	2.563	0.169
16	1.925	0.263
25	1.653	0.318
35	1.412	0.376
50	1.09	0.47
65	0.666	0.63
75	0.318	0.802
84	-0.086	1.061
90	-0.479	1.394
95	-0.986	1.981

Table 2-10. Sediment size distribution of bedload in Bear Canyon off Sabino Canyon Road.

Particle size (mm)	Particle size (Phi units)	Cumulative Percent Finer—raw data
64	-6	100.0
32	-5	99.4
16	-4	99.0
8	-3	95.1
4	-2	81.0
2	-1	57.1
1	0	28.3
0.5	1	11.7
0.25	2	3.1
0.125	3	0.7
0.063	4	0.2
Percent Finer	**Modeled particle size (Phi units)**	**Modeled particle size (mm)**
5	1.673	0.314
16	0.691	0.619
25	0.163	0.893
35	-0.251	1.19
50	-0.762	1.696
65	-1.295	2.454
75	-1.709	3.269
84	-2.157	4.461
90	-2.52	5.736
95	-2.987	7.929

Table 2-11. Sediment size distribution of bedload in Sabino Canyon below Sabino Canyon Dam at road.

Particle size (mm)	Particle size (Phi units)	Cumulative Percent Finer—raw data
32	-5	100.0
16	-4	97.5
8	-3	94.1
4	-2	87.0
2	-1	69.5
1	0	38.9
0.5	1	14.4
0.25	2	3.8
0.125	3	0.3
0.063	4	0.0
Percent Finer	**Modeled particle size (Phi units)**	**Modeled particle size (mm)**
5	1.819	0.284
16	0.92	0.529
25	0.503	0.706
35	0.133	0.912
50	-0.356	1.28
65	-0.843	1.793
75	-1.267	2.406
84	-1.795	3.47
90	-2.356	5.119
95	-3.206	9.225

Table 2-12. Sediment size distribution of bedload in Sabino Canyon 300 ft above Sabino Canyon Dam.

Particle size (mm)	Particle size (Phi units)	Cumulative Percent Finer—raw data
16	-4	100.0
8	-3	98.1
4	-2	86.1
2	-1	58.2
1	0	27.9
0.5	1	10.2
0.25	2	2.2
0.125	3	0.4
0.063	4	0.1
Percent Finer	**Modeled particle size (Phi units)**	**Modeled particle size (mm)**
5	1.503	0.353
16	0.605	0.657
25	0.129	0.914
35	-0.253	1.192
50	-0.739	1.669
65	-1.203	2.303
75	-1.533	2.893
84	-1.903	3.74
90	-2.199	4.591
95	-2.565	5.919